DESIGN OF NOVEL COPPER(II) BASED ANTI-INFLAMMATORY DRUGS FOR THE ELEVATION ASSOCIATED WITH RHEUMATOID ARTHRITIS

A Dissertation submitted to the

UNIVERSITY OF CAPE TOWN

In fulfilment of the requirements for the degree of

MASTER OF SCIENCE

By

ZIZILE MHLAMBISO

B.S.c (NMMU)

Department of Chemistry

University of Cape Town

Rondebosch 7700

South Africa

December 2009

Dedication

Yonela

Aviwe

Dumile

Phefumlela Sibulele

Phumeza

Thando

Irene Nomvuyiso

Welcome Mandlenkosi

Agnes Zinitha

ACKNOWLEDGEMENTS

- My supervisor, Professor Graham Ellis Jackson, for his patience and support throughout the course of this study.
- Professor Gert Kruger and O.Onajole at the University of KwaZulu Natal for synthesising the ligand.
- UCT Chemistry department technical stuff.
- Fellow members of our research group, Grace, Gadzikano, Pumeza, Mamohale, Everast, for the encouragements.
- Members and staff and fellow students in the Chemistry Department (UCT)
- The University of Cape Town Equity Scholarship, Harry and Crossley Post Graduate Scholar, Mintek and National Research Foundation (NRF) for financially assistance.
- My parents for their love and support.
- My partner Thobela

CONFERENCE PROCEEDINGS

This research study has been presented at the following conferences

- Development of copper based anti-inflammatory drugs (adamentane derivatives), Z. Mhlambiso and G.E Jackson. October 2008, Cape Organometallic Symposium, Cape Town, South Africa.
- Copper(II) anti-inflammatory drugs: A potentiomentric and spectroscopic study, Z.Mhlambiso and G.E Jackson, November-December 2008, South African Chemical Institute, Stellenbosch, South Africa.

ABSTRACT

It has been shown that copper complexes are able to alleviate inflammation associated with Rheumatoid Arthritis (RA). Serum copper levels are elevated in RA and it has been postulated that endogenous copper might have a protective function in chronic inflammatory conditions.

In designing Cu(II) anti-inflammatory drugs, one needs to know the stability constants of the ligand together with Cu(II) and the competitive metal ions, Zn(II) and Ca(II) in blood plasma. For this purpose glass electrode potentiometry, infrared (IR) spectroscopy, nuclear magnetic resonance (NMR) spectroscopy, UV/Visible spectroscopy as well as blood plasma modelling were used to explore the coordination chemistry of a newly designed ligand, PCUL (Bis-(3-aminoethy-2-aminomethylpyridine)-oxahexacyclo-dodecane).

PCUL protonation and formation constants with Cu(II) and Zn(II) were investigated by potentiometric analysis at 25°C and 0.15mol/dm^3 $Na^+(Cl^-)$. The potentiometric analysis showed that Cu(II) formed far more stable complexes at physiological pH with PCUL than the in *vivo* competitor Zn(II).

In this study the IR spectroscopic analysis was used to determine the Cu(II)-PCUL complexation sequence. The IR spectra show that the central amines are coordinated to the metal ion first. The small frequency shift between pH 4.02 to 6.91 proves that the pyridyl nitrogen atoms are also coordinated to Cu(II).

The sequence of protonation and the coordination site of Cu(II) were determined using NMR spectroscopy. UV/Visible spectroscopy was used for determining the number of possible chemical models present in solution.

The blood plasma simulation studies using speciation modelling calculations shows that PCUL is poor in mobilizing Cu(II) *in vivo*. PCUL substantially mobilizes Zn(II) and there is little ligand left to complex with Cu(II). Therefore PCUL is not good for mobilization of Cu(II).

CONTENTS

GLOSSARY

PCUL	Bis-(3-amnioethy-2-aminomethylpyridine)-oxahexacyclo dodecane
cageL	3,5-diaminodiamido-4-oxahexacyclo dodecane
pyN	2-(aminomethyl)-pyridine
gly	Glycine
555-N	N^1-(2-aminoethyl)-N^2-(pyridine-2-ylmethly)ethane-1,2-diamine
en	ethylenediamine
BETA	ESTA task for initial estimates of stability constants values
ESTA	Equilibrium Simulation for Titration Analysis
DMARD	Disease modifying antirheumatic drugs
NSAID	Non-steroidal Anti-inflammatory Drugs
RA	Rheumatoid Arthritis
ECCLES	Equilibrium of Constituent Concentrations in Large Equilibrium Systems
p.m.i	plasma mobilizing index
l.m.w	low molecular weight
emf	electromotive force
R_f	Hamiltonian R-factor
R_{lim}	Hamiltonian R-lim
pH	–Log of the activity of the hydrogen ion
$Log\beta_{pqr}$	Logarithm of the overall stability constant

OBJE	Task to minimise the objective function in terms of the emf
OBJT	Task for optimising parameters with respect to reactant concentrations
ZBAR	Task to calculate the complex formation function
Z-bar	Complex formation function
QBAR	Task to calculate the deprotonation function
Q-bar	Deprotonation function
σ_{pqr}	denotes standard deviation in $\log\beta_{pqr}$ for species pqr
T_H	total proton concentration (mol/dm^3)
T_L	total ligand concentration (mol/dm^3)
T_M	total metal concentration (mol/dm^3)
[L]	free ligand concentration (mol/dm^3)
K_w	dissociation constant of water
E_{cell}	electrode potential (volts)
E^o	electrode response intercept (volts)
R	universal gas constant
T	absolute temperature (Kelvin)
F	Faraday constant
$[H^+]$	hydrogen ion activity
s	electrode response slope
a_i	activity
γ_i	activity coefficient
c_i	concentration of i^{th} ionic species
I	ionic strength (mol/dm^3)
G	Gibbs free energy or chemical potential ($kJ\ mol^{-1}$)
G^o	Standard Gibbs free energy ($kJ\ mol^{-1}$)
U_{obj}	Objective function

n_T	total number of experiments
n_P	number of parameters being optimized
n-bar	number of protons bound to ligand in the absence of complexation
R_f^H	Hamiltonian R-factor
R_{lim}^H	Hamiltonian R-limit
10Dq	ligand field splitting
g	gerade
u	ungerade
λ_{max}	wavelength of maximum absorption
h	Planck's constant
c	speed of light
I^o	intensity of incident radiation
I	intensity of transmitted radiation
ε	molar extinction coefficient
ν_{max}	frequency of maximum absorption

LIST OF FIGURES

LIST OF TABLES

Figure 1: Structural formulae of ligands discussed in this study

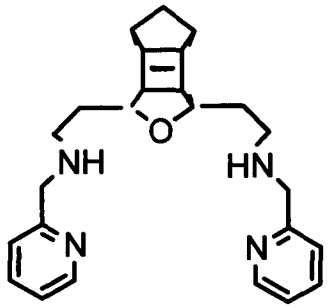

PCUL

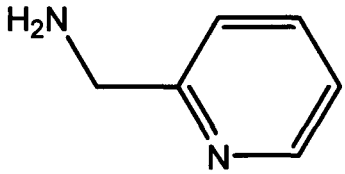

2-(aminomethyl)-pyridine

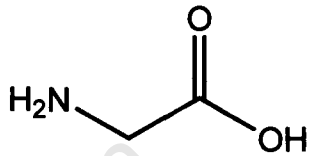

glycine

ethylenediamine

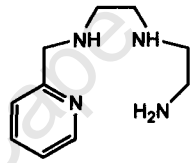

[555-N]

CHAPTER 1

INTRODUCTION

1. INTRODUCTION

1.1 RHEUMATOID ARTHRITIS

Rheumatoid arthritis (RA) is an autoimmune disease that causes chronic inflammation of the joints [1]. RA is characterized by massive synovial proliferation and subintimal infiltration of inflammatory cells, which along with angiogenesis leads to the formation of a very aggressive tissue, the pannus shown in Figure 1.1 [2].

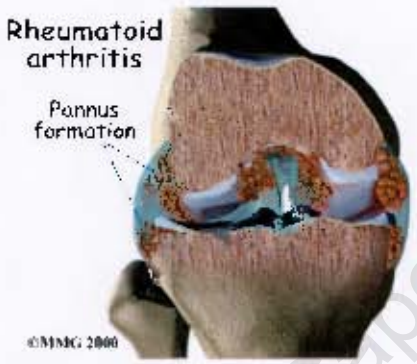

Figure 1.1: The pannus formation in RA.

The RA pannus consists of a hypertrophic synovial membrane composed of hyperplastic synoviocytes and inflammatory cells that infiltrate the synovial membrane [3]. The loss of joint function occurs when expansion of the pannus induces bone erosion and cartilage thinning. One of the earliest phenomena observed in RA is synovial neovascular formation delivering nutrients and oxygen to this proliferating pannus [4]. It has been shown that, angiogenesis inhibits the growth of the pannus in animal arthritis models. Vascular endothelia growth factor (VEGF) plays an important role in the pathogenesis of RA.

Immunohistochemical and in *situ* hybridization studies indicate that VEGF is strongly expressed in subsynovial macrophages, in fibroblasts surrounding microvessels, in vascular smooth muscle cells and in synoviocytes [4]. In the early stages of RA, VEGF expression is active and it continues throughout the course of the disease [4]. The VEGF level in synovial fluid and tissues correlates with the clinical severity of RA and with the degree of joint destruction [4].

Bone destruction also occurs when VEGF mediates the recruitment, chemotaxis, proliferation and osteoclast precursor macrophages. Macrophages and macrophage-like cells form the interface between the innate and adaptive immune systems and in addition to presenting antigens; they are responsible for amplifying inflammatory response and mediating tissue injury [3].

RA is also characterized by increased production of the inflammatory cytokines tumour necrosis factor alpha (TNF-α), Interleukin-1α(IL), IL-1β, and fibroblast growth factor (FGF-1). TNF-α appears to be a key mediator in the disease process, and IL-1β plays a permissive role by acting to shift the whole-body protein metabolism towards net catabolism, to elevate resting energy expenditure and to increase joint pain and stiffness [5]. In an experimental mouse models, treatment with antibodies against TNF-α, IL-1α, and IL-2β attenuated RA. FGF-1 (Fibroblast growth factor) is important for the growth of synoviocytes in the course of RA [5].

RA is referred to as a systemic illness, sometimes called rheumatoid disease since it can affect multiple organs of the body. This occurs because patients with autoimmune disease have antibodies in their blood that target their own body tissues, where they can be associated with inflammation. RA can last for years, meaning that it is a chronic illness, hence patients may experience long periods without any symptoms [1].

The diagnosis of RA is based upon clinical manifestations or findings [6]. The initial indication of this disease is usually polyarthritis affecting the small joints of the hands and feet in a systematic fashion. Cervical spine and large joints may also be involved but the thoracic and lumbar spines are usually spared. The presence of subcutaneous rheumatoid nodules in radiologic demonstration and detection of an antibody in the serum called rheumatoid factor may confirm the diagnosis of the disease [6].

The etiology of RA remains unknown; hence, its pathophysiology is poorly understood. Recent results show that rheumatoid synovial cells have a transformed phenotype. Synovial membrane (SM) immunohistological examination shows it to have all the hallmarks of a T-cell driven lesion: an accumulation of predominantly

$CD4^+$ T-cells belonging to the memory phenotype, activated macrophages and synoviocytes or specialised synovial fibroblasts and lysosomal enzymes.

The aetiology of early events of RA remain unknown, the search for a bacterial or viral agent initiating the disease has been unrewarding, despite the variety of molecular and cellular approaches used [3]. It is, therefore possible that there is no single cause but rather a combination of genetic and environmental factors that contribute to the initiation of RA [3]. One hypothesis suggested that RA is an antigen-driven, T-cell dependent disease and that the inflammatory events are initiated by $CD4^+$ T-cells recognizing antigens in the synovial tissue. However, to date, no specific, common antigen has been identified in the synovium of different RA patients [3]. It is possible that a variety of antigens is involved in the T-cell response and that the antigen or epitopes presented to T-cells vary during the course of the disease [3]. T-cells also appear to play a pivotal role in the conversion of the synovium into lymphoid tissue [3]. Free oxygen radicals (e.g., superoxide and hydrogen peroxide) have been implicated as mediators of tissue damage in RA, along with proinflammatory cytokines, particularly (TNF-α) [5]. In the synovial fluid of RA patients, free radical oxidation products have been identified and these products are thought to be generated by activated macrophages, monocytes, granulocytes, as well as by anoxic reperfusion reactions that may occur with the movement of affected joints [5].

In metabolism of aerobes, the superoxide radical anion $O_2^{\cdot -}$ is encountered via one-electron reduction of molecular oxygen [7]. The superoxide radical is very toxic because it is an intermediate or occasional byproduct during respiration and as an immune response product of phagocytes during respiratory burst. Superoxide has been implicated in oxidative damage phenomena, along with hydrogen peroxide (H_2O_2) and hydroxyl radical ($^{\cdot}OH$), related to aging, inflammation and postischemic injury via reperfusion. Nature utilizes superoxide dismutase (SODs), in order to provide cellular defence against the oxidative stress by catalyzing $O_2^{\cdot -}$ disproportionate into the less toxic dioxygen and hydrogen peroxide. (Shown by the following reaction)

$$2O_2^{\cdot -} + 2H^+ \xrightarrow{SOD} O_2 + H_2O_2$$

So far, three unrelated kinds of SOD's have been characterized, all being metalloenzymes [5]. These clases have been classified depending on their active site metal ion content mainly: Cu-and Zn-dependent SODs [7]. Copper and zinc containing enzymes among SODs are probably the most abundant found in all eukaryotes and many prokaryotes.

RA is a common disease affecting 5% of the Western World, afflicts equally all races of people with women afflicted more than men, in a ratio of 2-3:1 [8]. In adults, the disease is prevalent in the age range 40-60 years although it can occur in any age [9]. Multiple members can be affected in some families, hence suggesting genetic basis for the disorder. The symptoms and progression of this disease can be controlled using immunosuppressive and anti-inflammatory drugs; however, there is no cure for this disease and treatment of chronic RA remains largely symptomatic [1].

Schematic representation of a normal Osteoarthritis and Rheumatoid arthritic joints are shown in Figure 2.1.

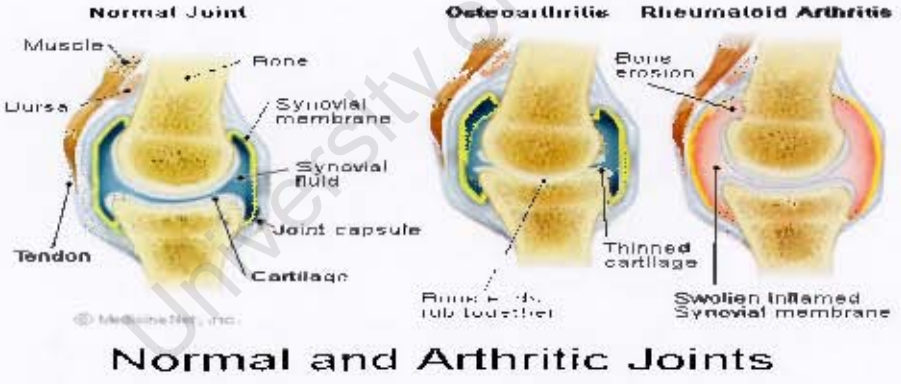

Figure 1.2: Cross section of a healthy and diseased joint

The synovial joint consists of six basic components, which are; joint capsule, joint cavity, synovial membrane (synovium), synovial fluid, bones coming together to form joints and hyaline cartilage [9].

The ability of a normal synovial joint to function properly as a load bearing structure depends on the integrity and correct alignment of the opposing surfaces of the articular cartilage, as well as the thickness and pattern of the subchondral bone. A

synovial capsule is composed of two layers, an outer fibrous and an inner synovium [9]. The outer layer is not well vascularised and it consists mainly of joint receptors innervating it, while the synovium is well vascularised but poorly innervated [9]. The functional characteristics of the connective tissue in the joints are determined by their chemical composition [9]. These tissues are composed mainly of proteoglycans, collagen and glycoproteins [9].

The articular cartilage has the ability to decrease stress on the contact joint surfaces by minimizing friction and wear between two opposing joint surfaces during movement and to dissipate forces on the joint over a wide area. There are two substances, which are found in the synovial fluid, namely: hyaluronic acid and a glycoprotein called lubricin, both of these substances are responsible for lubrication of the joints. Hyaluronic acid lubricates the joint capsule and lubricin lubricates the cartilage. Nutrients are carried to and wastes are carried from the vascular components of the joint via the synovial fluid that serves as the transport medium [10].

The ends of the long bones that form the synovial joints are composed of a soft, spongy bone called subchondral bone, which is covered and protected by hyaline cartilage [11]. Proliferation of synovial granulation tissue takes place at the cartilage in regions where the bone is not protected. The cartilage then becomes exposed to destructive enzymes from the synovial fluid and the pannus, which remove proteoglycans from the cartilage by redial cleavage [11].

The superficial layers of the cartilage, which are assumed to be deposited by the immune complex, act as chemoattractents from the synovial pannus, causing the granulomatous response to spread throughout the joints. Thus, the chronicity and persistence of rheumatoid inflammation occurs due to the presence of cartilage together with immune complex [11]. This therefore constitutes the mechanism of joint destruction leading to erosion of articular cartilage and subchondral bone (as shown by Figure 1.2) resulting in the permanent and debilitating structural damage that is associated with chronic unremitting RA [11].

1.2 Drug therapy for RA

The acceptable treatment for RA should have the following features; highly efficacious, devoid of side effects, affordable and acceptable to the patient. Traditionally, copper rich diets such as crayfish and peanuts were administered as a way of treatment of RA [12]. Antioxidant micronutrients play a vital role as part of the mechanism that protects against tissue damage caused by reactive oxygen species [5]. Antioxidants also suppress the expression of cytokines and collagenase induced by tumor necrosis factor-α, which suggests additional mechanisms of protection against RA [5]. This suggests that antioxidant compounds may provide protection against the development or progression of RA. Diets high in fruits or vegetables have also been suggested to be protective against RA [6]. Copper jewellery was accepted as a standard treatment. However, scientific therapeutics have been slowly replacing this traditional approach.

Such therapeutic drugs can conveniently be classified into three categories:

1. Nonsteroidal anti-inflammatory drugs (NSAID)s
2. Glucocorticosteroids and
3. Disease-modifying antirheumatic drugs (DMARD)s.

1.2.1 NSAIDs

NSAIDs are characterized by an absence of steroid moiety in their structure as the name indicates [10]. They are referred to as first class drugs and are medications that can reduce tissue inflammation, joint pain, stiffness and swelling. The NSAIDs include salicylates, for instance aspirin and large number of non-salicylates, which are generally weak carboxylic or enolic derivatives [13]. These drugs are used in doses higher than the doses required for treating headaches and fever, aspirin acts as an effective anti-inflammatory medication for RA. Aspirin has been used for joint problems since the ancient Egyptian era [1].

The new NSAIDs require fewer doses per day, hence are just as effective as aspirin in reducing inflammation and pain. Beside their anti-inflammatory activities, NSAIDs also possess analgesic and antipyretic properties and are thought to function by

inhibition of the cyclo-oxygenase pathway of prostaglandin (PG) synthesis. Since NSAIDs suppress PG synthesis, gastric acid production is increased whereas the production of gastric mucosa is also decreased, thus impairing the normal protective mechanism of the stomach [14]. Several other PG-independent mechanisms of action has been proposed such as inhibition of collagenase, stabilization of lysosomal membranes and disruption of membrane-associated enzymatic functions, which generate the superoxide radical [14].

While these drugs are generally well tolerated, they are also associated with a wide range of potential clinical toxicities. The most common side effects of asprin and other NSAIDs include gastrointestinal tract (GIT) irritation and stomach upset. The damage to the GIT mucosa by NSAIDs can occur via a number of mechanisms [15]. Such mechanisms include direct topical irritation to the GIT epithelium, impaired barrier properties of the mucosa, reduced gastric mucosal blood flow, interference with the repair of superficial injury and suppression of gastric prostaglandin synthesis [15].

1.2.2 Glucocorticosteroids

These drugs are used in treatment of RA because of their anti-inflammatory and immunosuppressive effects [4]. They include compounds such as cortisone, prednisone and dexamethasone amongst others. They have numerous metabolic and physiological effects, affecting lymphocytes, granulocytes, macrophages, cell membranes as well as inhibiting the immune system. The mechanisms which result in such effects produced by glucocorticosteroids are rather complex. Steroids are believed to inhibit phospholipase A_2, which release arachidonic acid from cell membranes [16]. Corticosteroids are not considered to have disease-remitting potential, although this has recently been questioned since protection against joint erosion has been reported [16].

Glucocorticosteroids are administered as oral and parenteral preparations [16]. The later are given inta-articularly or at peri-articular sites of local inflammation and are effective at relieving pain and swelling [16]. Hydroxylation of prednisone to prednisolone and cortisone to cortisol at the C_{11} site is necessary for activity. Active

drugs such as prednisolone or methylprednisolone are preferred in patients with faulty hydroxylation systems or else the patient will appear unresponsive to these medications. Suppression of the pituitary-adrenal axis for about one week can occur in patients taking 50 mg of prednisone daily after only 5 days [17].

Disadvantages of glucocorticosteroids include inhibition of collagen synthesis and stabilization of lysosomal membranes. Many serious side effects are associated with the use of corticosteroids, especially their effects on bone and the GI tract. Glucose intolerance, increased susceptibility to infections and impaired wound healing are other complications of glucocorticosteroids. It is difficult to discontinue their use as some patients may develop a steroid-dependence [18].

1.2.3 Disease-modifying antirheumatic drugs (DMARD)s.

These drugs are aimed not only in treating the symptoms of RA but also at suppressing the disease at the source by diverting the course of the pathologic reaction [19]. DMARDs are referred to as 'second-line' or 'slow –acting' medicines. They are used for long period at varying doses and may take weeks or months for benefits of the drugs to be noted. DMARDs promote remission, thereby retarding the progression of the joint destruction and deformity if effective. Recent studies show that patients who respond to DMARDs with control of the rheumatoid disease may actually decrease the known risk of lymphoma that exists from simply having rheumatoid arthritis. However, the mechanism of action of DMARDs remains unknown. DMARDs include sulfasalazine (SSZ), D-penicillamine, various antimalarial and gold compounds, as well as the more recent immunoregulators cyclophosphamide, azathioprine (AZA) and methotrexate (MTX) [18].

Disadvantages of DMARDS include; clinical toxicity and patients need frequent evaluation by their physicians. Toxicity varies from 20% in sulfasalazine up to 60% in penicillamine [20]. Other side effects include renal toxicity, dermatitis, nausea and anaemia.

(a). D-penicillamine.

D-penicillamine has been used as a therapy for RA for many years [4]. Previous studies suggested that D-penicillamine might reduce rheumatoid synovial hyperplasia via Fas-mediated apoptosis, but the mechanism of the effect of D-penicillamine is still unknown [4]. Side effects of such drugs include fever, chills, mouth sores, metallic taste in the mouth, skin rash, kidneys and bone marrow damage, stomach upset and easy bruising [1]. Routine blood and urine tests are required to patients on such medication. This medication increases the level of histidine while hydroxychloroquine stabilizes the level [21]. D-penicillamine resembles one of the amino acid, cystein, hence it is thought to be very effective in altering the course of the disease. Its mode of action is thought to be via its ability to bind firmly to plasma proteins, including albumin, α-globulin and ceruloplasmin via the disulfide linkage [21].

(b). Antimalarials

The antimalarials are among the least effective and the least toxic of the slow-acting agents and their efficacy is largely a matter of opinion. Among the currently available antimalarial drugs, only chloroquine (CQ) and hydroxychloroquine (HCQ) are widely used. The actions of these compounds are identical; the only difference between them is that HCQ has an –OH on the ethyl group attached to the terminal nitrogen that occurs only in HCQ. The absorption of both HCQ and CQ after oral administration is essentially complete [20]. The drugs are plasma bound (<60%; albumin, α1-acid glycoprotein) but distributes widely and due to the extensive tissue biding and ion trapping, accumulates to impressive degree in the lung, kidney, spleen, melanin-containing tissues and also leucocytes [20].

Binding reflects intercalation in DNA, binding to macromolecules, such as melanin, and binding to phospholipids. [20]. HCQ exists in both ionised and unionised forms at physiological pH, where the unionized forms can diffuse throughout membranes and the ionized one cannot. The free permeable, unionized species allow initial movement of the drug into the cells and subcellular structures. However, once the drug is inside subcellular structures where pH is low, it becomes completely ionized and hence no longer able to diffuse through membranes (thus ion trapping occurs) [3].

Since melanin has a high capacity for HCQ/CQ, very significant quantities of the drug accumulates during chronic administration. The retina has high melanin content; hence, accumulation of the drug to the retina is associated with occurrence of visual difficulties, including blindness. Vision also may be impaired by drug deposition in the cornea, although the relative frequency of such deposit is unclear [20].

(c). Sulfasalanine (SSZ)

SSZ is a diazo conjugate of 5-aminosalicylic acid (which has some inflammatory activity) (5-ASA) and sulfapyridine [20]. After oral administration, the intact drug is poorly absorbed. Orally absorbed drug is reduced in the liver and its component liberated [20]. In the gut lumen, intact drug can be broken down to its components in the upper gastrointestinal tract, after which sulfapyridine is rapidly absorbed. These drugs are thought to modify lymphocyte function and inhibit rheumatoid factor (RF) synthesis as well as cyclo-oxygenase and proteolytic enzyme activity [20]. Basic cellular processes such as thiol-disulphide exchange, the collagenase enzyme reaction and nucleoprotein interaction are the effects of antimalarial drugs. They also inhibit anti-inflammatory properties, such as inhibition of prostaglandin (PG) synthesis and superoxide release by neutrophils, as well as stabilizing lysosomal membrane and suppressing phagocytosis [18]. Previous research indicated that gold affects complement activation and decreases serum concentrations of immunoglobulins through effect on macrophages and B-lymphocytes [18].

The side effects of SSZ are common to most sulphonamides and include gastrointestinal effects, hypersensitivity reactions and blood dyscrasias [20]. Mechanisms are generally not known for most of the aforementioned side effects [7]. Macrocytic anaemia can occur during sulfasalazine therapy since the sulfapyridine acts to prevent microbial synthesis of folic acid and because humans are entirely dependent on folic acid produced by their gastrointestinal flora. The above effect can be prevented by supplementation with folic acid [20].

(d). Azathioprine (AZA)

This drug is a prodrug that is metabolized to its active form 6-mercaptopurine (6MP) [20]. AZA is converted to (6MP) in *vivo.* Both AZA and 6MP have essentially identical properties and activities. AZA possess better oral absorption characteristics, which combined with its longer time action, accounts for its use in preference to 6MP [20]. AZA is a substituted analog of the naturally occurring purine, guanine [20]. Although effects on S-phase are primary, AZA can also affect RNA and protein synthesis in growth phases (G), G_1 and G_2, although higher doses may be required [20]. G_1 is much more sensitive to drug effects; hence, since it precedes the S-phase, high drug level effects at G_1 can actually prevent entry into the S-phase and thus limit the degree of cytotoxicity [20]. That is why AZA (6MP) is sometimes referred to as an S-phase specific, self-limited drugs [20]. This drug targets proliferating cells and has a differing degree to effect in proportion to the degree of proliferative activity [20].

AZA has anti-inflammatory and immunoregulatory activity, inhibiting monocyte production, B cell proliferation and γ-globulin synthesis [20]. This effect has been observed upon its conversion to 6MP. After several month of administration, AZA has been noted to cause a peripheral lymphopenia to RA patients. The reduction includes both B- and T- lymphocytes, with greater reduction occurring in T-helper. AZA appears to modify the function of B-lymphocytes, because T-suppressor function is very sensitive to AZA, more so than B-cells in general, B-antibody responses may actually be accentuated by low doses of AZA [20].

The unwanted side effects of AZA therapy include; bone marrow suppression, expressed as leukopenia of thrombocytopenia, or both [20]. The production of bone marrow suppression, hepatic damage and gastrointestinal effects probably occur via biochemical mechanisms [20]. An alkylating agent that inhibits DNA replication, cyclophosphamide acts by affecting B cell function that results in decreased immunoglobulin production [18]. AZA decrease serum immunoglobulins and suppress antibody response [18]. 6MP can produce severe hepatic toxicity, but this is usually in antineoplastic doses. However, lower doses of 6MP produce less toxicity. AZA hepatotoxicity is lower than that of 6MP, possibly reflecting both lower usual

doses and the relatively slow release of 6MP from the prodrug [20]. The unwanted gastrointestinal toxicity as a side effect of AZA, is diminished in 6MP [20].

(d). Methotrexate (MTX)

MTX is an analog of folic acid and its basic action is that of an antimetabolite [20]. This drug is a weak organic acid that is primarily in an ionized very water soluble form above pH 7, below pH 7 it is relatively insoluble [20]. Almost complete absorption occurs in doses used orally in the therapy of RA. Following absorption, this drug is widely distributed and actively taken up into the cells via the transporters for 5-methyltetrahydrofolate (5-methyl-FH_4), for which 5-formyl-FH_4 (leucovorin) is also a ligand [20]. In the synovial fluid and the surrounding cells, significant levels of MTX are found. MTX can be polyglutamylated, once inside the cells, with one to four glutamyl residues possible and two common.

The polyglutamated forms remain inside the cells since they are charged and too large for diffusion to occur. Differing rates and extents of polyglutamylation of MTX are demonstrated by different types of cells. Cells with low capacity accumulate less MTX and are less likely to develop toxic side effects, while those cells with high capacity and rate will accumulate significant quantities of MTX and are more likely to develop toxicity. Since MTX also affects RNA and protein synthesis, it can be classified with AZA/6MP, i.e., MTX is an S-phase (proliferation)-specific self-limited antimetabolite [20]. Unlike AZA, MTX is not metabolised to any extent, although small amounts of 7-OH-MTX may be formed [20]. 7-OH-MTX is insoluble than MTX, however it is less toxic. MTX is renally eliminated by both filtration and active secretion via the tubular organic acid transporter.

When MTX is used in therapy of RA at low doses, side effects related to bone marrow suppression (leukopenia, thrombocytopenia), damage to gastro—intestinal mucosa (nausea, anorexia, diarrhea and vomiting, mucositis, stomatitis) and skin rashes, (alopecia) which occur in any agent that inhibits cell replication are uncommon, in the order of 5%. MTX serious adverse reactions affect; the liver, lungs, GIT, renal production and central nervous systems. Hence, the use of MTX is discontinued because of this toxicity [20].

1.3 Background to study

1.3.1 The involvement of Copper in RA

Long before the extensive biochemical studies of the affected tissue, copper was already associated with RA [4]. Copper occurs as the metal in oxidation states (0), (I), (II) and unstable (III) [4]. Copper occurs as Cu(II) ion in an aqueous solution, which mainly depends on pH, temperature, presence of bicarbonate and sulphide and the presence of potential complexing agents such as amino acids, certain peptides and detergents [4]. Copper is an essential trace element that acts as a cofactor for a variety of enzymes by virtue of its ability to accept and donate electrons under physiologic conditions [4]. Copper is an essential component of a number of important enzymes, including:

1. The free radical scavenger- superoxide dismutase (SOD) – required for the destruction of superoxide radicals [22].
2. Tyrosine –for the synthesis of dihydroxyphenyl-alanine which is subsequently transformed to melanin, required for pigmentation [22].
3. Cytochrome c oxidase – involved in oxidative metabolism, brain functioning haem synthesis and phospholipid synthesis [22].
4. The neurotransmitter, dopa-β-mono-oxygenase-for conversion of dopamine to norepinephrine, which is a neural hormone important in the transmission of nerve impulses [22].
5. Lysyl oxidase - required for connective tissue in the lungs and bones [23].

Most of the copper in living organisms, including humans, plays the role of a cofactor for specific enzymes and electron transport proteins involved in energy or antioxidant metabolism [23]. Copper ions have recently demonstrated to be required for the assembly of multiprotein release complexes in the process of stress-induced nonclassical release of FGF-1 and IL-1α [4]. These two proteins lack a signal sequence in their primary structures and cannot be released through the classical endoplasmic reticulum-Golgi pathway [4]. Copper is also known to play a vital role in the development and maintenance of the immune system.

Copper, in its metal form, is malleable, ductile and a good conductor of heat and electricity. It is a major constituent of most alloys and has been termed one of man's most important metals, the ore having been mined for over 5000 years [24]. Copper is in fact the third most abundant metallic element in the human body following iron, calcium, potassium, magnesium and sodium. The normal adult body contains between 75 and 50 mg of copper, the average person consuming about 3 mg daily [24].

Copper and its complexes can have a dual nature [25]. The copper amino acid complex of glycine has been found to be an irritant, a response that is observed in copper salts and metallic copper [25]. Copper does not exist in any significant amount in free ionic states, hence its beneficial effects supercedes the adverse side.

1.3.2 Copper Biochemistry

Copper enters mammals through the alimentary tract, it does not enter mammals through skin, unless, for instance, it is applied in high concentrations in the form of specific ointments or if copper bracelet is worn, where it was observed that through sweat bracelets were solubilised and promoted dermal absorption of copper into the blood stream [23]. In mammals, absorption of copper occurs exclusively in the small intestines after digestion of food in the stomach and duodenum [23]. On entering cells, copper normally finds its way readily to the different sites where it is needed [23]. Most of the incoming copper rapidly finds its way into the hepatocytes of the liver and the brain, with less amounts entering the heart, spleen, kidney and blood [23] The iris and choroid of the eye have very high copper levels [23]. The data from human studies indicated that, in the range of normal intakes, there is some adaptation of absorption relative to need; higher percentages of the available copper are absorbed at lower intakes and vice versa [23].

Absorption of copper across the brush border into the cells of the intestinal mucosa, and its subsequent transfer across the basolateral membrane into the interstitial fluid and blood occur by different mechanisms [23]. Transfer across the mucosal barrier probably occurs by non-energy-dependent diffusion [23]. Transfer of copper across the basolateral membrane appears to be rate limiting and is mediated by a saturable,

energy-depended mechanism. Additional diffusion or carrier-mediated systems in the basolateral membrane come into play at higher intakes of copper and it seems these are the sites where competition for absorption between copper and other transition metal ions take place [23].

Most of the ingested copper is excreted via the bile, the major excretory route, thus preventing tissue toxicity [26]. Trace amounts of copper are excreted via urine except in cases of copper overload [26]. Excess copper in the tissue leads to the production of damaging free radicals and subsequent DNA cleavage [26]. Specific proteins are required in each step of copper transport pathway. These proteins are cell receptors, membrane transporters involved in metal influx and efflux and a series of intracellular transporters [26].

The design and synthesis of a peptide molecule mimicking the specific Cu(II)-transport site of human serum albumin provided an ideal opportunity to study in detail the coordination equilibria existing in approximated physiological conditions [27]. Serum albumin is a major metal binding protein in the body, with about 40 μg of copper able to bind to the albumin in one of the most extensively studied binding site of any protein [12]. Cu(II) bound to albumin is exchangeable and is known to be the transport form of Cu(II) in the blood. [27]. The proposed structure of major Cu(II) binding site in HSA is shown in Figure 1.3. This structure involves the α-NH_2 nitrogen, two peptide nitrogens and the imidazole nitrogen of the N-terminal Asp-Ala-His residue [29].

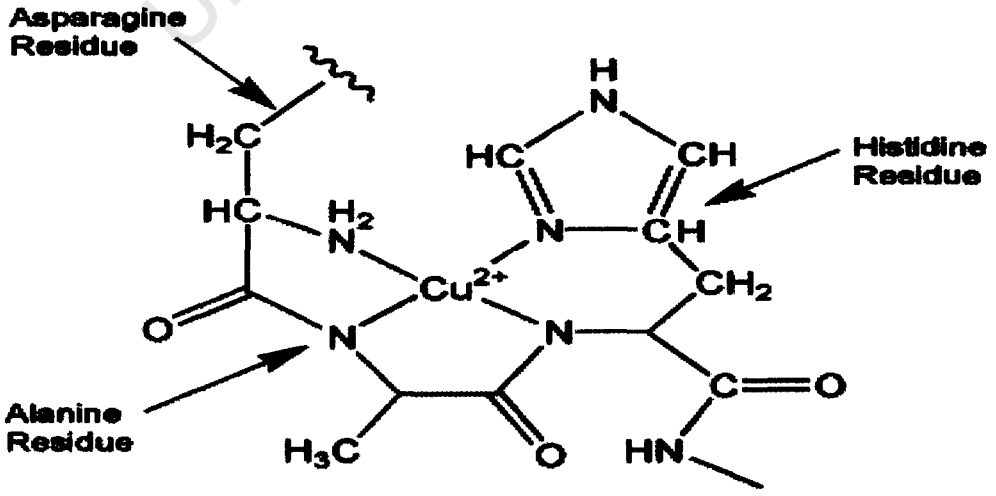

Figure 1.3: Copper binding site in Human Serum Albumin (HSA).

Sarkar and Co-workers have suggested that the ternary complex L-histidine-Cu(II)-albumin acts as an intermediate in the exchange of Cu(II) in blood between a macromolecule such as albumin and low molecular weight substances like amino acids [27]. Because Cu(II) bound to the designed peptide diglycyl-L-histidine simulates many characteristics of Cu(II)-albumin, the ternary system L-histidine-Cu(II)-diglycyl-L-histidine can be considered as the representative of the ternary complex L-histidine-Cu(II)-albumin [30].

Initially, Cu(II)-transport site was suggested to involve the α-amino nitrogen, two intervening peptide nitrogens and the imidazole nitrogen of the histidine residue in position 3 [12]. Subsequent investigations were carried out by Laussac and Sarkar with simple tripeptide molecules, e.g., glycylglycyl-L-histidine and glycylglycyl-L-histidine *N*-methyamide that were designed to mimic the proposed Cu(II)-transport site of human serum albumin (HSA). The results showed many similarities between HSA and these peptides in their Cu(II)-binding properties [12].

The Cu(II) cation is well known for its ability to interact with histidyl residues in peptides, especially with those containing the N-terminal sequence X-Y-His that is encountered in serum albumin [29]. Tripeptides with histidine in the 3rd position were widely studied for the complexation of Cu(II) ion as mimicking fragment for the N-terminal sequence of serum albumin [29]. These peptides contain a carboxylate group on the histidyl residue that does not exist in the protein structure [29]. This draw back is avoided by substitution of the histidyl residue by histamine. Hence, the pseudopeptides X-Y-Ha (Ha: histamine) can be used to evaluate the complexing ability towards the Cu(II) ions, although other models are possible, namely those using histidine residue in the amide form [29]. Previously this was done with Gly-Gly-Ha, which gave rise to the formation of the 4-N complex MLH_2, as with Gly-Gly-His with slightly lower formation constant [31].

The carrageenen foot oedema model of RA has been used in clinical studies on mice, and it was found that irrespective of the complex administered, at a moderate dose of 9.3mg/kg, approximately 60% reduction in inflammation was obtained [29]. Although RA is currently controlled by immuno-suppressive drugs and symptoms

treated with anti-inflammatory drugs, the use of metal chelating agents has grown [29]. There has been an upsurge of interest in the metal ion therapeutics, within the last decade for both diagnosis and treatment [29]. Cu(II)-$_L$-histidine, for instance, has been used in the treatment of Menkes disease [2, 3,]. Such interest has been due to the biochemical and pharmacological properties of the metal-ligand system, with extensive research carried out to determine the role of the ligands in copper uptake into the cells [29]. The effective role of various copper chelating agents in the alleviation of inflammation associated with RA have appeared in many articles, indicating the physiological importance of these agents as well as their therapeutic applications [29].

1.3.3 Anti-inflammatory mechanisms of copper complexes

Generally, copper is believed to possess anti-inflammatory activity since patients with RA exhibit changes in copper distribution in the blood. An increase in total serum copper is observed in arthritis suffers compared with the controls. This was observed as an increase in CP-bound copper and a decrease in albumin-bound and low molecular weight (l.m.w) copper resulting in low levels of bio-available copper in the blood [18]. Altered copper concentrations have also been observed in the synovial fluid of RA patients and some researchers suggest that alterations in copper are a cause of the disease while others do believe that it is a physiological response to the disease and that copper plays an essential role in its control and treatment [32].

It has been suggested that copper complexes of clinically used antiarthritis drugs were formed in *vivo* and that they were responsible for the beneficial effects of these drugs [32]. In a comparison of the effectiveness of copper, gold and silver thiomalate and thiosulphate in models of inflammation, the copper complexes were effective; while the activity of the gold and silver complexes was much lower [29].

There are several possible mechanisms for the anti-inflammatory activity of copper complexes [12]. The copper may induce lysyl oxidase activity, modulate prostaglandin synthesis, induce or mimic superoxide dismutase activity, decrease the permeability of human synovial lysosomes and modulate the physiological effects of histamine [12]:

(a). Induction of Lysyl Oxidase

The repair of damaged tissue requires cross-linking and extracellular mutation of the tissue components, collagen and elastin [33]. Lysyl oxidase that is copper dependent enzyme is responsible for this process [33]. It has been observed that lysyl oxidase activity is induced in copper deficient chickens with copper(II) sulphate [33].

(b). Modulation of Prostaglandin Synthesis

Copper complexes have been shown to decrease the synthesis of pro-inflammatory (vasodilator) prostaglandin, PGE_2 and a concomitant increase in the synthesis of the anti-inflammatory prostaglandin (vasoconstrictor), $PGF_{2\alpha}$ [32]. Modulation of the biosynthesis by copper complexes is an attractive mechanism for the action of copper [32].

(c). Induction of Superoxide Dismutase and Dismutase-Mimic Activity

Superoxide dismutase is known to have anti-inflammatory and arthritic activity [32]. The human superoxide dismutase contains copper at the site and is required for its dismutase activity [32]. This enzyme [32] disproportionate the superoxide anion that initiates inflammation.

(d). Stabilization of Lysosomal Membranes

Copper is reported to decrease the permeability of human synovial lysosomes, thus decreasing the release of free lysosomal enzymes [32]. Lysosomal enzymes are found in synovial fluid and are destructive towards cartilage [32].

(e). Modulation of the Activity of Histamine

Modulation of the physiological effects of histamine may also be an important biochemical role for copper complexes. It is found that copper-histamine complexes are the active form of histamine [22].

Some reports reveal that the possibility of inhibiting both fibroti response and inflammatory response by copper chelation is due to the suppression of transforming growth factor beta and TNF-α production [4].

1.3.4 Computer Based Approach

Most of the serum copper is non-reversibly bound to ceruloplasmin, the fraction of copper, which will be concerned with a localised deficiency, is the labile component comprising the albumin and low molecular weight (l.m.w) bound copper and the free metal ion [34]. The l.m.w fraction is thought to be important in the transport of metal ions across cell membranes and between biological sites [34]. However, their role in biological systems is not easy to investigate as the concentration of these complexes is generally below the analytical means of detection [34].

A computer simulation of the equilibrium reactions between transition metal ions and low molecular weight ligands was considered the only reliable way to determine which of the thousands of possible complexes would be important under biological conditions [34]. A blood plasma model developed by May *et al* (May, Linder, and Williams, 1997) has been successfully used to account for several processes in drug therapy [34]. Computer simulation in this regard is the calculation of the equilibrium concentrations of the individual species formed in the solution of metal ions and ligands [34]. The model requires the thermodynamic formation constants for all the complexes present in the mixture and the overall concentrations of components [34].

The computer program called ECCLES (Evaluation of Constituent Concentrations) was developed to permit the simulation of large and comprehensive systems [35]. Concentration scans are done in simulation data to ensure that the imposed free concentrations of the metals do not influence their distribution among low molecular

weight ligands [35]. In the free metal concentration range that was scanned, the extent of complexation of low weight ligands is far greater than total concentration of metal ligand complexes [35]. This is because of the very low total concentration of the transition metal, the weak bonding abilities of calcium(II) and magnesium(II) and the decrease in metal ion concentration due to protein binding [35].

Computer modelling using ECCLES has provided evidence in support of the hypothesis that the administration of l.m.w copper complexes would be beneficial in the treatment of RA [35]. The use of chelating drugs to displace the labile albumin in favour of the tissue is the most convenient way of utilizing endogenous copper reserves [35]. For this to occur it requires a drug, which is able to complete effectively with the protein for the metal ion and that the predominant metal complex formed in plasma should readily diffuse into the affected synovial tissue [35].

The extent to which administered therapeuticals may be able to fulfil these conditions can be judged by simulating their effects in plasma using ECCLES [35]. Plasma Mobilising Index (P.M.I) is a function used to ascertain whether the agent is sufficiently powerful and copper specific. Drugs that successfully bind copper ion in *vivo* in the presence of competing endogenous ligands produce large P.M.I values, which for copper are calculated as follows [35].

$$\text{(P.M.I)} = \frac{\text{Total low molecular weight (l.m.w) concentration in plasma in presence of the drug}}{\text{Total l.m.w Cu(II) concentration in normal plasma}}$$

Several investigations were carried out by researchers based upon the above information to further the use of copper complexes in alleviation of inflammation and or RA.

1.3.5 Ligand design

The design of a therapeutic generally requires knowledge of the difference between the health and disease state at a molecular level [36]. The most straightforward way of administering the copper is by injection, unfortunately, this is associated with several undesirable side effects [36]. Two general routes, as illustrated by scheme below [36] may achieve the increase in the local concentration of copper complexes.

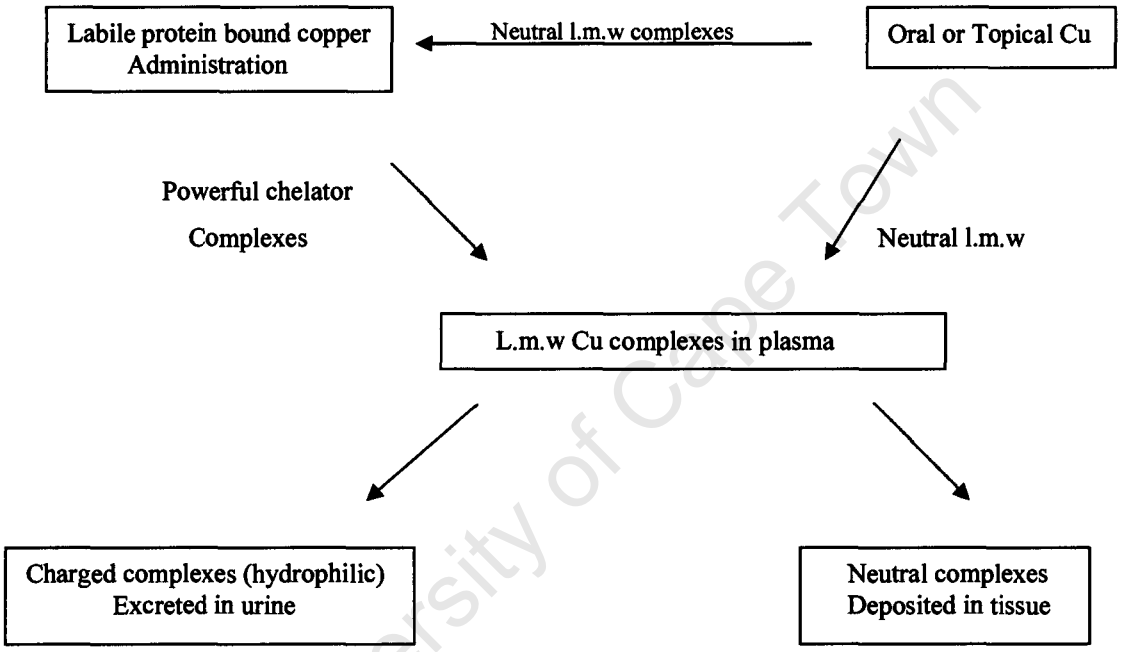

Figure 1.4: Routes for increasing the concentration of L.m.w copper complexes in Blood plasma [6].

Endogenous rather than exogenous sources seem appropriate for short term therapy [12].

There are three ways of achieving this aim:

1. By equilibrium competition for the labile protein-bound copper.
2. By decreasing the affinity of serum albumin for copper by allosteric effects.
3. By extracting copper from inert metalloproteins.

1.3.6 Ligand requirements

It has been shown that copper complexes are able to alleviate the inflammation associated with RA [37]. In order to achieve successful metal ion administration and subsequent mobilization in the body fluids, several general requirements have to be fulfilled [37]. The most important requirements of a ligand which will complex copper and increase its bioavailability and at the same time not disrupt the homeostasis of other endogenous metal ions are listed below [6];

1. The ligand must be a strong chelator in order to form thermodynamically stable complexes with the metal ion at physiological conditions of temperature and pH, thus minimizing loss to competing serum proteins [38].

2. The complex should also be primarily a nitrogen donor ligand so that the selectivity for the soft Cu(II) is increased over the harder Zn(II) and Ca(II) [38].

3. The complex must be formally uncharged and hence lipophilic to enable transport across cell membranes and prevent urinary excretion [38].

4. If the complex is to be administered orally, an addition requirement of stability at the low pH's encountered in stomach fluid must also be satisfied [38].

5. For dermal absorption the complex cannot be too lipophilic otherwise it will become trapped in the dermis.

1.3.7 Choice of ligands

Potential ligands must possess several thermodynamically desirable characteristics, in order to be able to meet the above requirements for metal ion mobilization [35]. Enhanced stability is not the only criterion for successful mobilization, but selectivity as well as other physical attributes of the complex plays an important role [35]. Ligands that have predominantly nitrogenous donor groups confer a high degree of selectivity towards Cu(II) upon such chelating agents [35]. Other cations, such as Ca(II) and Zn(II) can drastically interfere with ligands designed to bind Cu(II) in *vivo*, particularly if predominantly oxygen donor groups are present [35].

The design of the copper-chelating agent for the alleviation of inflammation associated with RA was based upon two important assumptions [36]. The therapeutic activity depends upon increasing the total labile Cu(II) concentration in some body compartments other than plasma and only neutral complexes will pass through a membrane separating these compartments whereas charged complex generally do not, in absence of a specific uptake pathway [36]. Ligands can be used to either mobilize copper endogenous or exogenous reserves, thus increasing the low molecular weight (l.m.w) fraction of copper complexes in the body fluids [36]. The major copper storage protein ceruloplasmin, which accounts for more than 90% of serum Cu, binds Cu irreversibly and would thus need to be denatured for its copper to be accessible [36].

Essentially, endogenous copper is only available from serum albumin (SA) which is the main copper transport protein in blood. Due to the fact that ceruloplasmin concentration increases in response to the development of RA, hence its concentration in RA sufferer increases [36]. Exogenous copper administration seems to be the only realistic means of increasing the body pool of labile uncharged low molecular weight (l.m.w) Cu(II) complexes [36].

Very strong or kinetically inert complexes which persist from the intestine through plasma to the tissue have been proposed [36]. This idea, is, however not effective since such complexes would be unlikely to yield Cu(II) ions to the biological mechanisms, that requires Cu(II) [36]. Alternatively, weakly bonded complexes

which would release the metal ions to proteins and amino acids in plasma can be chosen [36]. Thus the design of the ligand in this instance should be focusing upon its role in enhancing Cu(II) absorption from the intestines [36].

A third alternative is to design a ligand which will not only increase absorption of exogenous copper, but also take advantage of the large pool of endogenous copper bound to serum albumin [36]. The difficulty in predicting the absorption of a chemical from simple diffusion theory is due to the multilayered structure of mammalian skin, with regions varying in their capacity to solubilise hydrophilic substances [37]. Previous research gave rise to the generalization that the stratum corneum is the main barrier to penetration of all but the most lipophilic substances. Substances with high lipophilicity readily penetrate the lipid environment of the stratum corneum, but penetrate deeper with difficulty due to poor partitioning in the more complex aqueous matrix of the epidermal and sub-epidermal tissue [37]. Hence, in this category ligands would have to be powerful enough to compete with serum albumin but not so powerful that they promote copper excretion [36].

1.3.8 Complexation and chelate effect

There are desirable features required for a ligand for RA therapy which exploits Cu(II) bound to serum albumin [36]. This can be made possible by designing a multidentate ligand with the structural characteristics that make it effective to mobilize Cu(II) in *vivo* [36]. Metal ion mobilizing agents are essentially organic molecules or inorganic ions which can form complexes with the metal ion of interest, thereby keeping it in solution [39].

Various concepts involved in metal ion complexation should be discussed prior to choosing a particular series of complexing agents for their potential Cu(II) mobilizing ability, as suggested for the treatment of RA [39]. In the simplest case, when metal ions are dissolved in aqueous solution they are essentially already complexes since they do not exist as discrete entities, but are present in the form of aqua ions [39].

Complexation can occur if the ligands are bidentate in which chelate rings are formed. Enhanced stability is associated with these chelate rings compared to that of similar complexes involving only monodentate biding [38]. This is known as chelate effect, first defined by Schwarznbach and is one of the oldest phenomena in chemistry [38]. The chelate effect defines those ligands containing two or more donor groups in such an arrangement that they are able to form five or six-membered rings on coordination to the metal ion yield complexes with substantially larger formation constants than those of the analogous complexes of corresponding monodentate ligands [38].

The chelate effect is observed in Cu(II) complexes of ethylenediamine, $[Cu(en)_2]^{2+}$ which is about 10^7 times more stable than $[Cu(NH_3)_4]$, ignoring for the moment the dependence of the magnitude of the chelate effect on the chosen standard state [39]. Hence, the tetradentate triethylenetetramine Cu(II) complex $[Cu(trien)]^{2+}$, consisting of three contiguous or fused 5-membared rings, is a further 10^6 times more stable than $[Cu(en)_2]^{2+}$ [39]. Cu(II) complexes of ligands which give rise to a 5,6,5 membered chelate system are generally more stable than their 5,5,5 chelate analogues. This is due to steric constrains of the three contiguous, small ring in the later [40]. However, in literature, it has been reported that the 5,5,5 chelate complex is more stable than the 5,6,5 complex [40]. Increasing the number of chelate rings also enhances the stability [38]. Entropy increase associated with formation of chelate complexes is the simplest explanation for the increase stability [41].

It is a well-known fact of coordination chemistry that an increase in the size of the chelate ring above 5 usually leads to a drop in complex stability [38]. This observation, originally modeled in terms of entropy effects associated with the increase in the size of the chelate ring, is almost entirely due to favourable enthalpy contributions as seen in the thermodynamics of complex formation of ethylenediamine and propylenediamine complexes or of trimethylenediaminetetra acetic acid and ethylenediaminetetra acetic acid [40].

Several ligands have been investigated in our laboratory with copper(II) in trying to fulfil the above mentioned requirements. Sulphur could be considered an alternate donor atom in the ligand system as it is preferred by the softer Cu(I) ion. However, thiol groups bring about reductive chelation of Cu(I) and are known to be toxic [23].

Because of this toxicity, ligands containing amine, imidazole and pyridine have been preferred. Such ligands can coordinate to a metal ion via four nitrogen atoms upon loss of amide protons giving rise to three chelate rings [23]. Although the unsaturated nitrogen donor pyridine is a stronger base than any of the saturated nitrogen in the gaseous phase, it is a weaker base than the saturated nitrogen donors in aqueous solution [23]. Thus, the order of basicity of nitrogen donors in an aqueous solution can be stated as follows; amino > imidazole > pyridine [23]. The unsaturated nitrogen donor is sp^2 hybridized, which leads to greater s character in the orbitals used for bonding to the metal ion and hence more covalent bonding [23]. Thus ligands where such hetero-aromatic donors are present can exert very high ligand field strength, even though their proton basicity may be significantly less than that of the sp^3-hybridised saturated nitrogen donors [23]. The low proton basicity of the unsaturated nitrogen can be of considerable use in designing ligands, since what ultimately counts in many situations is not the formation constant of the metal ion with the ligand alone but also the relative difficulty of removing protons from the donor groups of the ligand so as to permit complex formation [23].

Since the study intends to archieve neutral Cu(II) complex, the ligand has to contain two anionic groups or dissociable protons [23]. The 3,6,9,12-tetra-azatetradecanedioic acid (ttda) ligand was investigated for the elevation of RA [23]. However from the animal tests this ligand proved to be too powerful a chelator of copper, such that it was rapidly excreted, unchanged in urine [23]. Even though such a complex was formally neutral, being dicarboxylic acids, it was still hydrophilic and hence cleared from the body via the kidneys [23].

In order to further improve lipophilicity, the pentacyclo-undecane derived ligand 3,5-diaminodiamido-4-oxahexacyclo dodecane (cageL) was designed [30]. This ligand has the amino/amido coordinating structure attached to a pentacyclo undecane derivative. Incorporating a rigid cage structure into bioactive compounds has its advantages;

- The cage moiety is able to cross various membranes quite efficiently due to their large lipophilic nature.
- The rigidity of the cage should increase the stability of the metal by forcing the ligand into an ideal conformation for complexation [30].

Research conducted by Odisitse and Jackson proved that cageL forms stable, lipophilic, Cu(II) complexes capable of surviving in *vivo* as demonstrated by speciation calculations using a blood-plasma model and animal experiments [30]. Further investigations indicated that the *N,N*-bis[2(2-pyridyl)-methyl]pyridine-2,6-dicarboxamide (PrDPr) is quite selective towards Cu(II) over zinc(II) and calcium(II) due to the ease with which copper(II) deprotonates the amide nitrogen groups [30]. The rigidity of the pyridyl moiety and pyridyl nitrogen that acts as an anchor enhanced the ionization of the amide protons in the presence of the metal ion [30].

The Bis-(3-aminoethy-2-aminomethylpyridine)-oxahexacyclo dodecane (PCUL), under study has a structure similar to that of PrDPr, but the central pyridine in PrDPr is replaced by the adamentane cage moiety. PCUL has pyridyl groups which are found in most of the non-steroidal anti-inflammatory drugs (NSAIDs) and Cu(II)-NSAIDs complexes are reported to be more effective than their parent compounds [30]. It is interesting to note that the stability of the Cu(II)-cageL complexes is greater than its non-cage analogue. It was anticipated that this would be the case because in cageL, the ligand is pre-formed in the correct conformation for metal-ion coordination [30]. Since the carboxylic groups reduced basicity in the pyridyl nitrogen due to its electron with drawing properties, they were replaced by ethyl groups in PCUL.

Adamantanes are generally of biological and medicinal interest because they possess a variety of therapeutic activities such as anti-inflammatory, anti-viral, antifungal and antimicrobial-anticancer activities [42, 43]. Adamentanes inhibit cycloxygenase isoenzymes (COX-1 and COX-2), preventing inflammation and pain [43]. Previous studies show that the presence of adamantine moiety in thiazolyl-*N*-substituted amides improved anti-inflammatory properties of this ligand, in comparison to the non-adamantane thiazolyl-*N*-substituted amide.

The coordination chemistry of 2-(aminomethyl)-pyridine (pyN) which forms part of the PCUL structure was explored by potentiometric analysis. The stability constants determined form pyN analysis was used to establish an estimation of PCUL stability constants. The glycine system in this study was used to validate the proposed experimental procedure.

1.3.9 Aims and objectives of the study

The search presented above indicates that increasing the local concentration of l.m.w copper complexes by means of an externaly ligand could be effective in relieving the symptoms of rheumatoid arthritis by stimulating anti-inflammatory activity [44]. The ligand designed to achieve this is a pseudo-mimic of HSA (Figure 1.5) that could possibly compete for and mobilize endogenous reversibly bound serum albumin Cu(II) [44]. The same ligand would be used for exogenous administration of Cu(II) orally or tropically as membrane-penetrable, low molecular weight complexes [44]. The broad objectives of this research were to develop and investigate such a ligand, using the following methodology:

- Design, synthesis and characterization of PCUL.
- Measure the formation constants of this ligand with Cu(II), Zn(II) and Ni(II) in aqueous solution using glass electrode potentiometry.
- Use a computer model of blood plasma, together with measured formation constants, to evaluate the plasma mobilizing ability of the ligand.
- Determine the structure of the Cu(II) complexes with the PCUL ligand in solution using UV/VIS spectroscopy.
- Determine the sequence of protonation and where exactly the metal ion would complex with the ligand.

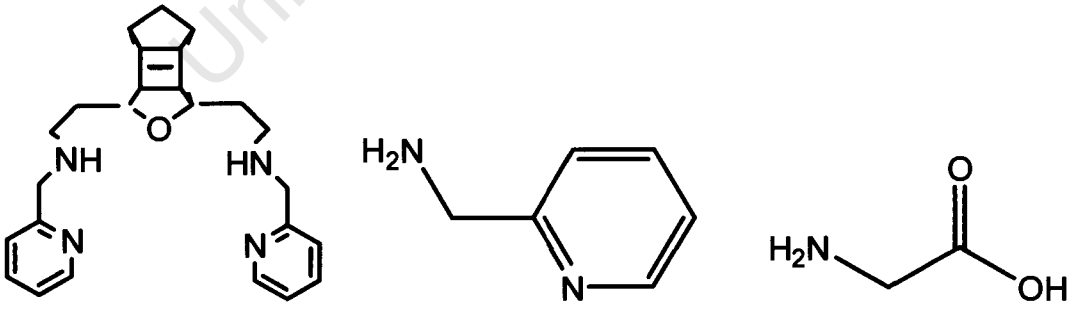

PCUL 2-(aminomethyl)-pyridine glycine

Figure 1.5: Structures of Bis-(3-aminoethy-2-aminomethylpyridine)-oxahexacyclo dodecane (PCUL), 2-(aminomethyl)-pyridine and glycine.

REFERENCES

1. http://www.medicinenet.com/rheumatoid_arthritis/page4.htm#5howisra
2. www.eorthopod.com/.../area/1
3. C.M.Weyand. *Rheumatology*.2000.**39**.3-8.
4. A.Omoto, Y.Kawahito, I. Prudovxky, Y.Tubouchi, M.Kimura, H.Ishino, M.Wada, M.Yoshida, M.Kohno, R. Yoshimura, T. Yoshikawa and H. Sano.*Copper chelation with tetrathiomolybdate suppresses adjuvant-induced arthritis and inflammation-associated cachexia in rats*, 2005, 7,1174-1182 BioMed Central Ltd, Japan.
5. J.R.Cerhan, K.G.Saag, L.A.Merlino, T.R.Mikuls and L.A.Criswell.American *J. Epidemiology*. 2003, **157**,345-354.
6. S.Odisitse. MSc *Dissertation,* 2003, UCT, Cape Town.
7. V.Pelmenschikov and P.E.M.Siegbahn, *J.Inorg.Chem,* 2005, **44**, 3311-3320.
8. G.E. Jackson and M. Kelly, *Inorg. Chim. Acta*, 1988, **152**, 251-217
9. J.N. Zvimba. PhD Dissertation 2005, UCT, Cape Town. J.M.H. Moll, *Arthritis and Rheumatism*, 1983, Churchill Livingstone, Edinburg
10. S.M.Krane, Arthritis and Allied conditions, 1989, 11th Ed, D.J. McCarthy (ed), Lea and Febiger, Philadelphia London.
11. E.D. Harris Jr, *Texbook of Rheumatology*, 1989, 3rd Ed, W.N. Kelly, E.D. Harris, S. Ruddy and C. Sludge (eds), W.B. Saunders. Company, Philadelphia London.
12. G.E. Jackson, L. Mkhonta-Gama, A. Voye, M. Kelly, *J.Inorg.Chem,* 1999, **79**.147- 152.
13. L.S. Goodman, A. Gilman, *The Pharmacological Basis of Therapeutics*, 5th Ed, pg 1407, McMillan, New York
14. L.C. Corman, C.L. Bell, N.L. Edwards, C.E. Harman, *Rheumatology for the House Officer*, 1990, **289**, 294.
15. S. Kuwano, S. Tsuji, *J. Gastroenterol. Hepatol*, 2000, **15**, D1.
16. M.A. Quinn, P.G. Gonaghan, P.E. Mercy, *Rheumatology*, 2001, **40**, 1211.
17. D.L Conn, *Arthritis Care Res.*, 2001, **45**, 462.
18. I.L Bonta, M.J. Parnham, J.E. Vincent, P.C. Bragt, *Prog. Med. Chem*, 1980, **17**, 186.
19. F.D. Hart, *Drug Treatment and Rheumatic Diseases*, 1978, 3rd Ed, MTP Press, England.
20. J.G. Hardin, G.L. Longernecker, *Handbook of Drug Therapy in Rheumatic Diseases*, 1992, 1st Ed, Little, Brown and Company, London.
21. M.M. Jones, P.M. May, *Inorg.Chim.Acta*, 1987, **138**, 66-73.
22. J.R.J. Sorenson, *Chem. In Britain*, 1984, **19**, 1110.

23. M.C. Linder and M. Hazegh-Azam, *Am. J. Clin. Nutr*, 1996, **63**, 7975, 8115.
24. R.C. Weast (ed), *CRC Handbook of chemistry and Physics*, 1982, 63rd Ed, CRC Pres.
25. C.H. Cashin, E.J. Lewis and (late) T. Buraen, *British J. Rheumatol*, 1985, **24**, 137-196.
26. D.W. Cox, *British Med. Bull*, 1999, **55**, 544.
27. T.P.A. Kruck and B. Sarkar, *J. Inorg. Chem*, 1975, **14**, 2383-2388.
28. P. Gizzi, B. Henry, P. Rubini, S. Giroux, E. Wenger, *J. Inorg. Biochem*, 2005, **99**, 1182-1192.
29. J.N. Zvimba and G.E. Jackson, *Polyhedron*, 2007, **26**, 2395-2404.
30. S. Odisitse and G.E. Jackson, *Polyhedron*, 2008, **27**, 453-464.
31. W. Sun, S. Tsujii, E.S. Gunawan, H. Sawaoka, N. Kawai, H. Iijima, A. Kimura, Y. Kakiuchi, M. Yasumaru, Y. Sasaki, S. Kawano, M. Hori, J. *Gastroenterology and Hpatology*, 2000, **15**, 752-761.
32. J.R.J Sorenson, *Prog. Med.Chem*, 1989, **26**, 437.
33. E. Edward-Bitter and H.K. Kleinman, *Advances in Molecular and Cell Biology*, 1993, **6**, 36, Jai Press Inc, Connecticut.
34. P.M. May and D.R. Williams, *J. Chem. Soc. Dalton*, 1978, 588.
35. G.E Jackson and P.M. Williams, *F.E.B.S. Letters*, **90**, 1978.
36. G.E. Jackson, P.M May, D.R. Williams, *J. Inorg. Nucl. Chem*, 1977, **40**, 1227.
37. J.N Zvimba and G.E. Jackson, *J. Inorg. Biochem*, 2007, **101**, 1120-1128.
38. G. Schwarznbach, *Helv. Chim. Acta*, 1952, **152**, 215.
39. A. E Martell and R.M. Smith, *Critical Stability Constants*, 1982, **6**, Plenum Press, New York.
40. G.E Jackson, P.W. May, A. Voye`, *Communication*, 1991, **10**, 8, 883.
41. C.G. Spike, R.W. Parry, *J. Am. Chem. Soc*, 1953, **75**, 2726.
42. www.journals, iucr.org, 2008.
43. O. Kouatly, A. Geronikaki, C. Kamoutsis, D. Hadjiparlou-Litina, P. Eleftherious, *Eu. J. Med. Chem*, 2008, 1-7.
44. S.K. Bai, A.E. Martell, *J. Am. Chem.* Soc, 1969, **91**, 126, 4412.

CHAPTER 2

GLASS ELECTRODE POTENTIOMETRY

2. GLASS ELECTRODE POTENTIOMETRY

2.1. Introduction

The aim of this experimental section was to determine the stability and type of complexes formed in solution under physiological conditions between the metal ions, copper(II), nickel(II), zinc(II) and the series of ligands previously described [1]. Several experimental methods can be utilized to investigate the chemical species that can potentially form in solution, for example, ultra filtration, calorimetry, solvent extraction, potentiometry, reaction kinetics, polarography as well as nuclear magnetic resonance, Raman, UV/VIS and infrared spectroscopy [2]. Potentiometry is one of the oldest analytical methods still in wide use because of its convenience and success for metal complex equilibrium measurements and hence the method of choice in this studies [3].

Whole body investigations must be performed in a nutrient medium that supports the life of the organism. However, it is also necessary for a solution chemist to choose working medium conditions for the chemical model [4]. In order to determine stability constants at constant ionic strength, several salts are used for the test solution and such salts include; potassium nitrate (KNO_3), sodium perchlorate ($NaClO_4$), sodium chloride (NaCl) and potassium chloride (KCl) [5]. However, in our experiments 0.15mol/dm^3 NaCl was used for the test solution. The choice of this salt was based on the fact that human blood is isotonic with 0.15mol/dm^3 NaCl [5]. The concept of ionic strength was introduced in 1921 by Lewis and Randall who stated that, 'in dilute solutions' the activity coefficient of a given strong electrolyte is the same in all solutions of the same ionic strength [3]. Since then many workers attempted to keep activity coefficient constant by using solution of constant ionic strength [3].

The correct temperature for work applicable to biological systems is obviously 37°C [1]. However they present some practical difficulties such as evaporation from the test solution and condensation on the roof of the reaction vessel [1]. As most potentiometric determinations are carried out at 25°C, it was decided to perform all experiments at this temperature, thus avoiding the problem of having to completely

insulate the titration setup and being able to directly compare the results with those reported in literature [1].

The enhancement in the accuracy and predictability of the values arising from glass electrode potentiometry requires full mastery of the principles behind electrode calibration [3]. Both glass and the reference electrodes require filling solutions, which over the decades has evolved to be potassium chloride (KCl) as the usual first choice because it seems to satisfy most of the criteria, especially that of the diffusion rates of anion and cation being equal [6]. There is a reference electrode that embodies an internal electrode such as silver/silver chloride cell (silver/silver chloride being inside the glass membrane and provides a constant potential) and an electrolytic solution contained in a glass/polymer salt bridge, which surrounds the internal electrodes and makes electrical contact with the test solution through the liquid junction. The body of the glass electrode is a nonconducting glass tube sealed to a bulb made of special conductive glass which is a pH sensing membrane [6]. The body is filled with a buffered electrolyte of fixed pH value and ionic concentration [6]. This design ensures that the constant potentials are developed on the inner surface of glass membrane and on the internal reference element [6].

The applicability of glass electrode potentiometry in the determination of stability constants is only possible when the proton displacement reaction can be monitored [4]. The monitoring of this reaction is also possible only when the interacting ligand is a weak Bronsted-Lowry acid or base and the displacement reaction is in equilibrium [4].

This chapter focuses on the general theory of potentiometry as a measurement method applied to complex equilibria, together with presentation and discussion of experimental results.

2.2 Theory

2.2.1 The Stability Constant

For simplicity, the term stability constant or formation constant will in this study refer to the values obtained for the overall formation constant of a metal-ligand species [7]. The stability constants provide a quantitative measure of the extent to which a metal will complex with a particular group or ligand [7]. The protonation constant is referred to as the chemical association of a ligand with protons [7].

The most accurate and reliable method for the determination of stability constants potentiometrically is to titrate one solution (acid or alkali) with another (of constant total metal and total ligand with 0.1mol/dm^3 alkali or 0.01mol/dm^3 acid), with the potential being determined after each addition of the titrant [8]. The study of stability constants essentially involves competition between two metal ions of which one may be H^+ [8]. The base titration of aqueous metal-ligand equilibria involves competition between the water molecules, the ligand molecules and hydrogen ions for the metal [8]. The hydronium ions and metal ions are also attracted by the donor ligand [8]. Several pre-complexation processes may be involved before the final complex species is formed and these would include loss of a coordination water molecule from the metal, followed by coordination of the ligand molecule accompanied by loss of the proton [8]. The overall stability constant is actually the product of stepwise stability constants [8]. However, the constants of the predominant chemical product species are selected to constitute the model that best describes the chemical system [8].

2.2.2 Factors that affect complex stability

The stability constants for a number of metal complexes had been reported by 1953 and it was feasible to ask the following question [9]:

- For a given ligand, how do the stability constants vary with changes in the central metal ion?
- How does the stability vary when the nature of the coordinating ligand, L, is changed?

Irving and Williams showed that for divalent ions of the first transition series the stability always follows the order: Mn <Fe < Co <Ni <Cu <Zn after reviewing all the data [9]. For each cation the stability increased when donor oxygen was replaced by donor nitrogen in either monodentate or bidentate ligands [9]. The stability increased with increasing number of chelate rings, but decreased with increasing ring size [9]. The known coordination sphere of a metal can also assist in postulating the kind of species that a ligand of a particular denticity will likely form with metal, which will also determine the extent to which the complex will be equated [9]. The concentration ratios of the reactants also influence the species that may predominate at equilibrium [7]. Polynuclear species may result from a high metal to ligand ratio [9].

2.2.3 The Potentiometric Cell

For the quantitative evaluation of data, the Nernst equation is used between the experimental electromotive force **(E)** value and the equilibrium hydrogen ion concentration **[H^+]** delivered by a glass electrode [10].

Consider an electrochemical cell in which a test solution surrounding a glass electrode is in electrical contact with a reference electrode through a salt bridge can be represented as follows [11];

First reference Half-cell (In glass electrode)		tests solution		second reference half-cell (External)
	g		**l**	

The boundaries, **g** and **l**, respectively, indicate the glass membrane and the liquid junction at the inter-face between the salt bridge and the test solution. The liquid junction potential may be affected by [10];

- pH and ionic mobility
- ionic strength
- colloids and suspension

- non aqueous-aqueous boundaries
- the salt bridge solution
- temperature and pressure

There are four contributions to the measurable potential difference between the two reference electrodes. Two arise from the electrode themselves; they will have opposite signs and will usually be of comparable magnitudes. Their contribution most importantly will be independent of the composition of the test solution and so may be represented as a fixed combination potential, $\mathbf{E_r}$.

On the other hand, the potential differences generated across the boundaries of **g** and **l** will depend on the activities of all the chemical species on either side of them. If these boundary potentials are represented by $\mathbf{E_g}$ and $\mathbf{E_l}$, the measured emf of the cell is given by the following equation;

$$\mathbf{E_{cell} = E_r + E_l + E_g} \qquad 2.1$$

In the case of the liquid junction, considerable changes in the composition of the test solution are required to alter $\mathbf{E_l}$ significantly, so, for the time being, this will be considered as a constant. Glass electrodes, in general, are found experimentally to exhibit a Nernstian response over a wide range of concentration. Equation 2.1 can be stated as follows;

$$\mathbf{E_{cell} = E_r + E_l + E_g^o - \frac{RT}{F} \ln\{H^+\}} \qquad 2.2$$

Where $\mathbf{E^o_g}$ is the standard glass-electrode potential at unit activity of hydrogen ions, **R** is the universal gas constant, **T** is the absolute temperature, **F** is the Faraday constant and $\{\mathbf{H^+}\}$ represents the hydrogen ion activity. The free hydrogen-ion activity, $\{\mathbf{H^+}\}$ can be expressed in terms of concentration as long as the ionic strength of the test solution remains constant. Hence, equation 2.3 is obtained by putting $\mathbf{s = 2.030RT/F}$ and collecting together all the constants (including the hydrogen-ion activity coefficient and factors arising from it) as $\mathbf{E_{const}}$ [10]:

$$E_{cell} = E_{const} + s \log[H^+] \quad 2.3$$

The activity of the hydrogen ion is defined with respect to concentration and the two are related by the following equation [10];

$$a_i = \gamma_i c_i \quad 2.4$$

where, γ_i is the activity coefficient of ion "i" and c_i is the concentration of the ionic species "i". The departure of activity from concentration for charged species is a function of the ionic strength **i** of the solution, given by the following equation [11].

$$i = 0.5 \sum c_i z_i^2 \quad 2.5$$

where c_i is the concentration of ionic species "i" and z_i is the charge on that ion [2].

The stability constants are also affected by temperature as represented by the Van't Hoff equation [3];

$$d\ln K/dt = \Delta H^o / RT^2 \quad 2.6$$

where ΔH^o is the standard enthalpy change of reaction and is related to Gibbs free energy ΔG^o and ΔS^o change of reaction, **T** is the absolute temperature in Kelvin and **R** is the natural gas constant in JK^{-1} mol^{-1} [3].

2.2.4 Calibration of Glass Electrode System

Before the electrode was calibrated, the glass electrode was stored in 3mol/dm^3 potassium chloride (KCl) solution which was stored in 25°C water bath. The glass electrode was repeatedly rinsed before each titration with boil-out distilled water and blotted dry. The electrode was not wiped with soft tissue paper, this was done in order to minimise the build up of static electricity [11]. The electrode was calibrated at 25°C and an ionic strength of 0.15 mol/dm^3 NaCl.

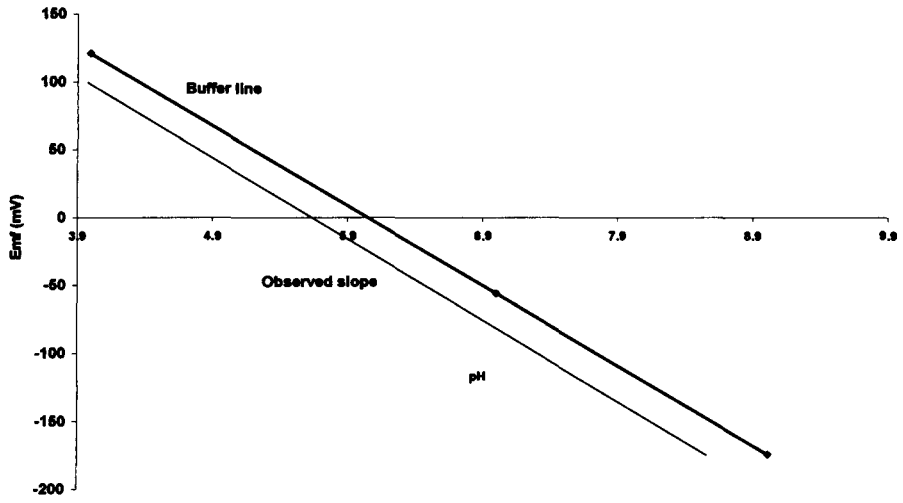

Figure 2.1: Electromotive force (mV) versus pH at 25°C.

The Nernstian slope was determined using commercially available reference buffer solutions of pH values 3.996, 7.001 and 9.012. Figure 2.1 shows a plot of electromotive force (emf) of each pH solution against pH. This graph gave a buffer line which varied between 58.83 and 59.03 which were within the acceptable working range of 58.60 to 59.16 at 25°C.

The final calibration of the electrode was achieved by performing strong-acid strong-base titrations in order to calculate the value of the response intercept, E^{o}, the value of 13.748 for the dissociation of water (pKw) was obtained from literature and was held constant during the optimization procedure [12]. The values of the intercept, E^{o} varied between 367.8mV and 363.499mV. The titration data obtained from strong-acid (HCl) strong-base (NaOH) titrations were introduced into ESTA library programs in order to obtain more precise slope and E^{o} values [12]. Equation 2.2 gives the activity of H^{+}, since $\{H^{+}\} = \gamma[H^{+}]$ equation 2.2 then becomes;

$$E_{cell} = E_r + E_l + E_g^{o} + \frac{RT}{F} \ln\gamma[H^{+}]$$

The intercept of the obtained emf of the cell from the NaOH and HCl potentiometric titration will be slightly lower than the intercept of the buffer line as shown in Figure 2.1.

From the NaOH-HCl potentiometric titrations the Gran plots were made to check carbonate contamination which is shown by the curvature in the region of equivalence point [12]. The two Gran functions used are given as;

$$\text{Gran function} = (V_i) \times 10^{-pH} \quad \text{.....before the end point} \qquad 2.8$$

$$= (V_o + Vi) \times 10^{pH} \quad \text{..... after the end point} \qquad 2.9$$

where V_o is the initial reaction vessel volume and V_i is the volume of added solution at the i^{th} point of the titration. Figure 2.2 shows how carbonate contamination may be viewed using the Gran functions from equations; 2.8 and 2.9.

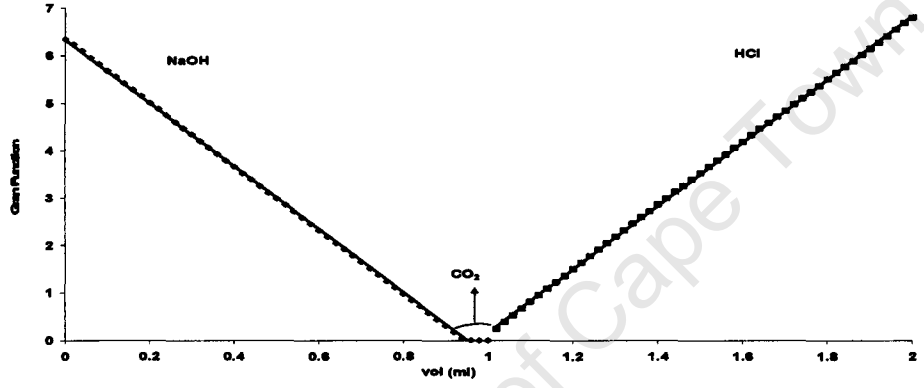

Figure 2.2: Gran Function versus volume of the titrant (ml).

The pH values used in the Gran functions at each titration point were calculated using the equation [12];

$$pH = -((E-E^{o})/s) \qquad 2.10$$

2.3. Data Analysis [13].

The major objective in ESTA is to provide a flexible tool for investigating phenomena associated with chemical interactions in solution and for their quantitative characteristics [13]. The collected data were used as input file into the ESTA file template in order to calculate the electrode parameters, protonation and formation constants [13]. The required parameters were calculated by making use of the task OBJE within the ESTA2A module of ESTA library computer speciation modelling programs [13]. The analysis was performed by fitting these constants to the titration

data, based upon minimization of the objective function, U_{obj}, with respect to emf [13]. The E^o, $[H^+]_{vessel}$, $[L]_{vessel}$ and $[M]_{vessel}$ have fixed values and therefore not refined. Hence the required logβ's were the only values refined. The results obtained were used to generate Z_H-Bar, Z_M-Bar and Q_M-Bar curves by making use of tasks Z-bar and Q-bar within the ESTA1 module of ESTA. The task SPEC also within the ESTA1 module calculates the species distribution taking part in an equilibrium system as a function of pH of all the $M_pL_qH_r$ species present in solution over the pH range of measurement [2].

The reproducibility and quality of the experimental data was always checked visually using the formation and deprotonation functions and repeat titrations were superimposable in every case.

2.3.1 Computational Data Analysis Theory [14].

After all the potentiometric data have been carefully collected in the laboratory, the stability constants which are the unknown parameters of interest are determined from the accurately measured known parameters. The known parameters may include volumes of reaction solution, temperature concentration of the solution and other parameters.

For a complex formation reaction occurring between a metal, **M** and a protonated ligand, **L**, forming a complex $\mathbf{M_pL_qH_r}$, the equilibrium process is given by the following expression,

$$\mathbf{pM + qL + rH \leftrightarrow M_pL_qH_r} \qquad 2.11$$

The formation constant for $\mathbf{M_pL_qH_r}$ is given by the following equation according to the law of mass action;

$$\mathbf{\beta_{pqr} = [M_pL_qH_r]/[M]_p^k[L]_q^k[H]_r^k} \qquad 2.12$$

and the concentration of each species $\mathbf{M_pL_qH_r}$ in the $\mathbf{k^{th}}$ point is given by

$$[M_pL_qH_r]_k = \beta_{pqr}[M]_k^p[L]_k^q[H]_k^r \quad 2.13$$

where β_{pqr} is the formation constant of the species under consideration, $[M]_k$, $[L]_k$, and $[H]_k$ are concentrations of the free metal, free ligand and hydrogen ion, while **p**, **q**, and **r** are stoichiometric coefficients for metal, ligand and proton respectively. **r** can be any negative number, when **r = -1**, the proton is either removed from a water molecule (which in principle, is the same as coordination of hydroxide ligand to the metal ion) or from the ligand molecule occurring only in the complex, like the peptide-NH.

The equilibrium conditions together with the mass balance conditions for the three components are given in the general case for the k^{th} point as follows;

$$T_{k,M} = [M]_k + \sum_{i=1}^{N} p\beta_{pqr}[M]_k^p[L]_k^q[H]_k^r \quad 2.14$$

$$T_{k,M} = [M]_k + \sum_{i=1}^{N} p\beta_{pqr}[M]_k^p[L]_k^q[H]_k^r \quad 2.15$$

$$T_{k,L} = [L]_k + \sum_{i=1}^{N} q\beta_{pqr}[M]_k^p[L]_k^q[H]_k^r \quad 2.16$$

$$T_{k,H} = [H]_k + \sum_{i=1}^{N} r\beta_{pqr}[M]_k^p[L]_k^q[H]_k^r \quad 2.17$$

where $T_{k,M}$, $T_{k,l}$ and $T_{k,H}$ are the analytical concentration of metal ion, ligand and hydrogen ion respectively. These mass balance equations are non-linear in the unknowns $[M]_k$, $[L]_k$ and β_{pqr} and the value $[H]_k$ is obtained from the potentiometric measurement. The complex $M_pL_qH_r$ may be considered to be formed by the reaction;

$$pM + qLH_n \leftrightarrow M_pL_qH_r + (qn-r)H \quad 2.18$$

The formation constant of this reaction denoted by $^*\beta_{pqr}$ can be transformed into β_{pqr} and vice versa with the aid of K_w, the autoprotolysis constant of water in experimental.

2.3.2 ESTA (Equilibrium Simulation for Titration Analysis) Program Library [15].

These programs were developed to provide a flexible, investigative tool for the quantitative characterization of chemical interactions in solution, especially those pertaining to the determination of formation constants. The program can take into account variations in ionic strength and the associated changes in activity coefficient. They also permit corrections of titration data affected by liquid-junction potentials and imperfect ion-selectivity of the electrode. The program library is used to calculate equilibrium distributions of chemical species, to analyse potentiometric titration data and to manipulate the titration data for a variety of other purposes.

The main calculation are done by two types of program modules, namely, simulation module **(ESTA1)** and optimization module **(ESTA2)** [2]. By setting up and solving the mass-balance equations, **ESTA1** can determine, on a point-by-point basis, single values for almost any titration parameter. On the other hand, **ESTA2** determine the best values based on a least square procedure over a whole system of titrations. The other program modules are error propagation modules **(ESTA3)** which performs a Monte Carlo error propagation analysis, the interative data preparation module **(ESTA8)** providing access to an extensive on-line help facility. The Gauss-Newton method is used to minimize the objective function, U_{obj}, in the ESTA program. This objective function is optimized by the task OBJE (optimization with respect to the observed emf) within the ESTA2 module. In contrast with the OBJT task, optimization is based on total concentration. Since the variations in total concentrations are smaller than the variation in emf, OBJT is more robust and faster than OBJE but less sensitive. Therefore in practice OBJT would often be used for initial optimization followed by OBJE for the final optimization.

Depending on the chemical systems being investigated, for instance, the binary and ternary systems, the formation function (Z-bar) and the deprotonation function (Q-bar) function are defined differently because the kinds of equilibria taking place in the different systems may vary depending on the number of the components that constitute each system. These functions are calculated by the tasks Z-bar and Q-bar within the ESTA 1 module for Z-bar function and Q-bar function respectively.

The task SPEC within ESTA1 module calculates the distribution of species taking part in an equilibrium system as a function of pH of the solution [16].

2.3.3 The Objective function (U_{obj}) [15].

The objective function to be minimized by the interactive refinement of the set of stability constants is given by;

$$U_{obj} = (N-n_p)^{-1} \Sigma n_e^{-1} \Sigma w_n (y_n^{obs} - y_n^{calc})^2 \qquad 2.19$$

where y_n^{obs} and y_n^{calc} may be either EMF_n or T_n

w_n is the weight applied at each point

N is the total number of experimental titration points and

N_p is the number of parameters to be optimized

A Gauss-Newton method is the most frequent approach used for minimizing U and this has been adopted in ESTA as the main means of optimization. The objective function assumes that the function is quadratic with respect to all the parameters; hence U_{obj} can be expressed as in the following equation;

$$U_{obj} = a + p^t b + (p^t H p)/2 \qquad 2.20$$

where **a** and **b** are Gauss-Newton quadratic parameter vectors, **p** is optimization parameter vector, p^t transpose of **p**.

The Hessian (H), is given by $H_{sr} = d^2U/dp_s dp_r$ 2.21

2.3.4 The Formation Function (Z-bar) and Deprotonation Function (Q-bar) [15].

Two important functions; the Z-bar and the Q-bar calculated from the titration data within the ESTA programs. They are defined differently depending on the presence or absence of a metal ion.

In the absence of a metal ion the protonation function is expressed as;

$$\mathbf{Z_H\text{-}bar = (T_H\text{-}H + OH) / T_L} \qquad 2.22$$

where $\mathbf{T_H}$ is the total hydrogen ion concentration, $\mathbf{T_L}$ is the total ligand concentration and $\mathbf{OH = K_w / [H]}$. Z_H may be plotted against pH and is the average number of hydrogen ions bound to the ligand at each pH.

The average number of ligands bound per metal ion at each concentration of the ligand is measured by the complex formation function, Z_M-bar and is given by the following equation;

$$\mathbf{Z_M\text{-}bar = (T_L - [L]) / T_M} \qquad 2.23$$

where, T_L, T_M, and L are the total ligand, total metal and free ligand respectively. The Z_M-bar function applies only to mononuclear binary complexes. A plot of Z_M-bar against the negative logarithm of free ligand concentration, defined as pL gives a pictorial representation of the equilibria taking place. The average number of protons released per metal ion, as a result of complexation is determined by the deprotonation function, Q_M-bar and is defined according to the equation;

$$\mathbf{Q_M = (T_H^* - T_H) / T_M} \qquad 2.24$$

where $\mathbf{T_H}$ and $\mathbf{T_M}$ are the total proton and metal concentrations respectively and $\mathbf{T_H^*}$ is the calculated total concentration of protons that would be necessary to give rise to the observed pH in the absence of the metal ions or rather if no complexation took place .

$$T_H^* = [H]-[OH] + \sum r\beta_{oqr}[L]^q[H]^r \quad 2.25$$

where **[OH] = Kw / [H]** and the summation is the overall protonated ligand species.

In binary systems, a formation function represents the number of protons that would be on the ligand in the absence of the metal ion, is defined by;

$$n_{bar} = (T_H^* - [H] + [OH]) / T_L \quad 2.26$$

The average number of dissociable protons in a complex would be given as in the following equation;

$$F = qn_{bar} - Q_{bar}p \quad 2.27$$

A set of theoretical titration data is generated by the selected and refined model. The agreement between the experimental plot and the theoretical plot is an indication of the validity of the proposed chemical model, a process termed pseudo-plotting.

2.3.5 Data Error Analysis [15].

In potentiometric titrations the determination of the protonation and stability constants requires minimal experimental errors. The optimization of stability constants may be affected by the magnitude of random and systematic errors inherent in the system. Hence a thorough examination of these errors has been done by studying a well known system for experimentally generated error, or by varying the reaction conditions for a particular system and observing its reproducibility. Random errors usually cancel each other out as the number of titration points increase as opposed to the systematic error.

2.3.5.1 Weighting

The neglect of weighting can undoubtedly, have very detrimental consequences [16]. As anyone who attempts to use an unweighted objective function based on residuals in emf soon discovers, manifestly bad results can be obtained because of the excessive influence of unbuffered regions in the data (for example, the points that occur near end-points, where small errors in titration volumes, etc.,) produce large errors in emf [16]. The purpose of weighting is to reduce, as much as possible, the adverse influences on optimized parameters that arise because errors in values held constant during the calculation tend to propagate differently at different points [16]. To obtain unbiased results, the data ought to be weighted so that those points likely to be distorted most by the experimental error are correspondingly reduced in their effects on the optimized values of parameters [16].

Basically, weighting takes into account the fact that some of the titration points will be more reliable than others and hence relatively greater importance should be placed on these on the optimization process [17]. Therefore large residual of an unreliable data point will not tend to be reduced in favour of increasing other smaller residuals less affected by such errors [17].

The weight of the $\mathbf{q}^{th}$ residual at the $\mathbf{n}^{th}$ titration point may be expressed as;

$$W_{nq} = [\Sigma \{(y_{nq}^{obs} - y_{nq}^{calc}) / \delta p\}^2 \sigma p^2]^{-1} \qquad 2.28$$

where y_{nq}^{obs} and y_{nq}^{calc} are observed and calculated variables of the $\mathbf{q}^{th}$ residual at the $\mathbf{n}^{th}$ point respectively [16]. $\sigma\mathbf{p}$ is the standard deviation in the parameter p to be optimized [16].

The goodness of fit between experimental and calculated data from the refined set of β_{pqr}'s is expressed by the Hamilton R-factor (R_f^H) [16].

$$R_f^H = [U / \Sigma ne^{-1} \Sigma w_{ni} (y_{ni}^{obs})^2]^{0.5} \qquad 2.29$$

The **R-factor** can be compared to **R-lim** which is an indication of the best possible fit that can be obtained under the conditions that have been imposed by the set of experimental errors [16]. The **R-lim** is calculated from;

$$R_{lim}^{H} = [N / \Sigma ne^{-1} \Sigma w_{nq} (y_{nq}^{obs})^2]^{0.5} \qquad 2.30$$

The R_{lim}^{H} is the best possible **R** value based on the random error in the analytical data and the number of variables [16]. Thus the closer R_f^{H} gets to R_{lim}^{H} the better the agreement between the theoretical model and the experimental data [16]. However, since the theory is strictly valid for random errors only, which is often not the case in actual titrations, the **R-factor** can become less than the R_{lim}^{H} and in such a case the model is within the maximum allowed experimental error [16].

The computational procedure employed for the determination of protonation and stability constants by using ESTA library programs is shown by Figure 2.3.

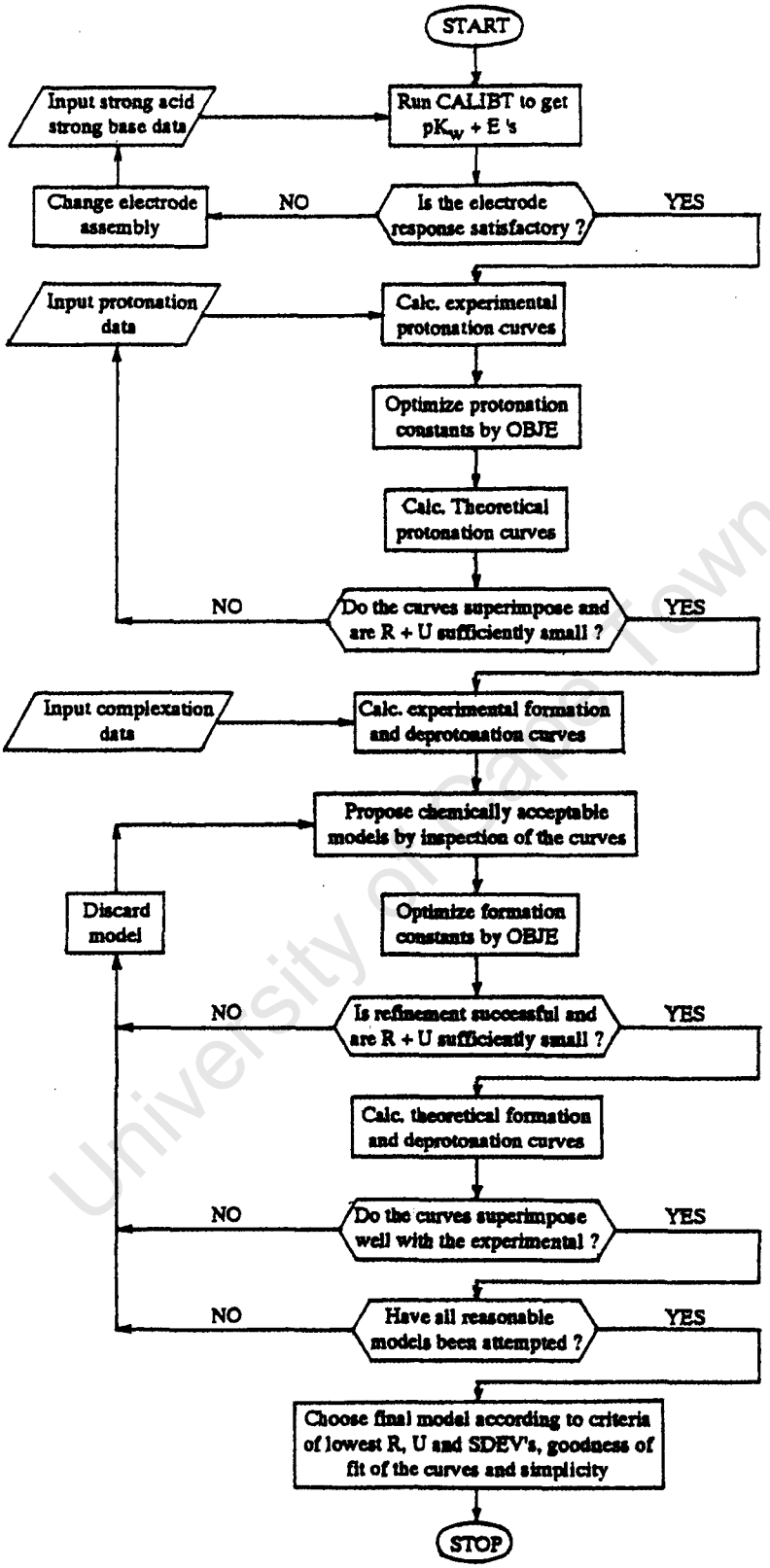

Figure 2.3: Flow chat describing the procedure for the determination of the protonation and complexation constants [17].

2.4 EXPERIMENTAL

2.4.1 Introduction

The procedure developed by Sillen and his colleagues over two decades ago are still widely accepted as the most accurate way of determining formation constants potentiometrically [18]. Solutions containing different metal to ligand concentrations and ratios are titrated potentiometrically with standardized strong base [18]. These titrations served to check the reversibility and reproducibility of each system, as well as to obtain protonation constants and electrode parameter values [19]. The data collected from these titrations were analysed by ESTA suit of programs to obtain the best fit of formation constants [20]. The resulting models were used to generate theoretical formation curves which could be compared with experimental curves [20].

2.4.2 Preparation and standardisation of solutions

In this study carbon dioxide must be excluded because it will react with NaOH to give bicarbonates and carbonates as shown in equations 2.31 and 2.32 respectively [21].

$$CO_2 + NaOH \rightarrow NaHCO_3 \qquad 2.31$$

Sodium Bicarbonate

$$NaHCO_3 + NaOH \rightarrow Na_2CO_3 + H_2O$$

Sodium Carbonate 2.32

Therefore this will render the potentiometric results inaccurate. In order to exclude carbon dioxide in solutions, the following procedures were used:

- Apart from ethylenediamine tetraacetic acid (EDTA), all solutions were prepared with NaCl as background electrolyte at an ionic strength of $0.15 mol/dm^3$.
- All solutions were prepared using glass distilled deionised water which had been boiled to remove carbon dioxide and cooled in a container protected by a carbon dioxide trap.

- The volumetric flasks were calibrated with distilled deionised boiled-water allowing for the Archimedes effect on standard weights, the volumetric expansion of glass and density changes of the water temperature [19].
- All chemicals were used with no further purification and were dried in a dessicator prior to preparation of the solutions.

2.4.3 Preparation of Stock base solution (NaOH)

0.1mol/dm^3 NaOH solutions were prepared under a nitrogen gas atmosphere to a concentration of 0.1mol/dm^3 from Merck ampoule (1.09959-Totrisol) [3]. This solution was standardised against recrystallized potassium hydrogen phthalate (KHP) using the Gran Method [22].

2.4.4 Preparation of Stock acid solution (HCl)

0.1mol/dm^3 and 0.01mol/dm^3 HCl solutions were prepared from a Merck ampoule (1.09973-Titrisol) in a background electrolyte [22]. 0.01mol/dm^3 HCl solution was standardised by titrating against the standardised NaOH using the Gran Method [22]. This titration data was also used to determine carbonate concentration of NaOH titrant solution by making use of the Gran method. The carbonate concentration will be shown by the curvature in the Gran plot.

2.4.5 Preparation of Stock Metal(II) ion solutions

The metal solutions were made up from the dehydrated chloride salt, as chloride was the choice of the background electrolyte. These solutions were then standardized against EDTA using Fast Sulphon Black (FSB), murexide and solochrome black as indicators for copper(II), nickel(II) and zinc(II) respectively according to the procedure given in Vogel [23].

The concentrations of the solutions varied between 0.0046mol/dm^3 and 0.0117mol/dm^3. In-order to prevent hydrolysis of the metal ions standardised 0.001mol/dm^3 HCl was added into the metal ion solutions. The metal hydroxide formation would give inaccurate concentrations of hydrogen ions present in the metal ion solution.

2.4.6 Preparation of Stock Ligand Solutions

Solutions of ligands under study were prepared by dissolving accurately weighed samples of PCUL and PyN in a background electrolyte. The concentration of these solutions was estimated based on the mass of each of the two ligands and were found to be 0.0180mol/dm^3 and 0.0200mol/dm^3 for PCUL and pyN-N respectively.

2.4.7 Preparation of Stock Glycine solution

For each titration the required amounts of the ligands was weighed and allowed to dissolve in 0.15mol/dm^3 NaCl solution in a reaction flask under N_2 atmosphere [11].

2.4.8 Equipment

The potentiometric titrations were performed under an inert atmosphere of purified nitrogen gas, at 25 °C, using a Radiometer PHM 84pH meter and Metrohm 665 Dosimet burette which were linked and controlled by a computer [24]. The calibrated combined pH glass electrode of 3M KCl internal filling solution was connected to the pH meter [24]. The electrode was immersed in a solution contained in a double-walled titration vessel, which was kept at constant temperature of 25°C by circulating water from a constant temperature thermostat bath [24].

The titrant solution **T** was delivered to the titrated solution **S** through an immersed capillary tip from a Metrohm Dosimat 665 piston burette using a Pascal program developed in this laboratory, to monitor the pH and the volume of **T** added at each titration point [25]. During titrations these solutions were stirred by Teflon magnetic stirrer bar, which allows a homogenous solution to be obtained giving a fairly fast response time but all calibration procedures were carried out at the same stirring rate. Care should be taken to ensure that the magnetic follower does not bump when rotating and thereby damaging the electrode [25].

The reaction solution was protected from the intrusion of atmospheric oxygen and carbon dioxide by passing a continuous flow of high purity stream over it throughout the titration. A gas bubbler attached to the gas outlet from the titration vessel prevented back diffusion [25]. To ensure the reproducibility of the titration data, all titrations were performed in duplicate. Before the high purity nitrogen was

introduced into the titration solution it was passed through five traps which included [26, 27]:

- 50% potassium hydroxide, to remove traces of carbon dioxide
- Fieser's solution consisting of 20g potassium hydroxide, 2g sodium anthraquinone-2-sulphonate and 15g sodium dithionite in 100ml water to remove traces of oxygen
- Glass wool
- Distilled water
- Background electrode of 0.15 mol/dm^3 to humidify the inert atmosphere

2.4.9 Data Analysis

The major objective in ESTA is to provide a flexible tool for investigating phenomena associated with chemical interactions in solution and for their quantitative characteristics [11]. The collected data were used as input file into the ESTA file template in order to calculate the electrode parameters, protonation and formation constants [2, 11]. The required parameters were calculated by making use of the task OBJE within the ESTA2A module of ESTA library computer speciation modelling programs [2]. The analysis was performed by fitting these constants to the titration data, based upon minimization of the objective function, U_{obj}, with respect to emf [2]. The E^o, $[H^+]_{vessel}$, $[L]_{vessel}$ and $[M]_{vessel}$ have fixed values and therefore not refined. Hence the required logβ's were the only values refined. The results obtained were used to generate Z_H-Bar, Z_M-Bar and Q_M-Bar curves by making use of tasks Z-bar and Q-bar within the ESTA1 module of ESTA.

The reproducibility and quality of the experimental data was always checked visually using the formation and deprotonation functions and repeat titrations were superimposable in every case [25]. It was rather difficult to work with our PCUL ligand because only ~0.2123g was provided which made a stock solution of 30ml and therefore small solution volumes were used for each experiment, hence high errors were observed in the refinement of PCUL concentration.

2.5 Results and discussion

2.5.1 Glycine system

The ESTA program library of computer speciation modelling programs was used to determine the protonation and stability constants [20]. The task OBJT was used with all the estimated stability constants for a more general adjustment, the output gave modified guesses and was optimised together with the acid concentration using the task OBJE to give the final values of the stability constants and the acid concentration describing the system [20].

2.5.1.1 Glycine protonation

H-glycine equilibria protonation constants were evaluated in the pH range of 2 -11. Figure 2.4 shows proton formation function, Z_H-bar plotted against pH for glycine. The Z_H-bar function rises slightly above 1 for this system indicating a stepwise protonation of two sites of which only one is fully protonated in the pH range studied. Glycine like all the amino acids in their pure state exists as a dipolar ion, a zwitterionic form being more favoured energetically both in solution and in solid state [11]. Depending on the pH of the aqueous solution, glycine exists as a zwitterion, the amino group being protonated ($-NH_3^+$) while the carboxyl group (CO_2^-) is deprotonated [11].

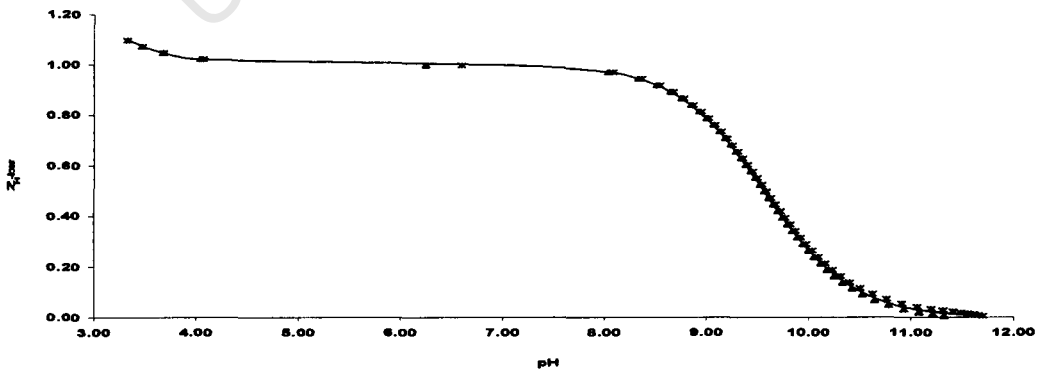

Figure 2.4: Protonation curves, Z_H-bar against pH for glycine at 25°C in 0.15mol/dm^3 (Cl^-) Na^+. The solid line indicates the theoretical curve.

Theoretically, the Z_H-bar should rise and level off towards the limiting value of 1 for mononuclear LH species formation indicating the presence of LH as a major species. Figure 2.4 is in good agreement with this theory, the levelling off of the curve at 1 indicates the protonated amino group which begins to lose a proton. The carboxyl deprotonation occurs at low pH where the accuracy of pH measurement is also low thus bringing about a slightly higher standard deviation than that of amino group [25].

Table 2.1: $\log\beta_{pqr}$ of H-glycine system determined at 25°C in 0.15mol/dm^3(Cl^-) Na^+. std Dev denotes standard deviation in $\log\beta_{pqr}$, R_f^H is the Hamilton R-factor and R_{lim}^H its limit. The general formula of a complex is $M_pL_qH_r$ denoted by the stoichiometric coefficient pqr.

Ligand	P q r	$\log\beta_{pqr}$	std Dev	logK	R_f^H	R_{lim}^H	n_T (n_P)	Literature[28]
H-glycine	0 1 1	9.56	0.021	9.56	0.017	0.039	2 (102)	9.59
	0 1 2	11.94	0.093	2.38				2.37

The complete overlap of the calculated and the observed Z_H-bar plots confirmed the overall protonation constants. The protonation constants determined by ESTA suit of programs (shown in Table 2.1) for glycine are pK_1 = 9.56 and pK_2 = 2.38 and are assigned for the amino group and the carboxyl group respectively [25]. The standard deviations are relatively small, the R-factor is less than its limit thus giving more confidence to this model.

2.5.1.2 Cu(II)-glycine complexation

The $\log\beta_{pqr}$ obtained from ESTA were entered into the input files of the tasks Z-bar and Q-bar of ESTA 1 module to give Z_M-bar and Q-bar plots respectively [25]. Z_M-bar measures the average number of ligands bound per metal ion due to complexation. This function is plotted against the negative logarithm of the free ligand concentration (pL) [25].

Figure 2.5 shows a plot of Z_M-bar as a function of pL for the Cu(II)-glycine system. The existence of bis complex of 1:2 M: L ratio is indicated by the levelling off of the function at the value of 2. In this system copper(II) coordinates with two molecules of glycine thus forming ML_2 species.

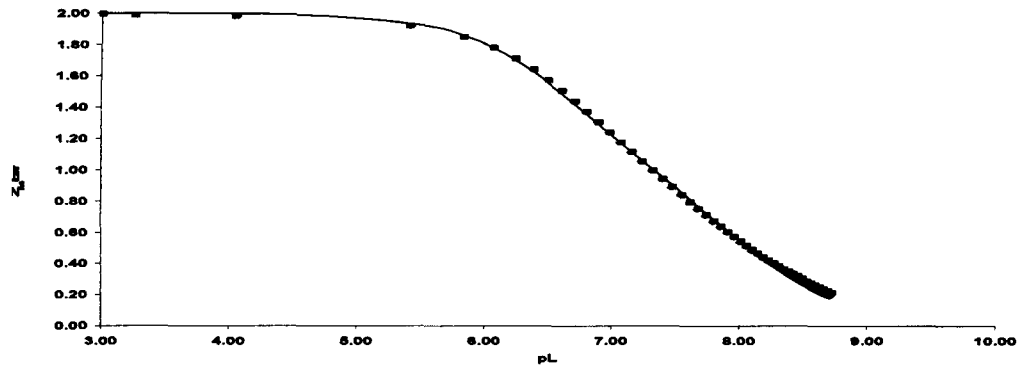

Figure 2.5: Formation function curve, Z_M-bar against pL for the Cu(II)-glycine at 25°C in 0.15mol/dm^3 (Cl^-) Na^+. M:L ratio 1:2 is displayed. The solid line represents the theoretical curve.

The deprotonation function, Q-bar, which indicates the average number of protons released upon complexation, is plotted against the pH of the solution [25]. This function is compared with n-bar function which measures the average number of protons that would be bound to the ligand in the absence of complexation [25].

In Figure 2.6, the deprotonation curve function rapidly rises, intersecting the n-bar at a value of 1 a pH 4. At this pH the n-bar = 1 indicating that the glycine has only one dissociable proton and no MLH_1 or and MLH_2 species formed. From the results given in Table 2.2, the divalent copper forms ML and ML_2 species with $\log\beta_{pqo}$'s 8.03 and 14.67 respectively. The deprotonation curve function continues to rise reaching a maximum value and levelling off at 2 at pH range 5-9. The rising of the Q-bar curve function is due to the formation of the hydroxo species 1 1 -1. Above pH 9.3, the Q-bar function runs parallel to the n-bar indicating that no further complexation take place.

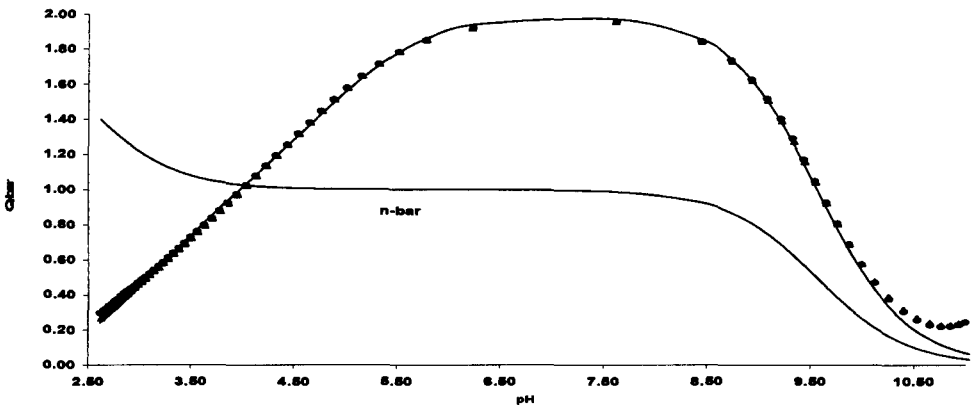

Figure 2.6: Deprotonation function curve, Q-bar against pH for the Cu(II)-glycine at 25°C in 0.15mol/dm^3 (Cl^-) Na^+. M:L ratio 1:2 is displayed. The solid line represents the theoretical curve.

The results obtained for the Cu(II)-glycine system are similar to those obtained in literature [28]. Table 2.2 also shows the hydroxo species which was never measured before. The low standard deviation, R-factor is less than its limit thus indicating that the model is within the maximum allowed experimental error. The agreement between the theoretical and the experimental curve gave confidence to the proposed model.

Table 2.2: $\log\beta_{pqr}$ of the Cu(II)-glycine system determined at 25°C in 0.15 mol/dm^3 (Cl^-) Na^+. std Dev denotes standard deviation in $\log\beta_{pqr}$, R_f^H is the Hamilton R-factor and R_{lim}^H its limit. The general formula of a complex is $M_pL_qH_r$ denoted by the stoichiometric coefficient pqr.

Metal-ligand complex	p q r	$\log\beta_{pqr}$	std Dev	R_f^H	R_{lim}^H	n_T (n_P)	Literature[28]
Cu(II)-gly	1 1 0	8.03	0.008	0.006	0.01	3 (273)	8.20
	1 2 0	14.67	0.01				15.07
	1 1 -1	0.011	0.02				

Figure 2.7 shows calculated species distribution curves for the Cu(II)-glycine system. According to the species distribution plot for Cu(II)-glycine system, complexation starts at pH ~2 forming ML species until pH 4.5 [25]. The formation of the predominant species, ML_2 begins at pH~2.9. Beyond pH 7 the solution contains mostly ML_2 species and this corresponds with the Q-bar curve function levelling at 2 [25].

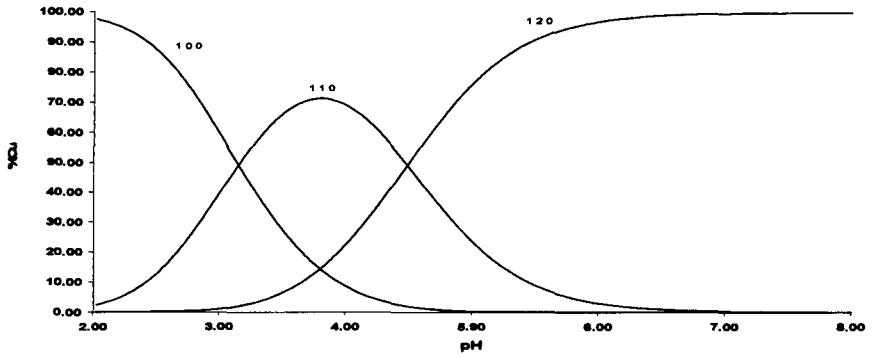

Figure 2.7: Species distribution curves of the Cu(II)-glycine as a function of pH.

2.5.1.3 Ni(II)-glycine complexation

Figure 2.8 shows a plot of Z_M-bar as a function of pL for the Ni(II)-glycine system. The curves are not superimposable indicating the presence of species other than simple mononuclear species [25]. The splitting is such that the bottom curve is for M:L ratio 1:1 and the top one for 1:3. The fanning back of the complex formation function at a pL of 6.5 is indicative of hydroxo and or mixed hydroxo species [25].

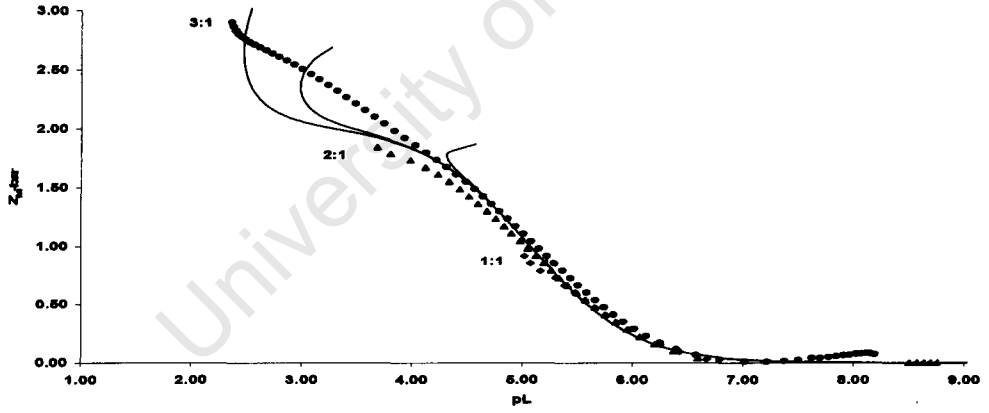

Figure 2.8: Formation function curve, Z_M-bar against pL for the Ni(II)-glycine at 25°C in 0.15mol/dm^3 (Cl^-) Na^+. M: L ratios 1:1, 1:2 and 1:3 are displayed. The solid line represents the theoretical curve.

Figure 2.9 shows a plot of Q-bar as a function of pH for the Ni(II)-glycine system. At pH value less than 4, the deprotonation function, Q-bar is zero indicating that no protons have been displaced due to complexation [25]. The n-bar has a value of about 1 at pH 4 confirming that the glycine is still protonated at low pH. At pH >4 Q-bar

function curves rapidly rise to intersect the protonation curve, n-bar at pH ~5. The Q-bar curve function rapidly rises to a value of 2 at pH range 7 to 8.4; this indicates that in basic conditions the predominant species in solution is MLH_{-1}. The curves are not superimposable and intersect the n-bar curve at pH~6 reaching a maximum value of ~1.9 at pH 7. Above this pH, the Q-bar curves run parallel to the protonation curve and then levels off at a value of 1.5 in a strongly alkaline solution indicating that no further complexation occurs at this point. The splitting is such that the bottom curve is for the ratio 1:1 and the top one for a 1:3 metal to ligand ratio.

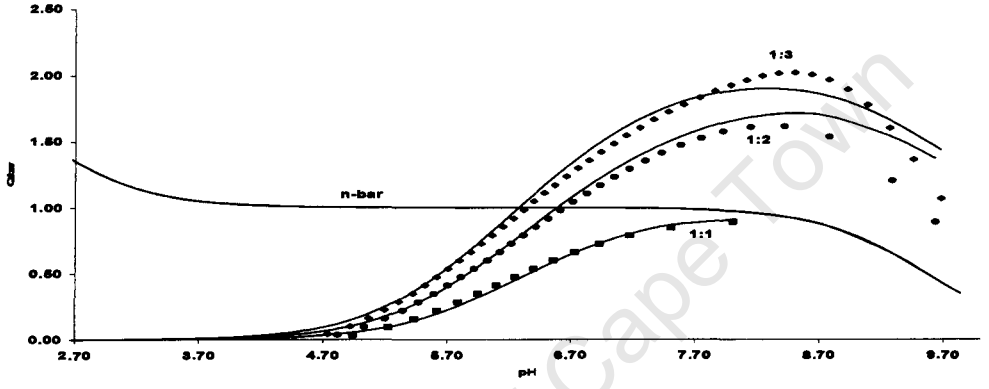

Figure 2.9: Deprotonation function curve, Q-bar against pH for the Ni(II)-glycine at 25°C in 0.15mol/dm^3 (Cl^-) Na^+. M: L ratios 1:1, 1:2 and 1:3 are displayed. The solid line represents the theoretical curve.

$\log_{\beta pqr}$ values for the Ni(II)-glycine system are given in Table 2.3. The R-factor is slightly higher than its limit indicating that it is not statiscally possible to improve the model. The similarity between the experimental and the literature results supported the proposed model.

Table 2.3: $\log\beta_{pqr}$ of the Ni(II)-glycine system determined at 25°C in 0.15 mol/dm^3 (Cl^-) Na^+. std Dev denotes standard deviation in $\log\beta_{pqr}$, R_f^H is the Hamilton R-factor and R_{lim}^H its limit. The general formula of a complex is $M_pL_qH_r$ denoted by the stoichiometric coefficient pqr.

Metal-ligand complex	p q r	$\log\beta_{pqr}$	std DEV	R_f^H	R_{lim}^H	n_T (n_P)	Literature[28]
Ni(II)-gly	1 1 0	5.05	0.008	0.04	0.02	8 (389)	5.59
	1 2 0	10.09	0.01				10.24
	1 1 -1	1.47	0.03				

Figure 2.10 shows calculated species distribution curves for the Ni(II)-glycine system. ML formation starts at pH 3 as indicated by Figure 2.10. The formation of the ML and ML_2 species pattern follows that of Cu(II)-glycine system. However, it is important to note that the stability constants obtained for the Cu(II)-glycine system are higher than those obtained for the Ni(II)-system. This is confirmed by the percentage formation of the ML species which is formed, at 70% for the Cu(II)-glycine system and 50% for the Ni(II)-glycine system .

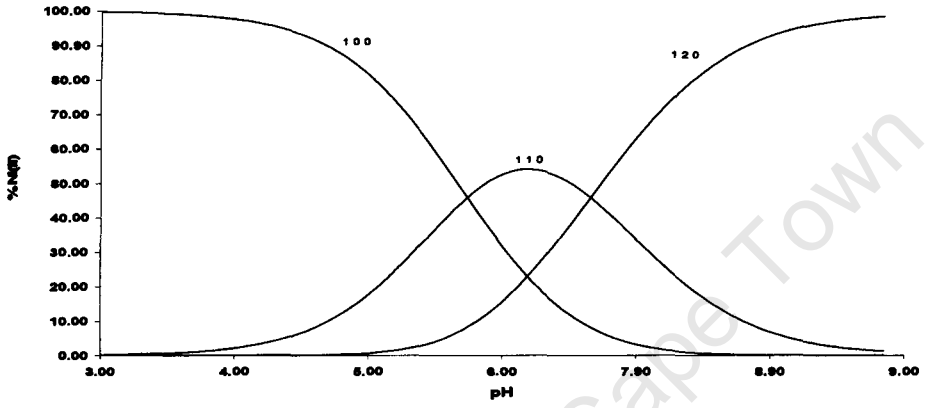

Figure 2.10: Species distribution curves of the Ni(II)-glycine as a function of pH.

2.5.1.4 Zn(II)-glycine complexation

Figure 2.11 shows a plot of Z_M-bar function curve against pL for the Zn(II)-glycine system. The ML species are not the only species present in solution and this is indicated by the Z_M-bar curve function not levelling off at 1 as found for the Ni(II)-glycine system. The fanning back of the complex formation function at pL 3.2 is an indication of the presence of the hydroxo and or mixed hydroxo species.

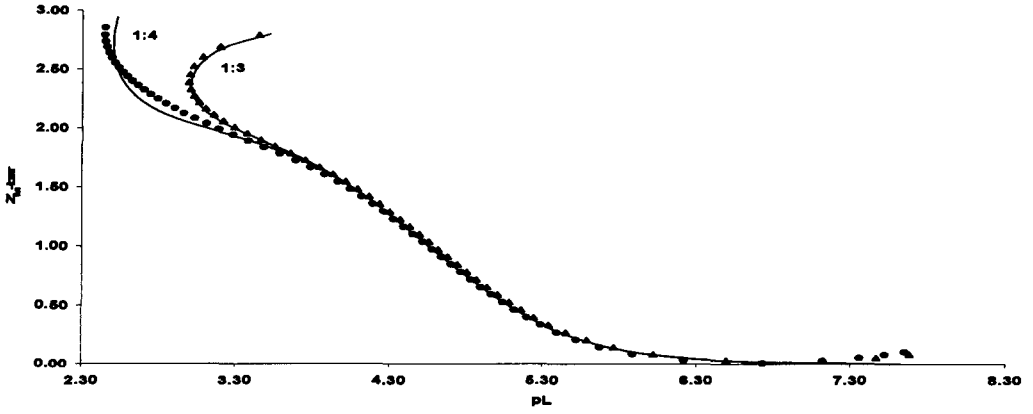

Figure 2.11: Formation function curve, Z_M-bar against pL for the Zn(II)-glycine at 25°C in 0.15mol/dm^3 (Cl^-) Na^+. M:L ratios 1:3, 1:4 are displayed. The solid line represents theoretical curve.

Figure 2.12 shows a plot of deprotonation curve function, Q-bar against pH for the Zn(II)-glycine system. Similar to the Ni(II)-glycine system, the n-bar have value of ~1 at pH 4 confirming that glycine is still protonated at low pH. At pH >4.5, Q-bar rapidly rises to intersect the n-bar at 1. Between pH 7 to 8 the Q-bar curves rapidly rise to a maximum value of 2 indicating that at high pH the predominant species in solution is ML_2. At pH >8.5, the Q-bar curves run parallel to the n-bar curve indicating that no further complexation take place beyond this pH. The R-factor is closer to its R-lim thus showing good agreement between the theoretical and the experimental data.

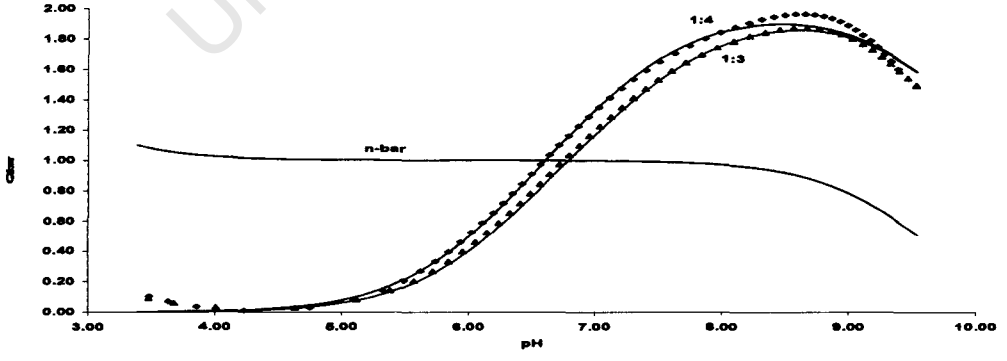

Figure 2.12: Deprotonation function curve, Q-bar against pH for the Zn(II)-glycine at 25°C in 0.15mol/dm^3 (Cl^-) Na^+. M:L ratios 1:3, 1:4 are displayed. The solid line represents the theoretical curve.

Table 2.4 shows three species obtained in the complexation of Zn(II) with glycine ligand together with their stability constants. The standard deviations are reasonably low and are lower than those obtained in the Zn(II)-glycine system. The obtained $\log\beta_{pqr}$ for Zn(II)-glycine system are similar to literature values. The R-factor ≈ R-lim therefore it is not statiscally possible to improve this model.

Table 2.4: $\log\beta_{pqr}$ of the Zn(II)-glycine system determined at 25°C in 0.15 mol/dm^3 (Cl^-) Na^+. std Dev denotes standard deviation in $\log\beta_{pqr}$, R_f^H is the Hamilton R-factor and $R_{lim}{}^H$ its limit. The general formula of a complex is $M_pL_qH_r$ denoted by the stoichiometric coefficient pqr.

Metal-ligand complex	P q r	$\log\beta_{pqr}$	std Dev	R_f^H	$R_{lim}{}^H$	n_T (n_P)	Literature[28]
Zn(II)-gly	1 1 0	4.931	0.007	0.026	0.018	4 (210)	4.90
	1 2 0	9.113	0.007				8.96
	1 1 -1	-0.309	0.012				

The calculated species distribution curves for the Zn(II)-glycine system are given in Figure 2.13. The formation of the ML species begins at pH 3.5. It is important to note that the formation of the ML species for Zn(II)-glycine system follows that of Cu(II)-glycine and Ni(II)-glycine systems. However, there is a difference in the percentage formation of this species, 30% of ML species is formed at pH 7.

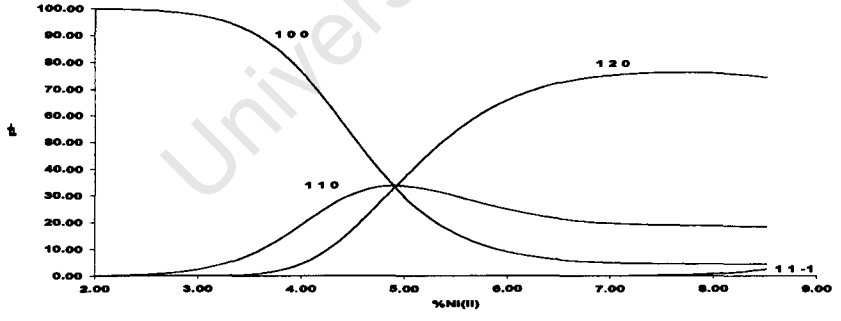

Figure 2.13: Species distribution curves of the Zn(II)-glycine as a function of pH.

From Table 2.1, the pK_a values obtained for H-glycine systems are in close agreement with those obtained in literature. Also from Tables; 2.2, 2.3, and 2.4 the obtained deprotonation constants are in close agreement with those obtained in literature. The variation is due to the fact that our experiments were performed at 25 °C in 0.15 mol/dm^3 (Cl^-) Na^+. Martell *et.al* carried out titrations at the same temperature but at

0.1 mol/dm^3 (Cl^-) Na^+[28]. The glycine potentiometric studies were done to directly compare our results with those reported in literature in order to validate the proposed experimental procedure.

2.5.2 pyN system

The determination of the protonation and stability constants for pyN system followed the same experimental procedure as that of the glycine system. For analysis, the potentiometric data was entered into the ESTA library of computer speciation modelling programs [25].

2.5.2.1 pyN-protonation

H-pyN equilibria protonation constants were evaluated in the pH range of 2 -11. Figure 2.14 shows a plot of Z_H-bar against pH which indicates that pyN contains one measurable protonation site as indicated by the levelling off of the Z_H-bar function at 1 at pH 5. This indicates that 1 proton is added to the ligand, resulting in a mono-protonated ligand at low pH. Above pH 7 the predominant species is pyN while below this pH the predominant species is $pyNH^+$. The stability constants given in Table 2.5 are similar to those obtained by Martell [28]. As with glycine system, the slight discrepancy is due to the ionic strength of 0.15mol/dm^3 (Cl^-) Na^+ used in literature.

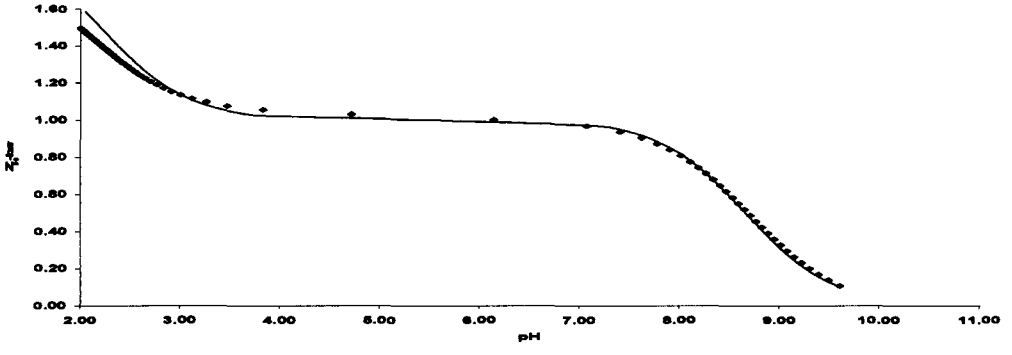

Figure 2.14: Protonation curves, Z_H-bar against pH for pyN at 25°C in 0.15 mol/dm^3 (Cl^-) Na^+. The solid line indicates the theoretical curve.

The complete overlap of the calculated and the observed Z_H-bar plots confirmed the overall protonation constants. The protonation constants determined by ESTA suite of programs for pyN are $\log K_1$ = 8.66 and pK_2 = 2.20 as shown in Table 2.5. These stability constants are assigned for the nitrogen in the amine group and nitrogen in the pyridyl group respectively. The low pK_a value of the second protonation is due to the electronic repulsion effect and base weakening effect of the protonated amine [24].

Table 2.5: $\log\beta_{pqr}$ of H-pyN system determined at 25°C in 0.15 mol/dm^3 (Cl^-) Na^+. std Dev denotes standard deviation in $\log\beta_{pqr}$, R_f^H is the Hamilton R-factor and R_{lim}^H its limit. The general formula of a complex is $M_pL_qH_r$ denoted by the stoichiometric coefficient pqr.

Ligand	p q r	$\log\beta_{pqr}$	std Dev	logK	R_f^H	R_{lim}^H	n_T (n_p)	Literature[28]
H-pyN	0 1 1	8.66	0.02	8.66	0.04	0.002	2 (122)	8.61
	0 1 2	10.86	0.05	2.20				2.00

The R-factor is greater than R-lim, however since the experimental and the theoretical protonation constants are relatively similar, the proposed model was considered reasonable correct.

2.5.2.2 Cu(II)-pyN complexation

Figure 2.15 shows a plot of complex formation function Z_M-bar plotted against the negative logarithm of the free ligand concentration (pL). This function rapidly rises to 1.5 at low pL value. The fact that the Z_M-bar does not level off at 1 indicates that:

- Mononuclear species are not the only species in solution.
- 1 proton is added to pyN.

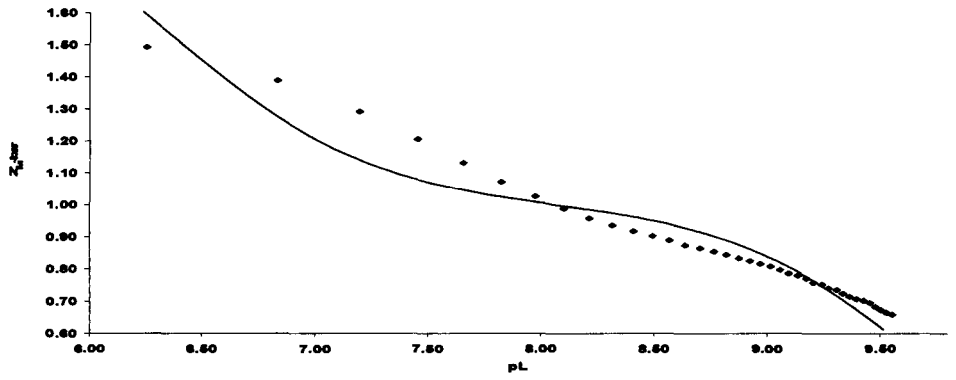

Figure 2.15: Formation function curve, Z_M-bar against pL for the Cu(II)-pyN at 25°C in 0.15mol/dm^3 (Cl^-) Na^+. M:L ratio 1:2 is displayed. The solid line represents the theoretical curve.

The deprotonation function, Q-bar is plotted against pH as shown by Figure 2.16. This function is plotted in conjunction with n-bar, which indicates the amount of protons that would be bound to the ligand in absences of the metal. Complexation with Cu(II) begins at pH 2.5. The Q-bar curve function rapidly rises to intersect the n-bar at Q-bar value of 1 at pH 3.5 indicating that a single proton is lost upon Cu(II)-pyN complexation, thus resulting in simultaneous formation of 1 1 0 and 1 2 0 with $\log\beta_{pqr}$'s 9.71 and 16.13 respectively as given in Table 2.6. The Q-bar curve function continuously increases reaching a Q-bar value of 1.8 at pH 6.5 indicating that the ligand lost a total of two protons and the predominant species at this pH is 1 2 0. Beyond pH 6.5 no further complexation takes place as the Q-bar curve function runs parallel to the n-bar.

At pH range 2.7-3.5 there is good agreement between the theoretical and the experimental curves. However, as the Q-bar rises with increasing pH, the agreement between these two curves slightly differs. This is of no concern as at this pH complexation is complete.

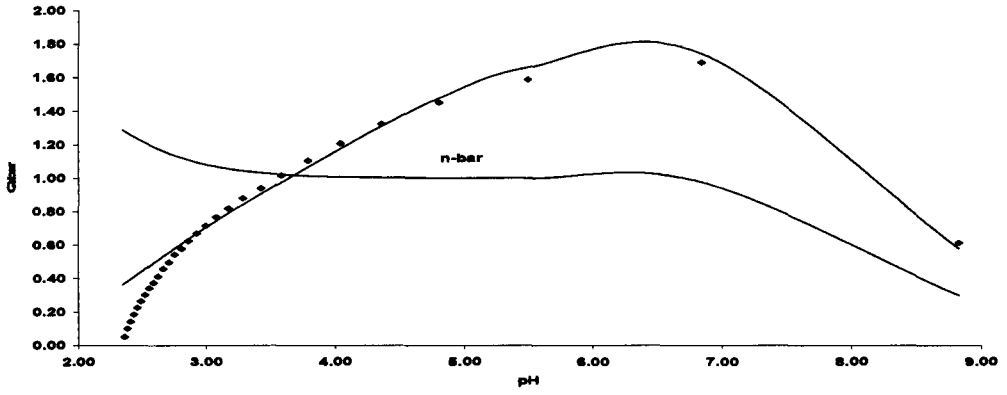

Figure 2.16: Deprotonation function curve, Q-bar against pH for the Cu(II)-pyN at 25°C in 0.15mol/dm^3 (Cl^-) Na^+. M:L ratio 1:2 is displayed. The solid line represents the theoretical curve.

The formation of 1 1 0 and 1 2 0 is confirmed by the species distribution plot against pH given in Figure 2.17, 70% of 1 1 0 species is formed at pH 3.5 and at pH 6, 100% of 1 2 0 species is formed.

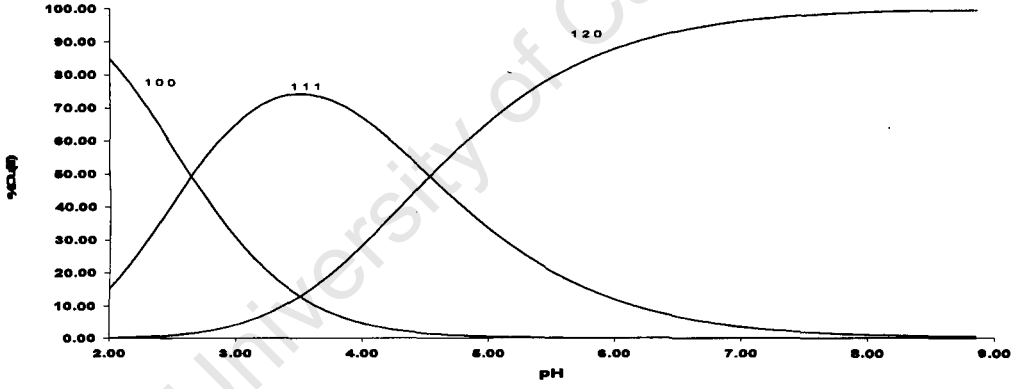

Figure 2.17: Species distribution curves of Cu(II)-pyN as a function of pH.

The two species determined by ESTA suite of programs are given in Table 2.6. From this table we can see that the experimental first $\log\beta_{pqr}$ is similar to the literature value while the second $\log\beta_{pqr}$'s slightly differ with each other. This discrepancy may be attributed to the fact that Martell conducted experiments at 0.1 mol/dm^3 (Cl^-) Na^+. The low standard deviations in $\log\beta_{pqr}$'s led confidence to the results. It is not statiscally possible to improve this model as the R-factor ≈ R-lim.

Table 2.6: $\log\beta_{pqr}$ of the Cu(II)-pyN system determined at 25°C in 0.15 mol/dm^3 (Cl^-) Na^+. std Dev denotes standard deviation in $\log\beta_{pqr}$, R_f^H is the Hamilton R-factor and $R_{lim}{}^H$ its limit. The general formula of a complex is $M_pL_qH_r$ denoted by the stoichiometric coefficient pqr.

Metal-ligand complex	p q r	$\log\beta_{pqr}$	std Dev	R_f^H	$R_{lim}{}^H$	n_T (n_P)	Literature[28]
Cu(II)-pyN	1 1 0	9.71	0.01	0.018	0.012	2 (60)	9.50
	1 2 0	16.13	0.01				17.20
	1 1 -1	-0.01	0.02				

2.5.2.3 Ni(II)-pyN complexation

.

Figure 2.18 shows a plot of Z_M-bar against the logarithm of free ligand concentration. From this plot, the Z_M-bar curve function reaches a maximum of ~1.7 at pL ~5.5 indicating that about two protons would be bound per metal ion due to complexation. The Z_M-bar curve function does not level off at 1, indicating that mononuclear species is not the only species in solution. Fanning back at pL 8-9 is an indication of hydroxo species formation.

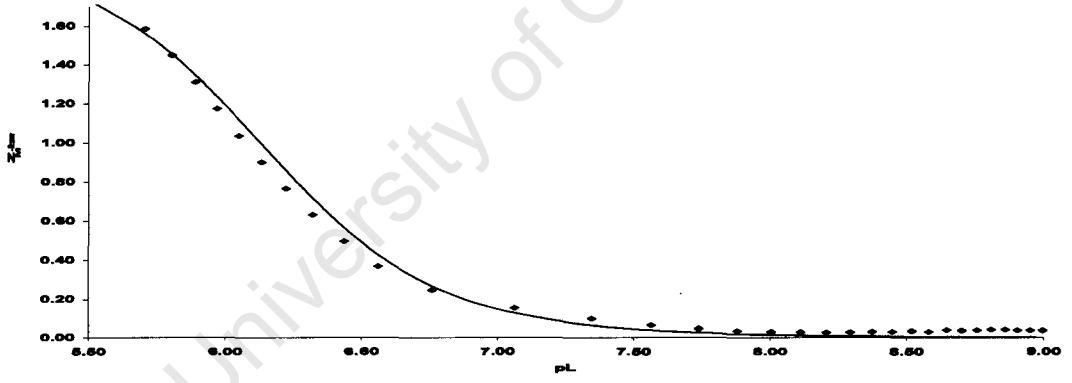

Figure 2.18: Formation function curve, Z_M-bar against pL for the Ni(II)-pyN at 25°C in 0.15mol/dm^3 (Cl^-) Na^+. M:L ratio 1:2 is displayed. The solid line represents the theoretical curve

The deprotonation function in Figure 2.19 shows that at pH ~2.13 the function is not zero, indicating that complexation has already started. The species distribution curve versus pH in Figure 2.20 indicates that complexation occurs at the onset of the titration at pH 1.9. The deprotonation curve function rises intersecting the n-bar at Q-bar value of ~1 at pH 5 losing one proton thus forming 1 1 0 species, however Figure 2.12 shows that 33% of 1 1 0 is formed in solution at pH 5.

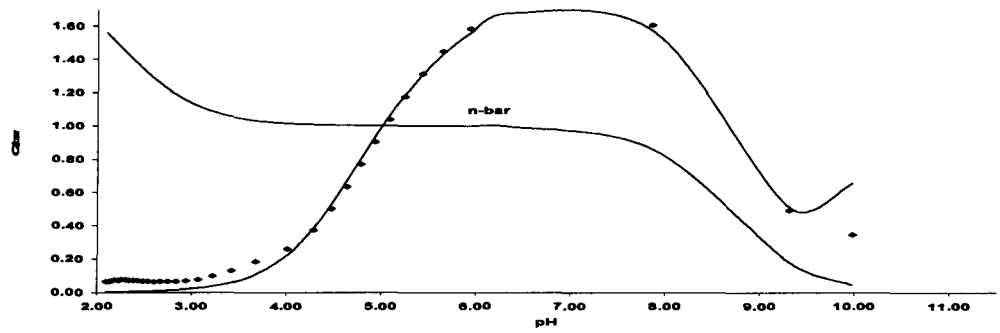

Figure 2.19: Deprotonation function curves, Q-bar against pH for the Ni(II)-pyN at 25°C in 0.15mol/dm^3 (Cl^-) Na^+. M:L ratio: 1: 2 is displayed. The solid line represents the theoretical curve.

The Q-bar curve function continues to rise, reaching a maximum of 1.7 at pH 6.4 indicating that almost two protons are lost upon Ni(II)-pyN complexation thus leading to the simultaneous formation of ML_2 species. Figure 2.20 shows that 76% of 1 2 0 is formed in solution at pH ~7.4. No further complexation occurs beyond pH 6.5 as the Q-bar curve runs parallel to the n-bar curve. Also at pH 6.5 the theoretical and the experimental curves differs slightly from each other. However, this occurs at the buffered region after complexation process has been completed, therefore this is not of concern. The formation of ML(OH) species occurs at pH 9.32. However, only 2.69% of ML(OH) is formed in solution as shown by Figure 2.13.

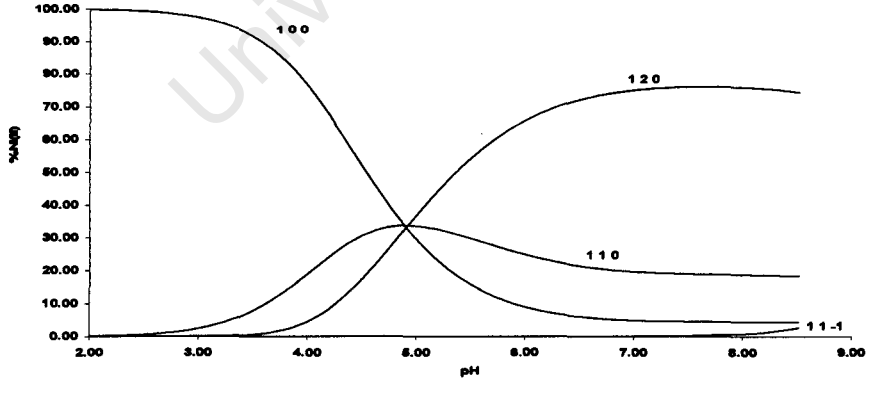

Figure 2.20: Species distribution curves of Ni(II)-pyN as a function of pH

The ESTA suite of programs gave the deprotonation constants shown in Table 2.7. The experimental $Log\beta_{pqr}$'s differs from those obtained in literature. This may be due to the fact that Martell performed experiment at 0.1 mol/dm^3 (Cl^-) Na^+ [28]. The standard deviations are relatively low, the agreement between the theoretical and experimental curve function at pH 4.5-5.5 supported to the proposed model.

Table 2.7: $log\beta_{pqr}$ of the Ni(II)-pyN system determined at 25°C in 0.15 mol/dm^3 (Cl^-) Na^+. std Dev denotes standard deviation in $log\beta_{pqr}$, R_f^H is the Hamilton R-factor and R_{lim}^H its limit. The general formula of a complex is $M_pL_qH_r$ denoted by the stoichiometric coefficient pqr.

Metal-ligand complex	p q r	$log\beta_{pqr}$	std Dev	R_f^H	R_{lim}^H	n_T (n_P)	Literature[28]
Ni(II)-pyN	1 1 0	6.136	0.04	0.031	0.013	2(70)	7.11
	1 2 0	12.26	0.03				13.34
	1 1 -1	2.30	0.06				

2.5.2.3 Zn(II)-pyN complexation

Figure 2.21 gives a plot of Z_M-bar curve function against free ligand concentration. Z_M-bar curve function reaches a maximum of ~1.7 at pL 4.5. As for the Cu(II)-pyN and Ni(II)-pyN systems, this indicates that two ligands would be bound per metal ion complexation. Fanning back at pL >7.5 indicates the formation of hydroxo species.

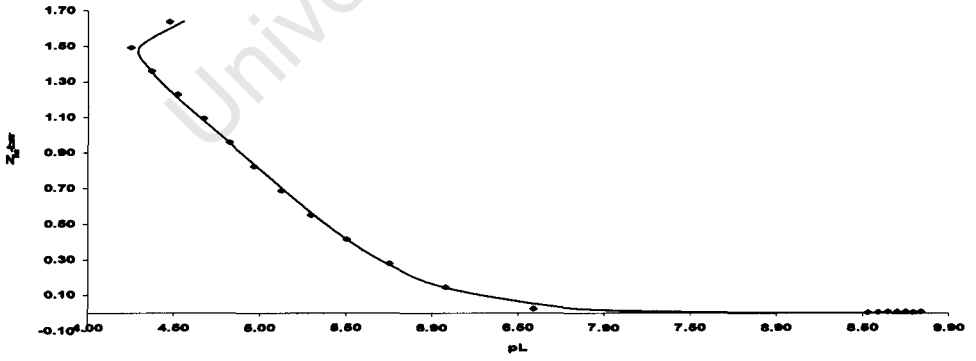

Figure 2.21: Formation function curve, Z_M-bar against pL for the Zn(II)-pyN at 25°C in 0.15mol/dm^3 (Cl^-) Na^+. M:L ratios 1:2 is displayed. The solid line represents the theoretical curve.

Figure 2.22 shows the complexation pattern of Zn(II)-pyN system. From this graph, the complexation process begins at pH 2.5 for this system. At pH ~6.6 the Q-bar curve function intersect the n-bar curve function at 1. Indicating that 1 proton is lost upon Zn(II)-pyN complexation and the predominant species at this pH is ML. The Q-bar curve function continues to rise reaching a maximum of 1.3 at pH 7.8 thus indicating a slight formation of ML_2 species. The Q-bar curve function then run parallel to the n-bar, indicating that no further complexation occurs beyond pH 7.8.

It is important to note that a good agreement between the theoretical and the experimental curves is observed for Zn(II)-pyN system at pH 2.5-7.4. At pH >9.3 the Q-bar curve function rises again reaching ~1.7, indicating the formation of ML(OH) species in this alkaline region. Rising of the Q-bar to ~1.7 indicates that the ligand has lost a total of two ligands due to Ni(II)-pyN complexation.

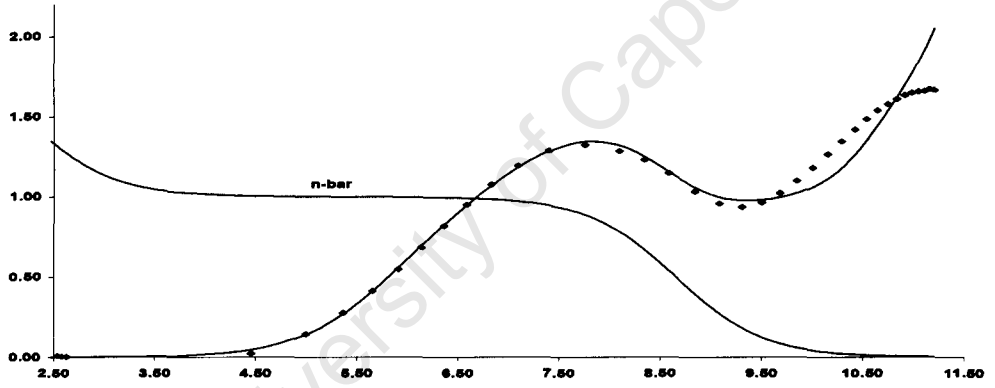

Figure 2.22: Deprotonation function curves, Q-bar against pH for the Zn(II)-pyN at 25°C in 0.15mol/dm^3 (Cl^-) Na^+. M:L ratio: 1: 2 is displayed. The solid line represents the theoretical curve.

The calculated species distribution curves for the Zn(II)-pyN system are given in Figure 2.23. The formation of the ML species starts at the beginning of the titration process at pH 2.7 and continues until pH 8.7. The formation of ML_2 species begins at pH 4.7 while that of ML species begins at pH 2.7 and continues until pH 8.7. At pH 6.4, ML species reaches 53% formation while ML_2 species reaches 59% formation at pH 8. This plot also shows that beyond pH 8.7 the formation of ML(OH) is 46%.

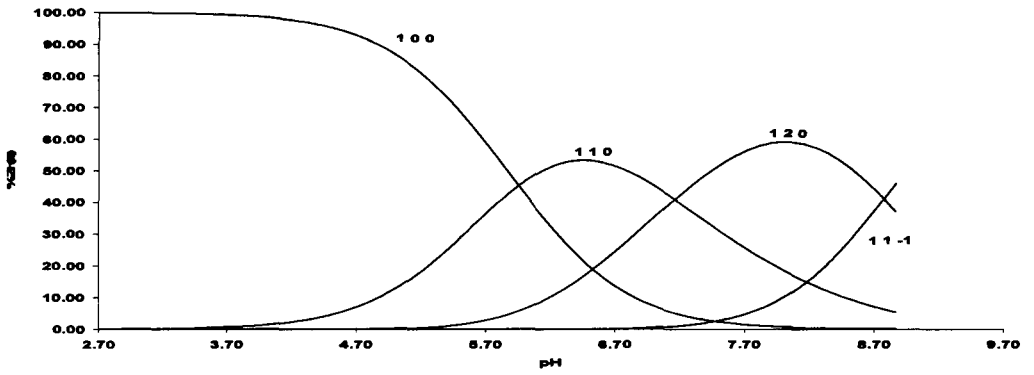

Figure 2.23: Species distribution curves of the Zn(II)-pyN as a function of pH.

The three species obtained for Zn(II)-pyN system are given in Table 2.8. The similarities between the experimental $\log\beta_{pqr}$'s values and the literature ones, and the low standard deviations gave confidence to the results. The theoretical and the experimental $\log\beta_{pqr}$ are similar and the standard deviations are relatively low and this led confidence to the results.

Table 2.8: $\log\beta_{pqr}$ of the Zn(II)-pyN system determined at 25°C in 0.15 mol/dm^3 (Cl^-) Na^+. std Dev denotes standard deviation in $\log\beta_{pqr}$, R_f^H is the Hamilton R-factor and R_{lim}^H its limit. The general formula of a complex is $M_pL_qH_r$ denoted by the stoichiometric coefficient pqr.

Metal-ligand complex	p q r	$\log\beta_{pqr}$	std Dev	R_f^H	R_{lim}^H	n_T (n_P)	Literature[28]
Zn(II)-pyN	1 1 0	5.282	0.02	0.019	0.011	4(132)	5.28
	1 2 0	9.393	0.02				9.44
	1 1 -1	0.323	0.02				

The results obtained for Zn(II)-pyN complex were satisfactory, hence validating comparison the use of pyN system as model system with PCUL system. pyN was included in this study since it forms part of the PCUL (ligand of interest) structure. The results from pyN potentiometry were compared with literature and gave us an idea of the PCUL protonation and deprotonation constants.

2.5.3. PCUL system

It was rather difficult to perform studies on the PCUL system because only 0.21230g of the ligand was provided. Also it was a hydroscopic oil which made accurate weighing of the ligand impossible. For these reasons, a 30ml stock ligand solution was prepared and, used for all experiments. Working with small volumes increased the associated error and meant that fewer titrations could be performed as compared to the glycine and pyN systems. For these reasons the standard deviations are quite high.

The determination of the protonation and stability constants for PCUL system followed the same experimental procedure as that of the glycine and pyN systems.

2.5.3.1 PCUL-protonation

PCUL equilibria protonation constants were evaluated in the pH range of 2 -11. The complete overlap of the calculated and the observed Z_H-bar plots confirmed the overall protonation constants. PCUL has three pK_a values corresponding to the nitrogens in the amines and the one corresponding to the nitrogen of the pyridyl group.

The Z_H-bar function in Figure 2.24 shows only one inflection point because the protonation constants of these amine groups are so close and that they are titrated virtually simultaneously. The difference of 0.86 log units between pK_1 and pK_2 indicates an electronic repulsion on addition of a proton to a charged species or rather to an already protonated molecule. The fourth protonation constant could not be determined because complete protonation of the pyridyl nitrogen occur below the reliable measurable pH range of our glass electrode [24].

From Figure 2.24, the protonation curve Z_H-bar versus pH obtained for PCUL is sigmoidal in shape with limiting Z_H-bar value of 2.5. It is important to note that the protonation constants obtained for PCUL are similar to those obtained for pyN as expected, since pyN forms part of the PCUL structure. At pH lower than 3 the function rises due to the protonation of the acidic pyridyl nitrogen [24].

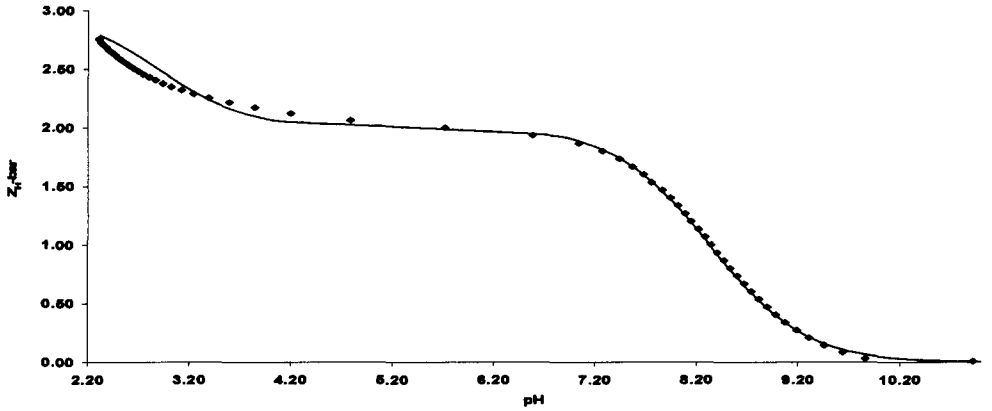

Figure 2.24: Formation function curves, Z_H-bar against pH for PCUL at 25°C in 0.15mol/dm^3 (Cl^-) Na^+. The solid line represents the theoretical curve.

At pH ~ 3 - 4, the function levels off at a Z_H-bar value of ~2 indicating that two protons have been added to the ligand, resulting in a di-protonated ligand at low pH. Below pH 7 the predominant species is PCUL while above this pH the predominant species is $PCULH^+$. The Z_H-bar rises to a limiting value of 2.5 indicating that LH, LH_2 and LH_3 are the predominant species in solution.

The three protonation constants determined by ESTA optimization of potentiometric data for PCUL are $pK_1 = 8.71$, $pK_2 = 7.95$ and $pK_3 = 2.89$ as shown in Table 2.9. The low pK_3 or rather the acidity of the pyridyl nitrogen is due to the electronic repulsion effect and base weakening effect of the protonated methylamine group [3]. The standard deviations are relatively low and the agreement between the theoretical and experimental curves gave confidence to the results.

Table 2.9: $\log\beta_{pqr}$ of the H-PCUL system determined at 25°C in 0.15 mol/dm^3 (Cl^-) Na^+. std Dev denotes standard deviation in $\log\beta_{pqr}$, R_f^H is the Hamilton R-factor and R_{lim}^H its limit. The general formula of a complex is $M_pL_qH_r$ denoted by the stoichiometric coefficient pqr.

Ligand	p q r	$\log\beta_{pqr}$	std Dev	logK	n_T (n_P)	R_f^H	R_{lim}^H
H-PCUL	0 1 1	8.71	0.025	8.71	1 (64)	0.028	0.012
	0 1 2	16.66	0.024	7.95			
	0 1 3	19.55	0.036	2.89			

2.5.3.2 Cu(II)-PCUL complexation

The complex formation function, Z_M-bar is only strictly defined for simple mononuclear complex formation [21]. From Figure 2.25 the Z_M-bar does not start at zero indicating that at the start of the titration complexation is already occurring. Therefore, the curves level off at 1, indication that the ML species is formed. In the pL range 13-4.5 the curve is horizontal indicating that no further complexation occurs. Below pL 4.5, fanning back of the Z_M-bar begun indicating the formation of the MLH_{-1} species. These observations are subsisted by the Q-bar curve.

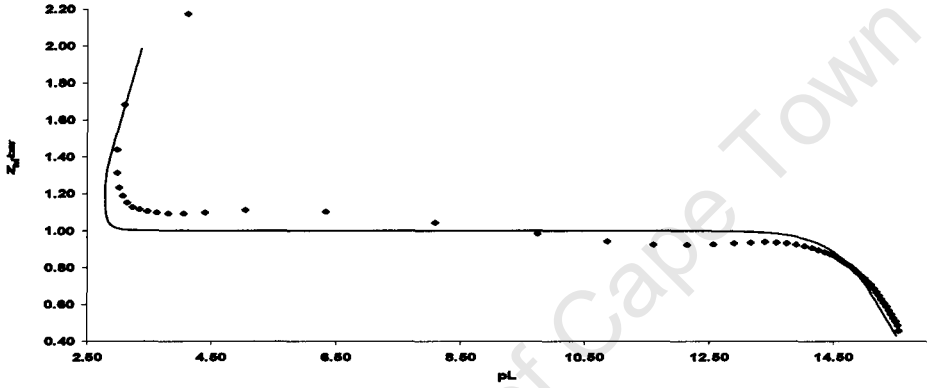

Figure 2.25: Formation function curve, Z_M-bar against pL for the Cu(II)-PCUL at 25°C in 0.15mol/dm^3 (Cl^-) Na^+. M:L ratio 1:2 is displayed.

A plot of the deprotonation curve function against pH is given in Figure 2.26. The Q-bar curve function is 2.3 at the point it is clear that for the Cu(II)-PCUL system, complexation occurs at the start of titration, since at pH 2.68 the Q-bar curve function is 2.3. At pH 5 the Q-bar curve function intersects the n-bar at 2, indicating that two protons are lost upon Cu(II)-PCUL complexation. The predominant species at pH 5 is ML reaching 99% formation at pH 3.5-8.5 as shown by Figure 2.27. The complexation of Cu(II)-PCUL is complete at pH >5 this is shown by the Q-bar curve function running parallel to the n-bar. At pH 9.94 Figure 2.27 shows the formation of ML(OH) species of which only ~1% is formed as indicated by Figure 2.27.

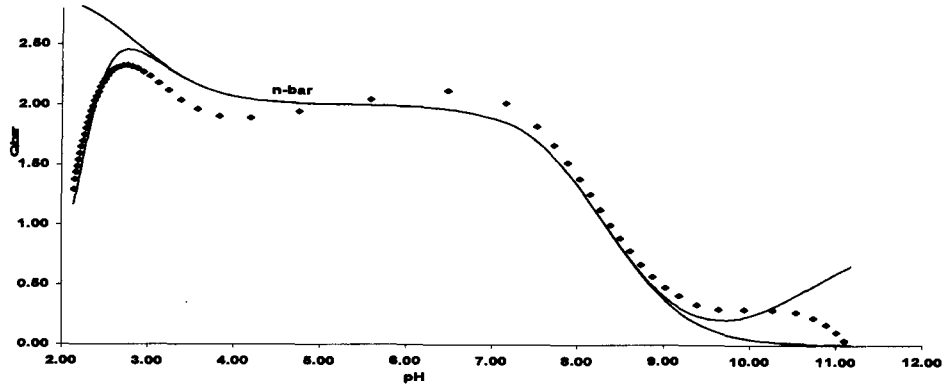

Figure 2.26: Deprotonation function curve, Q-bar against pH for the Cu(II)-PCUL at 25°C in 0.15mol/dm^3 (Cl^-) Na^+. M:L ratios 2:1 is displayed. The solid line represents the theoretical curve.

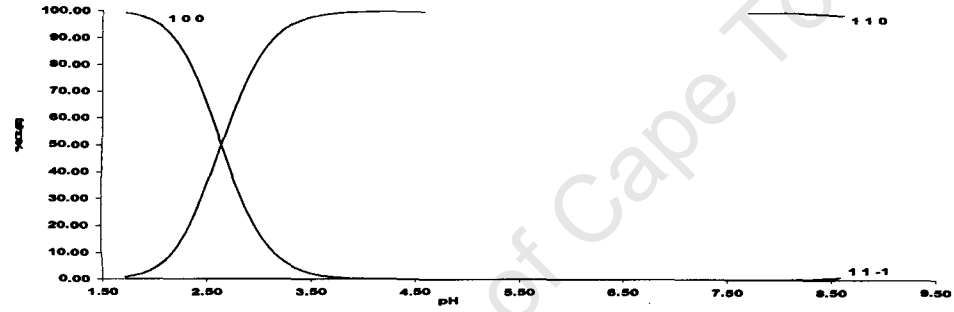

Figure 2.27: Species distribution curves of Cu(II)-PCUL as a function of pH.

Three protonation constants derived from the experimental data and are quantitatively related to the formation constants ($\log\beta_{pqr}$'s) which were used to investigate the reproducibility of the experimental data and the reliability of the evaluated β_{pqr} values. The ESTA suit of programs yielded the results given in Table 2.10, the standard deviation, R-factor and R-lim are relatively high because of small error associated with small volume of PCUL used.

Table 2.10: $\log\beta_{pqr}$ of the Cu(II)-PCUL system determined at 25°C in 0.15 mol/dm^3 (Cl^-) Na^+. std Dev denotes standard deviation in $\log\beta_{pqr}$, R_f^H is the Hamilton R-factor and R_{lim}^H its limit. The general formula of a complex is $M_pL_qH_r$ denoted by the stoichiometric coefficient pqr.

Metal-ligand complex	p q r	$\log\beta_{pqr}$	std Dev	n_T (n_P)	R_f^H	R_{lim}^H
Cu(II)-PCUL	1 1 0	15.38	0.14	1 (64)	0.04	0.01
	1 1 -1	7.45	0.18			

2.5.3.3 Zn(II)-PCUL complexation

Figure 2.28 shows a plot of Z_M-bar as a function of pL for the Zn(II)-PCUL system. The Zn(II)-PCUL complexation pattern follows that of Cu(II)-PCUL system. At pL 8.5, the theoretical and the experimental curves are similar, however, at pL lower than 8.5 the two curves differ from each other.. Since this occurs at the buffered region where no complexation is taking place, it is therefore not of concern. At pL 3.5-9.5 the Z_M-bar curve function is essentially horizontal indicating that Zn(II)-PCUL complexation is complete

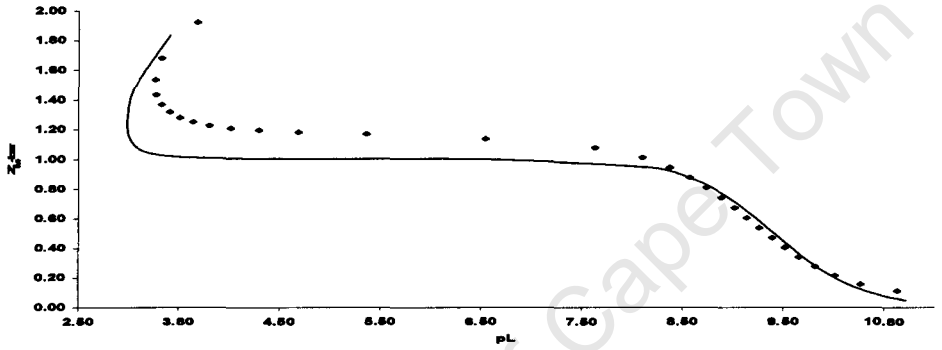

Figure 2.28: Formation function curve, Z_M-bar against pL for Zn(II)-PCUL at 25°C in 0.15mol/dm^3 (Cl^-) Na^+. M:L ratio 1:2 is displayed.

The deprotonation function Q-bar is plotted against pH for the Zn(II)-PCUL system in Figure 2.29. At pH 3.5 the Q-bar curve function is not zero, indicating that complexation of Zn(II) with PCUL occurs at the beginning of the titration. The Q-bar curve function rises and intersects the n-bar at 2 indicating that two protons have been lost upon Zn(II)-PCUL complexation at pH 5. This indicates that at this pH region the predominant species is Ml. The speciation graph in Figure 2.30 shows that at pH range 3 to 9, ~99.9% of the ML species is formed in solution. It is important to note that at pH 4- ~4.5 the theoretical and the experimental curves are similar. At pH 5-8 the Q-bar curve function run parallel to the n-bar indicating that the complexation of Zn(II) with PCUL is complete. The theoretical and the experimental curves are different to one another at pH 5 to 8; however, this is not of concern since it occurs at the buffered region where no further complexation occurs. At pH >9, ML(OH) species is formed, Figure 2.30 shows that less than 1% of this species is formed at pH range 3 to 9.

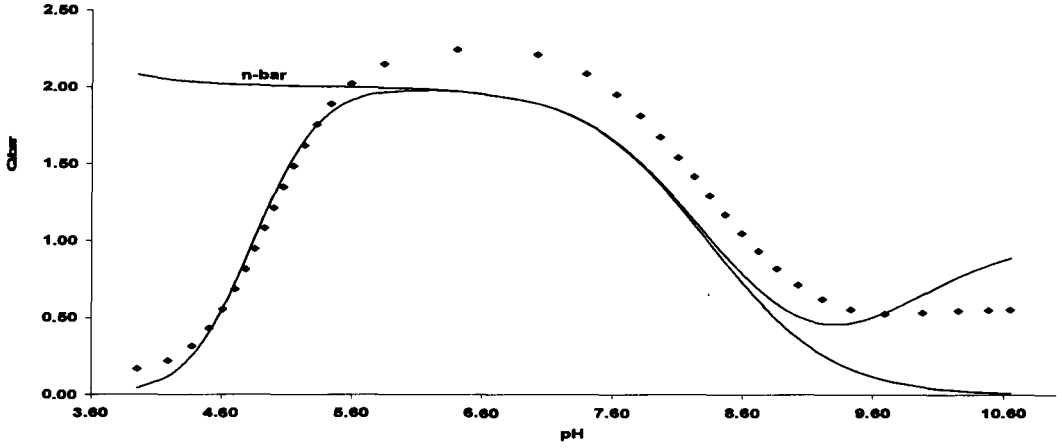

Figure 2.29: Deprotonation function curve, Q-bar against pH for Zn(II)-PCUL at 25°C in 0.15mol/dm^3 (Cl^-) Na^+. M:L ratio 1:2 is displayed. The solid line represents the theoretical curve.

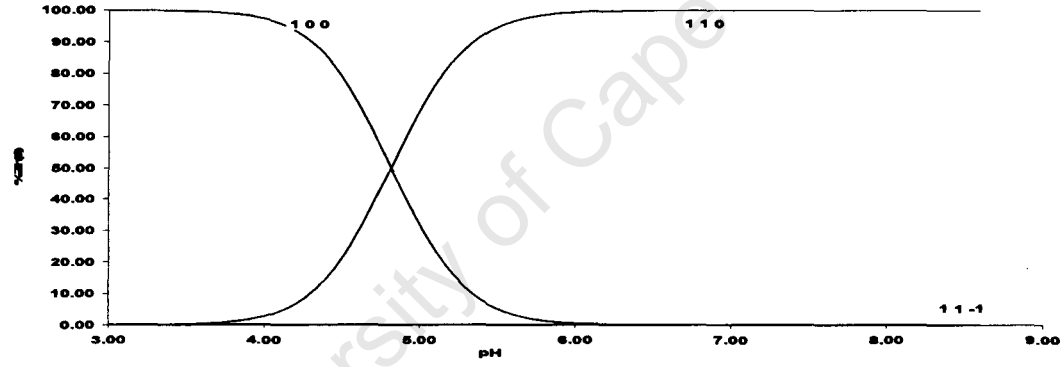

Figure 2.30: Species distribution curves of Zn(II)-PCUL as a function of pH.

The model presented in Table 2.11 resulted from the analysis of Z_M-bar curve function using the ESTA suite of programs. Similar to Cu(II)-PCUL system, R-factor and R-lim are relatively high because of small error associated with small volume of PCUL used.

Table 2.11: $\log\beta_{pqr}$ of the Zn(II)-PCUL system determined at 25°C in 0.15 mol/dm^3 (Cl^-) Na^+. Std Dev denotes standard deviation in $\log\beta_{pqr}$, R_f^H is the Hamilton R-factor and R_{lim}^H its limit. The general formula of a complex is $M_pL_qH_r$ denoted by the stoichiometric coefficient pqr.

Metal-ligand complex	p q r	$\log\beta_{pqr}$	std Dev	n_T (n_P)	R_f^H	R_{lim}^H
Zn(II)-PCUL	1 1 0	9.411	0.11	1 (58)	0.13	0.017
	1 1 -1	-0.394	0.17			

2.5.4 Discussion

The protonation constants of PCUL and the stability constants obtained from complexation of PCUL with Cu(II) and Zn(II) are discussed in relation to amine and the pyridyl groups. Figure 3.31 shows the structures of PCUL and related ligands to pyridine and amine. The proposed coordination structures for the various species found in this study are given in Figure 2.31.

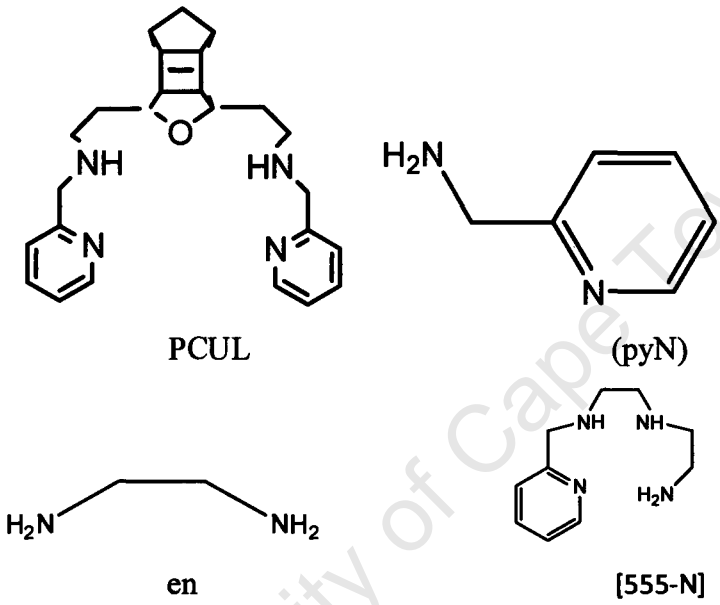

Figure 2.31: Structures of Bis-(3-aminoethy-2-aminomethylpyridine)-oxahexacyclo dodecane (PCUL), 2-(aminomethyl)-pyridine and glycine

Table 2.12: Comparison of the stepwise protonation constants of PCUL and related ligands with pyridine and amine performed in 25°C in 0.15mol/dm^3 (Cl^-) Na^+.

Species	pyN	PCUL	en[21]	555-N[21]
0 1 1	8.66	8.71	9.9	9.57
0 1 2	2.20	7.95	7.1	7.91
0 1 3		2.89		4.16

Table 2.12 shows the protonation constants determined by ESTA optimization of potentiometric data for pyN, PCUL, en and 555-N. The third equilibrium constant obtained for 555-N is higher than that of PCUL. The reason for this is that PCUL has two unsaturated n-donor pyridyl groups whereas 555-N has one pyridyl group and en has none. The unsaturated n-donor pyridyl group is a weaker base in aqueous solution than the saturated nitrogen found in en and 555-N. However, the second protonation constants obtained for PCUL and 555-N are relatively similar differing by 0.04 log units. This suggests that the secondary nitrogen donor atoms are protonated during the first stage of the protonation process in both PCUL and 555-N, while the primary nitrogen donors are protonated in the second stage of the protonation process in these two chelating agents [21]. The first protonation constant obtained for PCUL is less than that obtained for 555-N. The first protonation constant obtained for PCUL is determined for the pyridyl group which requires a very acidic solution, while for 555-N the same protonation constants is obtained for the amine group.

2.5.4.1 Complexation with Copper(II)

The Cu(II)- PCUL complexation reaction was evidences by a colour change from blue to light blue. The ESTA suit of programs gave the following species 1 1 0 and 1 1 -1 as shown in Table 2.13.

Table 2.13: Formation constants of copper(II) with PCUL and ligands related to pyridine and amine performed in 25°C in 0.15mol/dm^3 (Cl^-) Na^+.

Species	pyN	PCUL	en[21]	555-N[21]
1 1 0	9.71	15.38	10.5	18.62
1 1 -1	-0.01	7.60		7.97
1 2 0	16.13		19.7	

Table 2.31 shows the formation constants of the ligands with Cu(II). The structural formular of PCUL has two unsaturated nitrogen donor atoms which are sp^2 hybridized, which lead to greater character in bonding to the metal ion and hence more covalent bonding [**2**]. Also incorporated to the PCUL is the adamentane moiety, the rigidity of the adamentane should increase the stability of the metal by forcing the ligand into the ideal conformation for complexation [10]. It is therefore expected that

PCUL would form far more stable complexes with Cu(II) as compared to 555-N. However, Table 3.13 shows that the equilibrium constants obtained for the formation of ML and ML(OH) species for 555-N are much higher than the equilibrium constants obtained for PCUL for the same species.

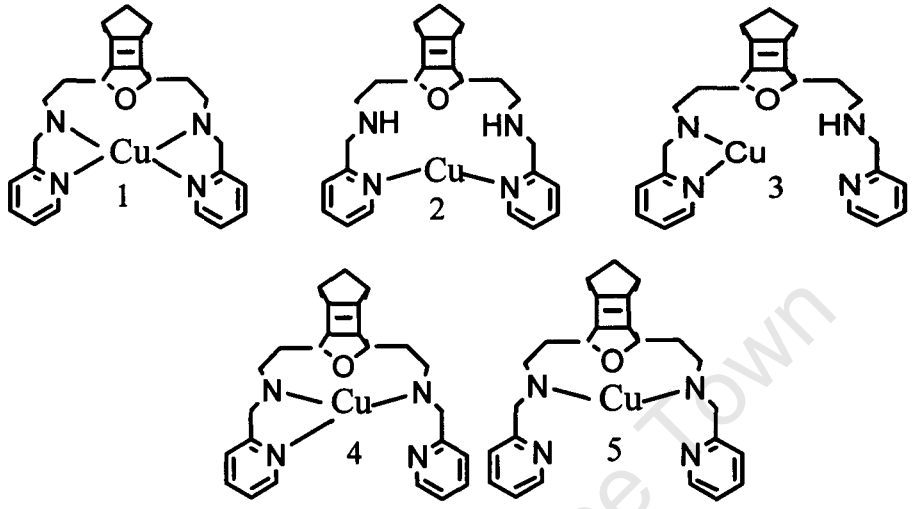

Figure 2.32: Cu(II)-PCUL coordination structures (coordinated water molecules have been omitted).

Figure 2.32 shows the proposed coordination structures which are used as a guideline for discussing the species formed in solution. 1 1 0 species seems to be the most predominant or most stable species as indicted by the results given in Table 2.13. The ML species may be formed by coordination with all four nitrogens of the PCUL ligand, resulting in structure 1. Cu(II) may coordinate with nitrogens of the pyridyl groups only resulting in structure 2, however this would be a very weak complex as the $pK_3 = 2.99$ (Table 2.12), is far less than pK_a's of both amine groups. Also, the 4th protonation could not be determined potentiometrically because it was beyond our electrode working pH range. Structure 3 represent another possible coordination pattern, the 1 1 0 species can be formed by coordination with one of the amine groups and one pyridyl group. However, this is the same as the coordination pattern of pyN system, which gave a low stability constant $\log K_{110} = 9.71$ (Table 2.13) as compared to PCUL system where $\log K_{110} = 15.38$, hence differing by 5.67 log units.

Cu(II) may coordinate with both amine groups and one pyridyl group resulting in structure 4. However, this structure is also not preferred since coordination occurs in

only three sites. Structure 5 represents a similar coordination pattern to en except that its stability would be lower than en because of the lack of a chelate effect. Since the formation constants for 1 1 0 complex of Cu(II)-en it is less than that obtained for Cu(II)-PCUL complex, structure 5 is unlikely. Therefore we can conclude that structure 1 is most likely structure for Cu(II)-PCUL complex.

1 1 0 species is subsequently converted to 1 1 -1 (pK_{11-1} = 7.60), through axial coordination of the water molecules (structure not shown).

2.5.4.2 Complexation with Zn(II)

The formation curves for Zn(II)-PCUL system follows the same complexation pattern as the Cu(II)- PCUL system. The Zn(II)-PCUL chemical model in Table 2.11 shows two complex species which are 1 1 0 and 1 1 -1 with logβ's 9.411 and -0.394 respectively. The Zn(II)-PCUL complexation begins at pH ~3.8 as compared to pH ~2.2 for Cu(II)-PCUL system. This is because the Zn(II) ion has large size as compared to Cu(II), Zn(II) does not favour the deprotonation of the amine nitrogen [3]. The stability constants obtained for the Zn(II)-PCUL system are lower than those obtained for the Cu(II)-PCUL system in accord with the expected Irving Williams stability series. Irving Williams showed that for divalent ions of the 1st transition series, the stability always follows the order Mn< Fe< Co< Ni< Cu< Zn after viewing all his data.

2.5.4.3 Conclusion

The Cu(II)-PCUL complexation reaction was evidenced by a distinct colour changes from sky blue to navy blue. The potentiometric data was put on ESTA suite of programs which gave the equilibrium and/ or formation constants. The three protonation constants obtained from ESTA optimization of potentiometric data for the H-PCUL system are pK_1= 8.71, pK_2= 7.95, and pK_3= 2.89 given in Table 2.9. The equilibrium constants together with the proposed model for the H-PCUL system were acceptable since the equilibrium constants for H-PCUL were similar to the equilibrium constants obtained for the H-Glycine and H-pyN systems. The pK_1= 8.66 and pK_2= 2.20 for the H-pyN system given in Table 2.5. For the H-Glycine system

we only compared the second equilibrium constants, pK_2= 2.38 which was assigned for the amino group. The first equilibrium constant for H-Glycine is assigned for the carboxylic group (CO_2^-) which is not found in PCUL ligand. It is important to remember that the glycine system was included in this study to check the reliability of the proposed experimental procedure.

The *in vivo* competitor, Zn(II) archived lower stability constants for 1 1 0 and 1 1 -1 species with logβ's = 15.38 and 7.60 for 1 1 0 and 1 1 -1 species respectively. Figure 2.31 shows the possible Cu(II)-PCUL structures of which through Cu(II)-PCUL, Cu(II)-en, Cu(II)pyN, and Cu(II)-555N stability constants comparisons in Table 2.13, structure 1 was the most preferred coordination structure.

References.

1. F.R. Hartley, C. Burgees, R. Alcock, *Solution Equilibrium*, 1980, 33-144, Ellis Horwood Limited, Chichester.
2. F.R. Hartley, C. Burgess, R. Alcock, *Solution Equilibrium*, 1980, 147-169, Ellis Horwood Limited, Chichester, John Wiley and Sons.
3. A.E Martell and R.J. Motekaitis, *Determination and Use of Stability Constants*, 1988, VCH, New York.
4. D.R. Williams (ed), *An Introduction to Bioinorganic Chemistry*, 1976, Charles C. Thomas Publisher, USA.
5. F.J.C. Rossotti and H. Rossotti, *The Determination of Stability Constants and other Equilibrium Constants in Solution*, 1961, 127, McGraw-Hill Book Company, Inc, New York.
6. H.H. Willard, L.L. Merritt, J.A, Dean, F.A. Settle, *Instrumental Methods of Analysis*, 1988, 7th Ed, Wadsworth Publishing Company, California.
7. M.M Hughes, *The Inorganic Chemistry of Biological Processes*, 1972, John Wiley and Sons, London.
8. M.T. Beck, I. Nagypal, *Chenistry for Hydrogen and other Cations, Principles and Practice*, 1967, Marcel Dekker, Inc, New York.
9. D.R Williams, *The Metals of Life*, 1971, Nonstrand Reinhold Company, London.
10. P.M. May, D.R Williams, *Talanta*, 1982, **29**, 249-256.
11. N.P. Nama, MSc, Dissertation, 2003, UCT, Cape Town.
12. G.Gran, *Analyst*, 1952, **77**, 661-671.
13. K. Murray and P.M May, (*ESTA*) '*Equilibrium Simulation for Titration Analysis*', 1989, version 3, UWIST, Cardiff, Wales.
14. P.M. May, K. Murray, D.R. Williams, *Tatanta*, 1985, **32**, 6, 483-489.
15. P.M. May and K. Murray, *Talanta*, 1988, **35**, 927-932.
16. A Vacca, A. Sabatini, M. A. Gristina, *Coord. Chem. Rev*, 1972, **8**, 45-53.
17. A. Voye`, PhD Dissertation, 1993, UCT. Cape Town.
18. L.G. Sillen, *Laboratory Methods in Current Use at Department of Inorganic Chemistry*, KTH, 1959, Stockholm.
19. G.E. Jackson, P.W. Linder, A. Voyer`, *Dalton*, 1996, 4605-4612.
20. K. Murray, P.M. May, *ESTA*, 1984, UWIST, Cardiff.

21. J.N. Zvimba and G.E. Jackson, *Polyhedron*, 2007, **101**, 148-158.

22. J.C. Rossotti, H. Rossotti, *J. Chem. Edu*, 1965, **42**, 375-378.

23. B.S. Furniss, A.J. Hannaford, P.W.G. Smith, A.R. Tatchell, *Vogel's Practical Organic Chemistry*, 5th Ed, Longman Scientific and Technical.

24. S. Odisitse and G.E. Jackson, *Polyhedron*, 2008, **27**, 453-464.

25. S. Odisitse, MSc Dissertation, 2003, UCT, Cape Town.

26. A. Voye`, PhD Dissertation, 1993, UCT, Cape Town.

27. J.N. Zvimba, PhD Dissertation, 2005, UCT, Cape Town.

28. A.E. Martell, R.M. Smith, R.J. Motekaitis, Texas University, College Station, Texa, 1993.

29. D.C. Cox, *Brit. Med. Bull*, 1999, **55**, 544-555.

30. M.T. Amorin, *Inorg. Chim. Acta*, 1999, **284**, 20-29.

CHAPTER 3

SPECTROSCOPY AND ANCILLARY STUDIES

3. SPECTROSCOPY AND ANCILLARY STUDIES

While potentiometry gives an accurate measure of the thermodynamic properties of the system, it does not provide any information about the structure of the species formed. For this reason spectroscopic studies were undertaken.

3.1 INFRARED SPECTROSCOPY

3.1.1 Introduction [1].

Infrared spectroscopy is certainly one of the most important analytical techniques available to today's scientists. One of the grate advantages of infrared spectroscopy is that virtually any sample in virtually any state may be studied. Liquids, solutions, pastes, powders, films, fibres, gases and surfaces can all be examined with a judicious choice of sample techniques. Infrared spectroscopy is a technique based on the vibrations of the atoms of a molecule. An infrared spectrum is commonly obtained by passing infrared radiation through a sample and determining what fraction if the incident radiation is absorbed at a particular energy. The energy at which any peak in an absorption spectrum appears corresponds to the frequency of a vibration of a part of a sample molecule. The visible part of the electromagnetic spectrum is by definition, radiation visible to the human eye. IR spectroscopy is included in this study to determine the Cu(II)-PCUL complexation sequence.

3.1.2 Experimental

$5.4x10^{-6}$ mol stock solution of PCUL was prepared in 5 cm^3 glass vial and 2.48^{-5} moles of Cu(II) was then added into the stock PCUL solution, resulting in 1:2 metal to ligand molar ratio. IR spectra were recorded at 25°C on a Perkin Elmer Spectra One FT-IR spectrometer (Overhead-ATR ZnSe top plate). The pH of the resultant solution was adjusted to pH's 2.33, 4.02 and 6.91 using NaOH or HCl. A micro-pH 2000 meter was used to measure the pH of the solution. Before running IR analysis the solutions were frees dried and the KBr discs were prepared by mixing the solid samples with KBr.

3.1.3 Results and discussion

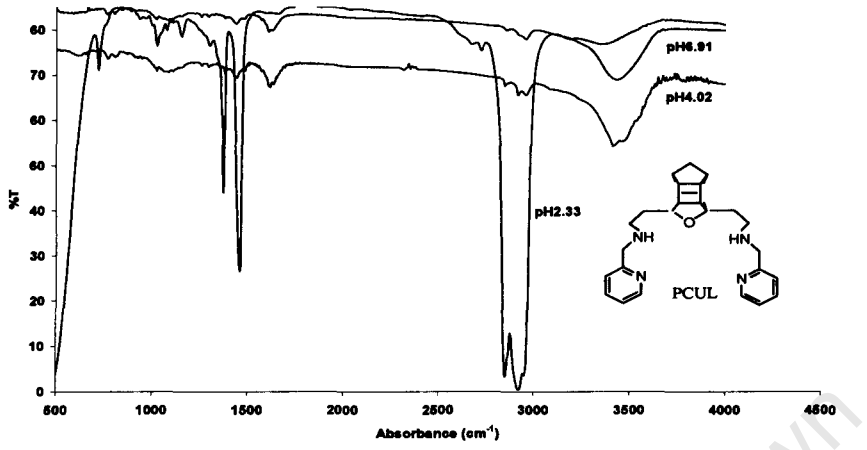

Figure 3.1: Infrared spectrum of Cu(II)-PCUL in KBr disc as a function of pH.

The infrared (KBr) spectra of Cu(II)-PCUL complex as a function of pH are shown in Figure 3.1. It was expected that the complexation would commence at pH 2.33 due to the attachment of the pyridyl groups [2]. From potentiometric results, at pH 2.68 the Q-bar curve function is 2.3 indicating that two protons are lost upon Cu(II)-PCUL complexation, Figure 3.1 confirms that complexation does occur at low pH. At pH 2.33 two absorption bands 1373 and 1459 cm^{-1} are observed. The 1373 cm^{-1} is assigned for the pyridium ion and the 1459cm^{-1} is assigned for pyridine. However as the pH of the solid complex is increased these bands disappear. At pH 4.02 the absorption bands at 3410 and 3454 cm^{-1} broaden and the intensity of these bands increases with pH. These bands are replaced by one absorption band at 3425 cm^{-1} at pH 6.91 which was assigned to the amine N-H stretching vibration in the PCUL ligand. This indicates loss of protons from the amine due to complexation. The predominant species at this pH is ML species reaching 99% formation as shown by Figure 2.27 from the potentiometric results.

All complexes exhibit a sharp maximum in the 1590-1600 cm^{-1} region attributable to the coupled stretching modes of the pyridyl C-C and C-N bands which have been shown to exhibit small frequency shift and a marked intensity increase on coordination of the pyridyl nitrogen atom [3]. At pH 4.02 the absorption band at 1609 cm^{-1} is shifted to 1607 cm^{-1} at pH 6.91. This indicates that the pyridyl nitrogen atom

is also coordinated. Steenland et.al, have assigned the 1591cm^{-1} band to a carbonyl group with strong coordination through oxygen [4]. The IR spectrum given in Figure 3.1 does not show the presence or existence of the 1591 cm^{-1} band. From this, we can therefore conclude that the adamentane oxygen is not involved in coordination.

3.2 NUCLEAR MAGNETIC RESONANCE

3.2.1. Introduction

NMR is an important tool in the investigation of chemical structures and reaction mechanisms and has been extended to whole body imaging in medical diagnosis [5]. In chemistry the use of this technique was initially restricted to the study of protons, but developments in instrumentation and procedures have resulted in the routine study of nuclei with spin other than ½ and with low natural abundances [5]. In this study, NMR was used to determine the sequence of protonation in PCUL and also to determine the coordination site of Cu(II).

The average pK_a of the protonation site can be estimated from the inflection point in a plot of the chemical shift against pH [6]. In both protonation and complexation reactions the presence of the proton or metal shifts the NMR signal arising from the protons attached to the neighbouring carbons [6]. The resulting signal is influenced by the nature of the bonding and the degree of complexation.

3.2.2 Experimental

In 5ml glass vials, 0.01358mol/dm^3 PCUL stock D_2O solution was prepared and the ^{1}H NMR spectra recorded at 300 MHz. The pH of these solutions was adjusted using concentrated NaOD or DCl. Tertiary butyl alcohol was used as an internal standard since it is not susceptible to pH changes. A micro-pH 2000 meter was used to measure the pH of the solutions. The pH of the solution may be calculated using the relationship [6]:

$$pD = pH + 0.4 \qquad 3.1$$

For copper(II)-PCUL complexation, solutions of 1:2 molar ratio of metal to ligand were prepared in D_2O and scanned in the pH range 2-11. The chemical shifts (ppm) of both protonation and complexation were plotted as a function of pH [5].

3.2.3 Results and Discussion

Figure 3.2 shows a plot of chemical shift as a function of pH where a, b, c, and d refer to chemical shift of protons attached to carbons of the pyridyl ring. Figure 3.3 shows the similar plots but for (e), (f), and (g) which refer to the chemical shift of the protons attached to the carbons next to the amine group.

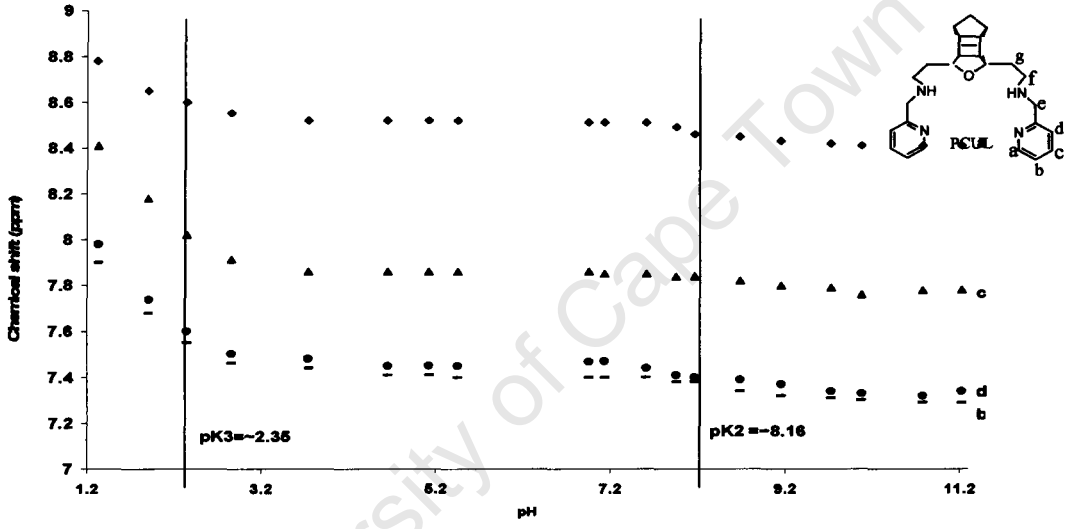

Figure 3.2: Change in proton chemical shift (ppm) for protons as a function of pH for PCUL (0.01358 mol/dm^3).

From Figure 3.2, a change in chemical shift is seen in the pH range 1.2 – 3.2. However as the pH of the solution increases, no dramatic change is seen as the chemical shift curves level off. The last protonation constant (pK_a) of 2.35 which is assigned for nitrogen of the pyridyl group was estimated from the inflection point in the chemical shift. This pK_a is similar to pK_2 = 2.38 of glycine and pK_3 = 1.95 of PCUL determined by potentiometry.

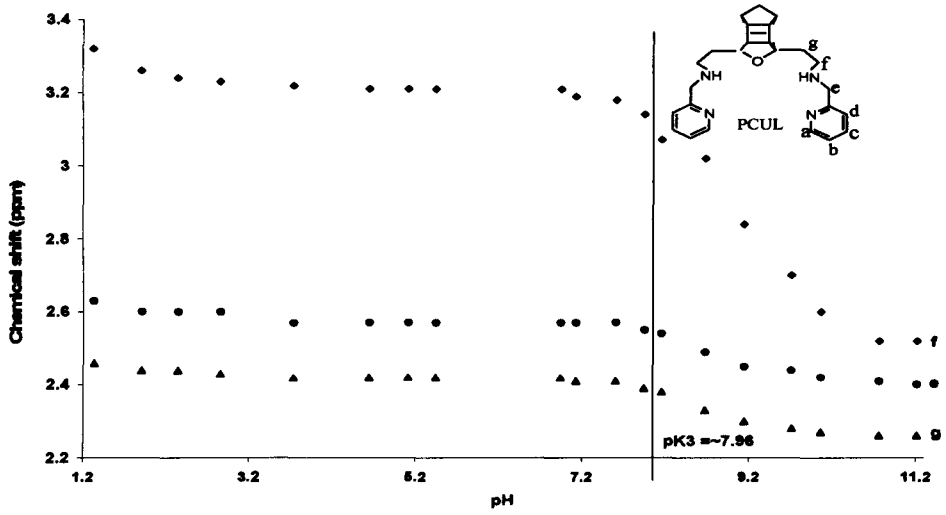

Figure 3.3: Change in proton chemical shift (ppm) for protons as a function of pH for PCUL (0.01358 mol/dm^3).

Figure 3.3 shows that there is no significant change in the chemical shift of e and g but for f proton signal, a dramatic change in chemical shift is observed at pH 7.2-9.2 region. This is a clear indication that the central amines are undergoing protonation. Theoretically, a significant change in chemical shift is observed in protons attached to carbons closest to the protonation site and Figure 3.3 confirms this theory. The protonation constant, pK_a 8.16 assigned for nitrogen of the amine group was estimated from the inflection point in the chemical shift and is close to the two pK_a's 8.17 and 7.56 determined potentiometrically.

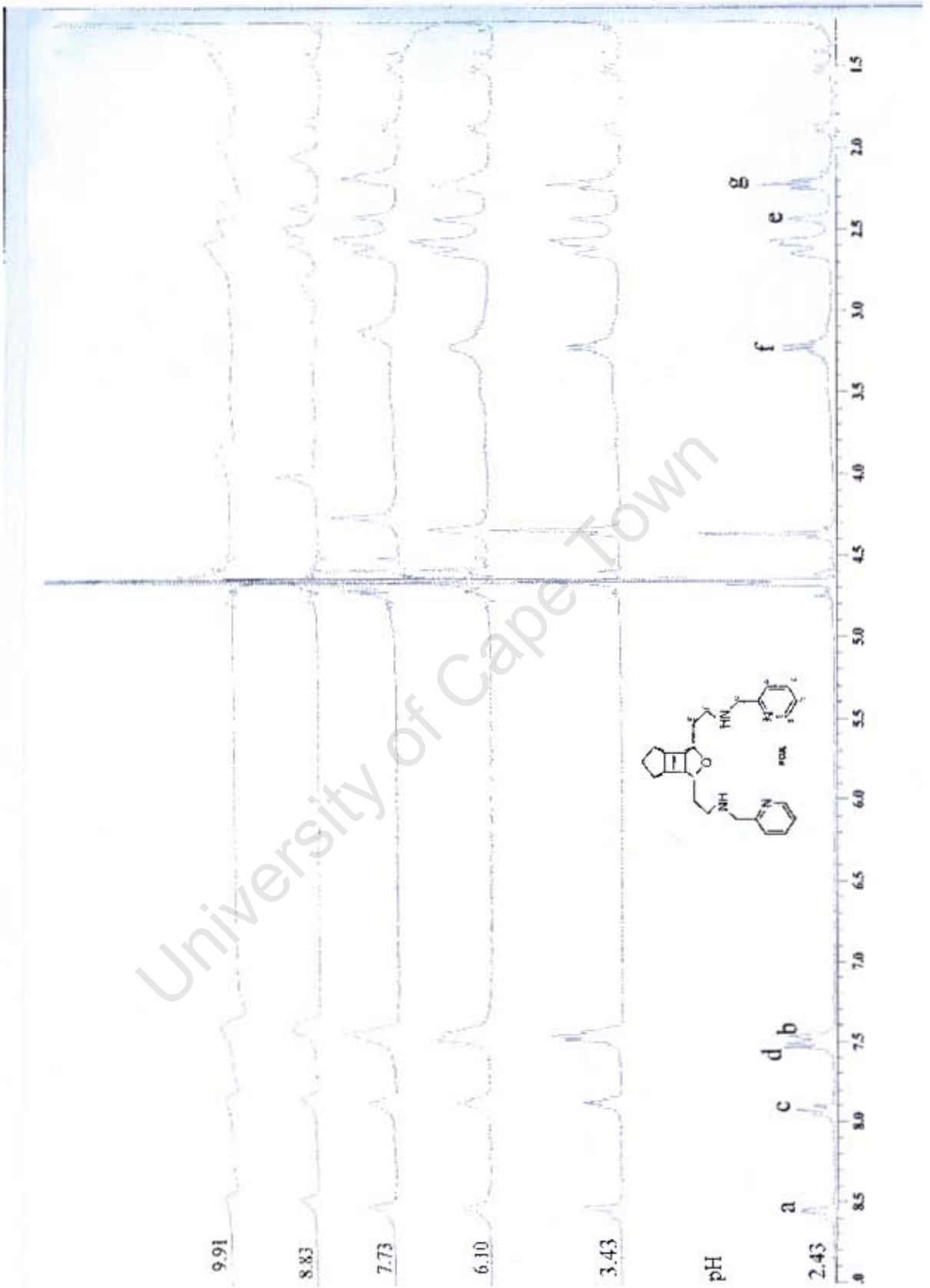

Figure 3.4: Proton NMR spectra for complexation of copper(II) with PCUL as a function of pH.

Figure 3.4 shows the effect of Cu(II) on the proton spectrum of PCUL. Cu(II) is paramagnetic, which can affect both the chemical shift and relaxation time of the protons [3]. This manifests itself as broadening and shifting of the NMR signals [3]. The broadening effect is usually more apparent unless there is pseudo-contact shifts. For non-macrocyclic ligands Cu(II) exchange is normally very rapid, hence only an average spectrum will be seen [3]. The spectrum shows that at pH 2.43 complexation occurs. The e proton signal remain relatively sharp while a, b, c, d, f, and g proton signals broaden with increasing pH and eventually disappear.

A significant broadening is observed for the f proton signal which disappears first. This suggests that complexation begins at the central amine. The fact that the pyridyl protons also broaden indicates that this group is also coordinated. The proton signals do not broaden at the same rate; this indicates that they are not at the same distance from the metal ion. Since this is a dynamic system it is not possible to conclude that both central amines are coordinated at the same time. It is possible for copper(II) to be rapidly exchanging between the two sites. Figure 3.5 shows a possible coordination pattern for the Cu(II)-PCUL complex.

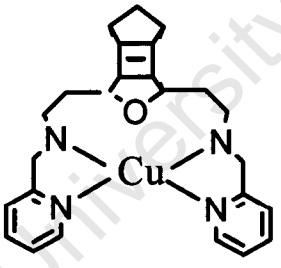

Figure 3.5: Cu(II)-PCUL coordination pattern.

The potentiometric results given in pages 77-80 show that the preferred coordination structure is structure 1. These findings confirm the NMR results since Figures; 3.2 and 3.3 indicated that the protons closest to the protonation site will be deprotonated first and hence Cu(II) will complex in those sites first (Figure 3.4). Thus Cu(II) complex with central amine 1st then coordinate with the pyridyl-nitrogens.

3.3 UV-VIS Analysis

3.3.1 Introduction

The formation of the different complexes can be followed by UV-visible spectrophotometry because distinct colour changes occur as a result of the changing speciation of the solution with pH [7]. The variety of colours among transition metal complexes arise from electronic transitions between energy levels whose spacing correspond to the wavelengths available in visible light [7]. These transitions in complexes are frequently referred to as *d-d* transitions because they involve molecular orbitals that are mainly metal *d* in character [7]. The electronic spectra of complexes can provide valuable information relating to bonding and structure since spacing depends on factors such as geometry of the complex, the nature of the ligand present and the oxidation state of the central metal ion [7].

UV-visible spectrophotometry can in fact be used as a supplementary technique to glass electrode potentiometry for quantitative analysis of equilibrium reactions, thereby determining formation constants [8]. This technique can be used diagnostically for determination of the number of possible chemical models present in solution not available with potentiometry, by carrying out a graphical or computer based rank analysis of the wavelength absorbance matrix [7, 9]. However, UV-visible spectroscopy does not evaluate stability constants as precisely as potentiometric data. This is due to the fact that UV-visible spectra of most complexes contain broad overlapping absorption bands and parameter correlation arises [9]. The potentiometric data may lead to a more precise analysis of the wrong model, whereas spectrophotometric data will indicate the correct model but give a less precise analysis of it [9]. Hence it is necessary to combine both spectrophotometric and potentiometric data for defining the chemical model and for evaluation of the stability constants respectively [9].

3.3.2. Electronic Spectra of Metal Complexes.

Electronic spectra from transition metal ions and complexes are observed in the visible and ultraviolet regions [10]. The spectra arise because electrons may be promoted from one energy level to another. The absorption spectra show the particular wavelengths of light absorbed, that is the particular amount of energy required to promote an electron from one energy level to a higher level, while emission spectra show energy emitted when the electron falls back from the excited level to a lower level [10].

The following selection rules are pertinent to electronic absorption spectroscopy:

1. Transitions between states of different multiplicity are multiplicity forbidden, i.e., electronic transitions in which the spin of an electron changes are forbidden [11].
2. In a molecule with a centre of symmetry, transitions between two gerade (g) or two ungerade (u) states (i.e., g→ g or u→ u) are Larport forbidden. The allowed transitions are g → u and u→g [11].

Rule 1 indicates that a d^2 configuration in an octahedral field would have three transitions that are spin allowed;

$^3T_{1g} \rightarrow {}^3T_{2g}$
$^3T_{1g} \rightarrow {}^3A^{2g}$
$^3T_{1g} \rightarrow {}^3T_{1g}$ [7].

As a result of rule number 2, *d-d* transitions in octahedral complexes are Larporte forbidden and therefore many complexes will not have intense colours [10]. However, there are mechanisms by which selection rules can be relaxed so that transitions can occur, even if only at low intensities [11]. Most ions do not have perfect symmetry and are distorted so that the centre of symmetry is destroyed, resulting in mixing (hybridization) of d and p orbitals [11]. Thus *d-d* transitions of octahedral complexes result in low-intensity spectra [10]. Tetrahedral complexes

often absorb more strongly than octahedral complexes of the same oxidation states [10]. The bands associated with formally spin forbidden transition gain enough intensity to be observed because the spin selection rule breaks down somewhat in complexes that exhibit spin-orbit coupling. The spin-orbit coupling and Jahn-Teller distortions often lead to more complex spectra than predicted with the spin selection rule [10].

3.3.3. Electronic Spectra of Copper Complexes

The aqueous chemistry of copper is largely devoted to copper(II) compounds because copper(I) compounds are quite unstable in aqueous solution [12]. Cu^{2+} has an incomplete *d* shell configuration (*Ar*) d^9 and its complexes are predominantly paramagnetic and highly coloured [12]. The d^9 electronic configuration is the whole equivalent of d^1 configuration [13]. Arising from these configurations is only the one Russell-Saunders term or free ion ground state, namely ^2D, which has the E_g and T_{2g} crystal field components [13]. In essentially an octahedral field the 5 degenerate d-orbitals are split, due to their spatial arrangement, into 2 higher energy E_g and 3 lower energy T_{2g} orbitals or electron wave-functions with energy difference of 10Dq (ligand field splitting). For the d^9 electronic configuration the ground state of the complex is given by ^2E_g and the excited state, at energy of 10Dq above this, by ^2T_g, which is the inverse of the d^1 case. Thus essentially only one absorption band occurs in the visible region of copper(II) complexes due to the *d-d* transition, of which λ_{max} is an indication of the ligand field stabilization energy,10Dq [13].

Furthermore, not only does the nature of the ligand but also the number of ligands in the coordination sphere of the metal ion affects the size of 10Dq [11]. For example the series of ammine aqua cupric complexes $[Cu(H_2O)_{6-n}(NH_3)_n]^{2+}$, shows absorption maxima at 790, 745, 680, 645, 590 and 640nm for n= 0 to 5, respectively [11]. Based on this trend it was thought that by evaluating λ_{max} of the individual species, this would indicate the particular coordination involved [11].

The ligand strengths of amines towards copper(II) are in the order NH_3> RH_2> R_2NH> R_3N [12]. In aqueous solution Cu^{2+} ion has absorption and magnetic spectra which can be interpreted in terms of tetragonally distorted $[Cu(H_2O)_6]^{2+}$ ion, the value

of difference in energy between orbitals (10Dq) being 12,500cm^{-1} [12]. The ligand field strength of water compared to other donors is shown by the order; Cl < H_2O < pyridine < NH_3 < 1,2-diaminoethane [14]. The ligands considered are those containing donor groups likely to be encountered in biologically-important molecules, especially proteins [15]. The donor atoms are: N(amino), N(peptide), N(imidazole), O(carboxylate), O (peptide), H_2O and OH^{-1} [12]. The λ_{max} (ν_{max}) of the *d-d* band (aqueous solution spectra) can be expressed as the sum of individual ligand-field contributions from the four donor atoms which, with copper, define the square plane [14].

Several complexes of copper(II) with polydentate ligands containing nitrogen have been studied and the type of complex formed by copper(II) with these ligands depend on both the number of the donor atom and the steric requirements of the ligand molecule [14]. Copper(II) peptide complexes have been studied as models for copper(II)-proteins interactions [14]. It was observed that strong copper(II)-N(peptide) bonds are formed when protons are ionized from peptide nitrogen atoms [14].

Billo has proposed a method for calculation λ_{max} for a tetragonally distorted Cu(II) complex, with axially coordinated water molecules [14]. This is calculated by the formula;

$$\nu_{calc} = \sum \nu_i \qquad 3.2$$

Where ν_i (x10^{3}cm^{-1}) is the energy contribution by atom i. From the above equation the contributions of each peptide and amino nitrogens to the ν_{calc} are:

$$\nu_{(amino)} = (4.53 \pm 0.07)\ x10^3\ cm^{-1} \qquad 3.3$$

$$\nu_{(peptide\ group)} = (4.85 \pm 0.04)x10^3\ cm^{-1} \qquad 3.4$$

$$\nu_{(carbonyl,\ H_2O,\ OH^-)} = (3.01 \pm 0.03)x10^3\ cm^{-1} \qquad 3.5$$

A value of 3.38x10^3 cm^{-1} was reported for oxime nitrogen [Cu(H_2dmg) Cl_2] (H_2dmg = dimethyloxime, λ^{max} = 770nm) [14]. The effect of the rest of the atoms of the ligand molecule is assumed to be either negligible or additive onto the direct effect of the coordinating atom via the molecular framework [14].

Billo's equation can predict λ_{max} of several of these types of complexes with good accuracy; however, the equation cannot predict absorption maxima of mixture which are likely to be present in solutions containing axially coordinating solvent molecules such as water [14].

3.3.4. Data Analysis

A solution of metal ion and ligands will normally contain a number of different species at different concentrations [9]. These species will contribute to the absorption spectrum and thus the spectrum will be the sum of all the species present [9]. Obtaining the spectrum of a single species is rather impossible unless it is the only species present.

The concentration of species in a system may be determined by measurement of the absorption of radiation by the species [9]. A relationship relating concentration of the absorption is the Beer-Lambert law, which can be expressed in the following formula [9];

$$\log_{10} (I_o/I) = \varepsilon \, cb \qquad 3.6$$

where $\mathbf{I_o}$ and **I** are the intensities of incident and transmitted radiation respectively, **c** is the molar concentration of absorbing species, **b** is the thickness of absorbing layer and ε is the extinction coefficient [9]. The term $\log (I_o/I)$ is called the absorbance and is represented by the symbol **A**, with this law becoming, $A = \varepsilon \, cb$ [11]. The Beer-Lambert Law can be expended to give a linear combination of terms for each individual species, for electronic absorption spectra of solution containing more than one absorbing species as follows;

$$A_{obs}^{\lambda} = \varepsilon_1^{\lambda} c_1 l + \varepsilon_2^{\lambda} c_2 l + \varepsilon_3^{\lambda} c_3 l + ... + \varepsilon_n^{\lambda} c_n l \qquad 3.7$$

where ε_1^{λ}, ε_2^{λ} and ε_n^{λ} are molar absorptivition coefficients of species 1,2 and n at the same wavelength λ and c_1,c_2 and c_n are their respective concentrations [9]. If the path length is given in cm, ε_n^{λ} is the molar absorption coefficient of the n^{th} species in

solution at wavelength λ and has value of ε_3 equal zero, then it does not absorb in the chosen spectral region and therefore does not influence A_{obs}^{λ} [9].

Complexometric solutions may be made up of a number of solutions of different metal ligand concentrations and pH [9]. The spectra of the individual species can be calculated by solving a set of linear equations (equation 3), if the UV/visible spectra of these solutions are obtained at a number of wavelengths [9]. It is advisable to adjust the pH of the metal-ligand complex solution by using strong acids and alkalis such as HCl and NaOH since they do not absorb appreciably in the spectral region of interest [9].

Calculation of ε can be done using a specially designed computer program that requires an input file with all the information relevant to the chemical system being studies, which includes amongst other parameters the concentration values of each chemical species present in the reaction [9]. These concentration values are calculated on the basis of the stability constants determined from potentiometric analysis [9]. The values of ε are then plotted against wavelength to give a spectrum showing the absorption bands of each chemical species [9]. The existence of a smooth spectrum is not inherent in the data analysis since the data is analyzed independently at each wavelength, so if one is obtained it lend confidence to the proposed potentiometric model [9]. A wrong chemical model is indicated by a disjointed spectrum, which will be formed when the stability constants and the concentrations are incorrect [9]. After having electronic absorption spectral information for each of the complex species the nature of the ligand field environment of the central metal ion can be deduced [9].

3.3.5. Experimental

Spectrophotometric titrations were performed for PCUL-Cu(II) complexation. An aqueous solution containing 1:2 metal to ligand ratio was prepared and measured over the pH range of 2-11. During titration the pH of this solution was adjusted by adding small amount of concentrated NaOH or HCl and the solutions were kept at 25°C. The titrations were carried out manually allowing for the measurement of absorbance versus wavelength measured out after each addition of the titrant . The absorbance readings were taken automatically at 2nm interval in the wavelength range of 340-820 nm Hewlett Packard 8452A Diode Array Spectrophotometer.

3.3.6 Results and discussion

Distinct colour changes were observed in Cu(II)- PCUL as the pH of the solution was increased.

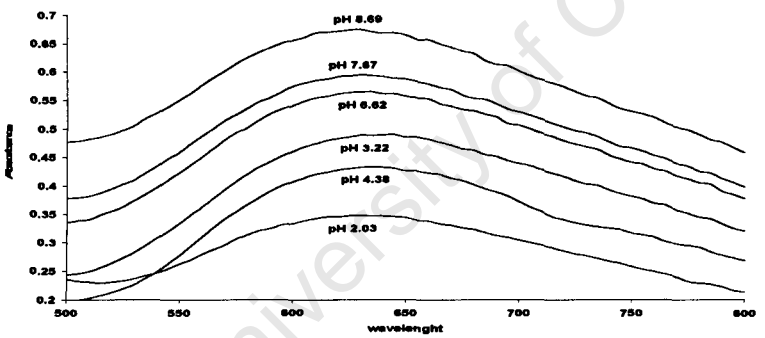

Figure 3.6: Electronic spectra of the Cu(II)-PCUL solution at 1:2 metal to ligand ratio as a function of wavelength (nm).

Figure 3.6 shows the absorption spectra for Cu(II)-PCUL system versus pH which are obtained in the pH range 2.03-8.69. The observed broad absorption bands for these species are due to the expected $^2A_{1g}$ $^2B_{1g}$, $^2B_{2g}$ ^2E_g $^2B_{1g}$, characteristic of d^9 tetragonally distorted Cu(II) complex [16]. As the pH of the solution is increased, a shift in absorbance (λ_{max}) is observed indicating the presence of different Cu(II)-PCUL species. Figure 3.6 shows that at pH 2.03, an absorption maximum of 645nm is observed indicating that there is already complexation at the beginning of titration.

At pH 2.03 the predominant species is 1 1 0 with $\log K_{1\,1\,0} = 15.38$ as given in Table 2.10. As the pH of the solution is increased a shift in absorbance (λ_{max}) is observed indicating an increase in the formation of the 1 1 0 species. This is also seen from Figure 2.26 where at pH 3.5 to 8.5 1 1 0 species is dominant. The predominant species at pH 2.03 to 8.69 is 1 1 0 species since 1 1 0 species reaches 99 % formation at pH > 8.5, thus only 1 % of 1 1 -1 species is formed at this pH therefore we did not need to calculate to calculate the absorbance of individual species.

Table 3.1: Wavelength absorbance maxima (λ_{max}) corresponding to molar extinction coefficient (ε) of the ML and ML(OH) species.

pH	Species	ε (dm^3/ mol/ cm)	Wavelength (nm)
2.33	1 1 0	36.06	645
8.69	1 1-1	50.04	630

From Table 3.1, the molar extinction coefficient (ε) and λ_{max} for 1 1 0 and 1 1 -1 species increase with increasing pH. However, the wavelength decreases with increasing pH. Hence the value of ε increase in the order 1 1 0 < 1 1 -1.

3.4 THE BLOOD PLASMA MODEL

In biological systems metal ions play an important role [17]. Metal ions such as calcium(II), magnesium(II), iron(II), cobalt(II), copper(II) and zinc(II) are considered to be essential for health in human [17]. The greater percentage of metal ions is bound to proteins in biological fluids [19]. Only a small fraction of these is bound to low-molar-weight (l.m.w) compounds, mainly amino acids [19]. There are also metal ions that are considered to be toxic to the human system and they tend to compete with the essential metal ions for binding sites on the ligands of blood plasma [20]. Such metal ions include; palladium(II), mercury(II) and cadmium(II) [20]. In biological fluids, free (hydrated) metal ions exist only at extremely low concentrations and these concentrations cannot play a significant role in physiological processes [19]. Metals bound to l.m.w. compounds play a major role in many biological and physiological processes such as; intestinal absorption, cell absorption and renal excretion [20]. The l.m.w complexes are believed to be involved [20];

1. as intermediates when metal ions are inserted into or removed from certain metalloenzymes or carrier proteins,
2. in the transfer of certain metal ions across membranes,
3. in keeping essential metals in solution and
4. in altering the potential of certain redox couples.

Copper is a biologically essential metal ion [15]. In blood plasma, 90% of the copper is irreversibly bound to ceruloplasmin, 10% is reversibly bound to serum albumin, and a small amount, <1%, is distributed amongst low molecular weight complexes, predominantly [Cu(hisdinate)(cystinate)] [15]. In patients with inflammatory disease, elevated plasma copper levels are found and these levels return to normal upon remission [21]. While the role of copper is unclear, it is thought that it is the low moleculer weight fraction which is responsible for the anti-inflammatory activity, possibly by making the copper available to superoxide dismutase [21].

It is important to note that the total concentrations of Mn(II), Fe(II), Cu(II), Zn(II) and Pb(II) in normal blood plasma are between $1x10^{-1}$ and $2x10^{-5}$ mol/dm^3 [19]. Hence the corresponding minute concentrations of the respective free ions are far below the limit of detection by any other analytical technique [19]. However, it is also very difficult to obtain information from large chemical systems due to their complexity [19]. Therefore it is not presently possible to set up a single simulation of blood plasma because of large number of compositions found in the plasma, as the model contains all the species present in blood plasma and as a result computer models simulating the complex systems have been developed [19, 17].

In order to understand the effect of the ligand on the equilibria, formation constants for the ligand together with the species determined *in vitro* are entered in the ECCLES (Evaluation of Constituent Concentration in Large Equilibrium Systems) [17]. ECCLES solves the relevant mass balance equations and displays the resulting species distributions in ordered way to enable changes in concentrations of major complexes to be readily monitored [17]. Formation constants of the ligand (drug) and the species of interest determined *in vitro* are incorporated into the database in order to understand the effect of the ligand on the equilibrium present in this model [17].

This database, on inclusion of the ligand concentration, is interrogated by the ECCLES computer program to yield results pertaining to the influence of this ligand on these equilibria [17]. MIX is one of the major features of ECCLES which generates estimate of the equilibrium constants for the many mixed (ternary) complexes that might be important in the blood plasma [17].

Considering the blood plasma compartments as a closed system, the blood plasma mobilizing index (p.m.i) is a convenient measure of the ability of the chelating agent, at a given concentration, to mobilize metal-ions from the labile protein-bound fraction [19].

The design of copper-based anti-arthritic agents is based amongst other properties on the ability of the ligand to bind strongly and selectively to the metal ion of choice as reflected by the p.m.i [18]. The p.m.i is defined as the ratio of the total concentration of low moleculer weight metal complex species in the presence of the drug to that of the normal plasma [17]. In addition, the p.m.i is a measure of the ability of the administered ligand to move metal ion to the low molecular weight (l.m.w.) fraction [17]. It is based on the premise that the free concentration of the metal ion is buffered and hence held constant during any reasonable perturbation [17]. The calculation of p.m.i takes into account competition between the ligand and all the endogenous metal ions and low molecular mass ligands present in blood plasma [17].

3.4.1 Simulation Studies

In order to establish the true selectivity of PCUL for Cu(II) over Zn(II) *in vivo*, the plasma mobilising index (p.m.i) was calculated. The inclusion of Zn(II) is due to its high concentrations in blood plasma relative to Cu(II) [20]. A comparison of the stability constants alone is not enough to conclude the stability of Cu(II)-PCUL in blood plasma because of high concentration of Zn(II) in plasma which may compete for the ligand [18]. The total ligand concentration in the calculations was raised over the range 10^{-00} -10^{-10} mol/dm^3.

The Cu(II)-PCUL p.m.i was calculated by incorporating the formation constants measured in potentiometric studies into the computer model of blood plasma [18].

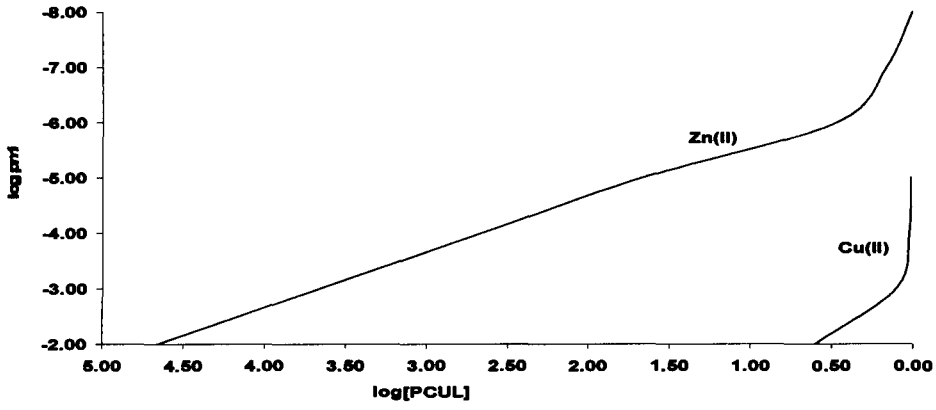

Figure 3.7: Logarithms of Cu(II) and Zn(II) plasma mobilizing indices as a function of log[PCUL].

The pmi curves for Cu(II) and Zn(II) with PCUL as a function of log[PCUL] are given in Figure 3.7. The potentiometric studies in Chapter 2 show that PCUL forms far more stable complexes with Cu(II) than with Zn(II). However, Figure 3.7 shows that PCUL mobilises Zn(II) more than Cu(II) in blood plasma. The reason for this is the relatively high affinity of PCUL for Zn(II) than Cu(II). This proves that looking at the stability of Cu(II) alone is not sufficient because as in this case Zn(II) being present in much higher concentration is able to compete for PCUL [22]. This also shows the importance for simulation models and inclusion of other completing metal ions in the study [3]. The curves in Figure 3.7 show PCUL mobilizing ability is in the order Zn(II) > Cu(II).

3.5 Octan1-1-ol/ water Partition Coefficient

3.5.1 Introduction

Hydrophobicity is often used to describe the free energy changes involved in the movement of a drug from the aqueous phase to the lipid bilayer but may also be important in the binding of the substrate to the macromolecular active site [23].

The most widely used physical property for predicting the biological effects of an organic chemical is the partition coefficient (P_{ow}) [24]. Since we intent to determine the hydrophobicity of Cu(II)-complex as a drug, P_{ow} is defined as the ration of the equilibrium concentration of a dissolved Cu(II)-complex in a two phase system consisting of two largely immiscible solvents, 1-octanol and an aqueous phase [25]. This can be expressed by the following equation [25]:

$$\log P_{ow} = \log ([Cu_2^+]_{org} / [Cu_2^+]_{aq}) \qquad 3.9$$

Where $[Cu_2^+]_{org}$ and $[Cu_2^+]_{aq}$ are the concentrations of Cu(II) in organic phase and aqueous phase respectively.

Speciation changes with pH and the different species have different partition coefficients, hence the amount of the Cu(II) transferred from aqueous solution to organic layer changes with pH [6]. In order to enhance the transport of a chelating ligand across membrane *in vivo*, it is useful to enhance the hydrophobicity of the chelating agent so as to improve its tissue permeation and therefore minimize loss of the complexes formed from the body via renal filtration [16]. In this study, 1-octanol/water partition coefficients were determined in order to predict and provide an estimation of the trans-dermal transport of the Cu(II)-PCUL complex

3.5.2 Experimental

Traditionally, the experimental method for determining $logP_{ow}$ is the shake-flask (SF) method, which is adapted as the standard OECD (Organisation of Economic Co-operation and Development) method [25]. The SF method is not suitable for highly hydrophobic compounds because of the formation of octanol emulsions in aqueous phase [25]. To overcome the formation of emulsions in the aqueous phase which is the limiting factor for SF a column generator technique and a slow-stirring (SS) methods were developed [25]. Since the SS method requires long equilibration times of between 2 and 5 days, SF technique became a method of choice in our study [16].

1ml of Cu(II) (0.005 mol/dm^3)-PCUL (0.018 mol/dm^3) solutions were mixed in 4 ml pill vials and adjusted to pH's 2, 3, 4 and 7 using NaOH. After adjusting pH, 1 ml of 1-octanol/water was added into each solution. The solutions were then shaken for 7 minutes and allowed to stand at constant temperature so as to allow the two phases to separate.

3.5.3 Results and Discussion

Table 3.2: $[Cu^{2+}]$ in 1-octanol and Cu(II) in water for the determination of $logP_{ow}$ as a function of pH.

pH	$[Cu^{2+}]_{organic}$	$[Cu^{2+}])_{aqueous}$	$logP_{ow}$
2.33	11.1	130	-1.069
3.34	7	141	-1.305
4.02	10.5	119	-1.055
6.91	6.8	132	-1.288

Average $logP_{ow}$ = -1.18

The results obtained for partition coefficient are given in Table 3.2. From these results the average $logP_{ow}$ for Cu(II)-PCUL complex was calculated in order to predict the lipophilicity of this complex. For a drug to be considered lipophilic, the $logP_{ow}$ value should be at least 0.6 [16]. Table 3.2 shows that at pH range 2.33-6.91

$logP_{ow}$ values are negative (-1.069, -1.305, -1.055, -1.288), indicating that Cu(II)-PCUL complex have some hydrophilic character which is enhanced by the adamentane cage moiety. Octan-1-ol/ water partition coefficient values have been reported recently for highly hydrophobic ($logP_{ow} > 6$) and highly hydrophilic ($logP_{ow} <-2$) substances [24].

The potentiometric studies in Chapter 2 show that the predominant species in solution is ML at pH range 2.33-7. Therefore we can conclude that at this pH range the ML species of Cu(II)-PCUL complex is hydrophilic and this is confirmed by the negative average $LogP_{ow}$ (-1.18) of this complex.

3.5.4 Conclusion

In this Chapter distinct colour changes from light blue to navy blue were observed for all experiments namely; blood plasma, infrared and octan-1-ol/ water partition coefficient. These colour changes were the result of increasing pH upon addition of of NaOH and or NaOD. These changes were the indication of Cu(II)-PCUL complexation pattern. Figures; 3.2 and 3.3 show that the deprotonation of PCUL ligand begun at the amine protons with logK's $_{011}$ = 8.71 and 7.91, then the pyridyl protons with $logK_{012}$ = 2.89. Figure 3.4 further proved that the Cu(II) coordinate to the amine group first with $logk_{110}$ = 15.38.

The absorption bands of interest were observed from the infrared KBr spectra in Figure 3.1. These bands are; 1373 and 1459 cm^{-1} which are assigned for the pyridium ion and pyridine respectively. The N-H bands are seen at 3410 and 3454 cm^{-1} at pH 4.02. These bands broaden with increasing pH and are replaced by one absorption band at 3425 cm^{-1} at pH 6.91. At pH 2.33 the pyridium ion and pyridine absorption bands showing complexation of Cu(II)-PCUL complexation were observed in Figure 3.1 with $logK_{110}$ = 15.38 at pH 2.0 from the potentiometric results. Cu(II)-PCUL complexation is also observed from Figure 3.6 at pH 2.02 with maximum absorbance of 645nm. It is important to note that at pH > 8.5, 1 1 -1 species formation was only 1%, thus 1 1 0 species is still dominant at pH > 8.5 reaching 99% formation in Figure 2.27.

PCUL mobilized Zn(II) more than Cu(II) in the blood plasma as shown in Figure 3.7. In blood plasma Zn(II) is available in much higher concentration than Cu(II), however since PCUL have pyridyl groups it was important to investigate if the pyridyl groups and adamentane incorporated in PCUL ligand would enhance the mobilization ability of the PCUL for Cu(II) over Zn(II).

References.

1. B.H. Stuart, *Infrared Spectroscopy: Fundamentals and Application*, 2004, John Wiley and Sons, Ltd.
2. D.J.Barnes, R.L.Chapman, F.Stephen & R.S.Vagg, *Inorg. Chim. Acta*, 1981, **51**, 155.
3. S. Odisitse and G.E. Jackson, *Polyhedron*, 2007, **27**, 453-464.
4. M.W.A. Steenland, P. Westbroek, I. Dierak, G.G. Herman, W. Lippens, E. Termmerman, A.M. Goeminne, *Polyhedron*, 1999, **18**, 3417.
5. P. Letkeman, *J. Chem. Edu*, 1979, **56**, 348.
6. S. Dougal, D. Hague, A. Morenton, *J. Chem. Soc, Dalt. Trans*, 1987, 2897.
7. J.E. Hunneey, E.A. Keiter, A.L. Keiter, *Inorganic Chemistry, Principles of structure and Reactivity*, 4thEd, 1993, Harper Collins College Publishers, New York.
8. H. Mailhot and R.H. Peters, *Environ. Sci. Technol*, 1988, **22**, 1479-1488.
9. F.R. Hartley, C. Burgees, R. Alcock, *Solution Equilibrium*, 1980, Ellis Horwood, Ltd, West Sussex.
10. J.D. Lee, *Concise Inorganic Chemistry*, 4th Ed, Chapaman and Hall, 1991, London.
11. H.H. Jaffe, M. Orchin, *Theory and Applications of Ultraviolet Spectroscopy*, 1962, John Willey and Sons, London, 509.
12. G. Wilkinson, R.D. Gillard, J.A. McCleverty, *Comprehensive Coordination Chemistry*, 1987, **3**, Pergamon Press, Oxford.
13. A.B.P. Lever, *Inorganic Electronic Spectroscopy*,1968, Elsevier, Amsterdam.
14. E.J.Billo, *Inorg. Nucl .Chem. Letters*, 1974, **10**, 613-617.
15. G.E.Jackson and M.J.Kelly, *Inorg. Chim. Acta*, 1988, **152**, 215-217.
16. J.N. Zvimba and G.E. Jackson, *J. Inorg. Bio*, 2007, 148-158.
17. P.M. May and D.R.Williams, *Febs Letters*, 1977, **78**, 134-138.
18. T.E. Nomkoko, G.E. Jackson, B.S. Nakani, W.K.A. Louw, J.R. Zeevaart, *Dalton*, 2004, 741-749.
19. H. Faure, A. Favier, in; *Handbook of Metal-ligand Interactions in Biological Fluids, Bioinorganic Chemistry*, **2**, 1163-1169, (Ed) Berthon G, Marcel Decker, Inc, New York,

20. P.M. May, P.W. Linder, D.R. Williams, *J. Chem. Soc, Dalt. Trans*, 1977, 588-595.

21. J.R.J. Sorenson, *in Metal ions in Biological Systems, Inorganic Drugs in Deficiency and Disease*, 1982, **14**, (Ed), H. Sigel, Chapter 4, Mercel Decker, Inc, New York.

22. S. Odisitse, *MSc Dissertation*, 2003, UCT, Cape Town.

23. J.W. Essex, C.A. Reynolds, W.G. Richards, *J. Am. Chem. Soc*, 1992, **114**, 3634-3639.

24. J.N.Zvimba and G.E.Jackson, *J. Inorg. Bio*, 2007, **101**, 1120-1128.

25. X.Q. Kong, D. Shea, W.A. Gebreyes, X.R. Xia, *Anal. Chem*, 2005, **77**, 1275-1281.

CHAPTER 4

GENERAL DISCUSSION AND CONCLUSION

GENERAL DISCUSSION AND CONCLUSION

It has been shown that copper complexes are able to alleviate the inflammation associated with RA [1]. Previous studies with a number of copper(II) chelating agents showed a reasonable good competition and selectivity for copper, with enhanced bio-availability of the metal for alleviation of inflammation associated with rheumatoid arthritis (RA) [2]. Research has been carried out in designing copper(II) chemically stable complexes for the use as anti-arthritic agents [1].

The research under investigating is aimed at contribute to the development of anti-arthritic agent. The ligand of interest should be capable of forming neutral species under physiological conditions as well as incorporating hydrophobic groups are very useful in enhancing exogenous dermal absorption of copper(II) and its subsequent endogenous mobilization to facilitates the bio-availability of the metal [2].

In our study the solution chemistry of Cu(II) and Zn(II) with PCUL ligand at 25°C in 0.15mol/dm^3 Cl^- Na^+ have been explored by glass electrode potentiometry. The potentiometric analysis was carried out in the pH range 2 to 11. Three protonation constants have been obtained for PCUL and these constants are similar to those obtained at the inflection point of chemical shift against pH graph. However, these protonation constants are slightly different from those of the related aminomethyl pyridine.

The potentiometric data analysis gave two possible species; ML and ML(OH). Looking at Figure 2.26, from pH 2.00 to 9.50 the predominant species is ML with $\log\beta_{110}$- 15.38. At pH > 9.50 there is the formation of the ML(OH) species through the axial coordination of the water molecules with $\log\beta_{11\text{-}1}$ = 7.45. Although the *in vivo* competitor Zn(II) gave lower stability constants than Cu(II) in blood plasma model, PCUL mobilized with Zn(II) over Cu(II). Table 3.2 shows that the Cu(II)-PCUL complex is largely hydrophilic with $\log P_{ow}$ giving negative values for all the pH's studied. This however was expected since adamantane incorporated into PCUL ligand is highly hydrophilic [3].

The NMR results supported the potentiometric analysis. As the pH was adjusted from 2.00 to 9.50 the protonation of the amine group was observed. The species distribution curve showed that at the acidic region the solution contains mainly ML species. IR and NMR studies show that the central amines are coordinated to Cu(II) first this indicates that the central amine is closer to the metal ion. The nitrogens of the pyridyl group are also coordinated to the metal ion. However since this is a dynamic system we cannot conclude that both central amines are coordinated at once.

UV/VIS, IR, and octan-1-ol/ water partition coefficient experiments were carried out until pH 8.69 for UV/VIS and pH 6.91 for IR and octan-1-ol/ water partition coefficient. This reason for this is that only 0.21230g of the ligand was available to carry out all experiments involved in this study. Before animal experiments may be undertaken it will be best to first study UV/VIS, IR, and octan-1-ol/ water partition coefficient beyond pH 8.68 and 6.91. The reason for this is to validate the complexation pattern observed in potentiometric and NMR analysis.

This study enlightened some of the problems and challenges associated with the development and design of copper-chelating agents for alleviation of inflammation associated with rheumatoid arthritis. Until the appropriate Cu(II)-ligand complex is formed the research for anti-inflammatory agent shall continue.

References

1. S.Odisitse, MSc Dissertation, 2003, UCT, Cape Town.
2. J.N.Zvimba and G.E.Jackson, *Journal of Inorganic Biochemistry*, 2007, **101**, 1120-1128.
3. O. Kouatly, A. Geronikaki, C. Kamoutsis, D. Hadjipavlou-Litina, and P. Eleftherious, *Eu. J. Med. Chem*, 2008, 1-7.